

MOLECULAR MODELING INSIGHTS INTO THE INHIBITION AND CATALYTIC
MECHANISM OF GOLGI α -MANNOSIDASE II

by

SAMEER PRALHAD KAWATKAR

(Under the Direction of Professor Geert-Jan Boons)

ABSTRACT

In this dissertation, we have employed a computational methodology in conjunction with experimental techniques to understand the mechanism of inhibition of Golgi α -Mannosidase II (GMI) by mannosatin A, and to determine the mechanism of the hydrolysis reaction catalyzed by GMII.

Ab initio calculations and molecular docking studies were employed to rationalize the inhibition data of mannosatin A analogues and to identify the mode of binding of mannosatin A. It was found that Mannosatin and aminocyclopentitretrol could bind to GMII in a similar mode as that of the known inhibitor Swainsonine. However, due to the flexibility of the five membered rings of these compounds, additional low energy binding modes could be adopted. The thiomethyl moiety of mannosatin was predicted to make favorable hydrophobic interactions with Arg228 and Tyr727, possibly accounting for its greater inhibitory activity.

In order to validate the docking predictions, the X-ray crystal structures of *Drosophila* Golgi α -mannosidase II (dGMII) complexed with the inhibitors mannosatin A and its *N*-benzyl analog have been determined. The X-ray structures were in excellent agreement with the predicted binding modes for mannosatin A analogues. Molecular dynamics simulations and

NMR studies have shown that the five-membered ring of mannostatin A is rather flexible. In the bound state, mannostatin A adopts a 2T_1 twist envelope conformation, which is not significantly populated in solution. Possible conformations of the mannosyl oxacarbenium ion and an enzyme-linked intermediate have been compared to the conformation of mannostatin A in the co-crystal structure with dGMII. It has been found that mannostatin A best mimics the covalent linked mannosyl intermediate. The thiomethyl group is able to make a number of additional polar and non-polar interactions increasing the affinity for dGMII.

Finally, a quantum mechanical investigation of the catalytic mechanism of the hydrolysis reaction catalyzed by GMII has been conducted. These calculations have revealed that in the transition state, the mannopyranosyl ring adopts a conformation that lies between an ideal $B_{2,5}$ and 1S_5 conformation. Superimposition of mannostatin A and swainsonine in their bound conformations onto the optimized transition state structure revealed that both inhibitors mimic the transition state.

INDEX WORDS: Mannosidases, Mannosidases mechanism, Glycosidase Inhibitors, Oxacarbenium ion, Mannostatin, Thiomethyl, X-ray, QM and QM/MM calculations

MOLECULAR MODELING INSIGHTS INTO THE INHIBITION AND CATALYTIC
MECHANISM OF GOLGI α -MANNOSIDASE II

by

SAMEER PRALHAD KAWATKAR

B. Sc., University of Mumbai, India 1996

B. Sc. (Tech), University of Mumbai, Institute of Chemical Technology, India 1999

A Dissertation Submitted to the Graduate Faculty of The University of Georgia in Partial
Fulfillment of the Requirements for the Degree

DOCTOR OF PHILOSOPHY

ATHENS, GEORGIA

2006

© 2006

SAMEER PRALHAD KAWATKAR

All Rights Reserved

MOLECULAR MODELING INSIGHTS INTO THE INHIBITION AND CATALYTIC
MECHANISM OF GOLGI α -MANNOSIDASE II

by

SAMEER PRALHAD KAWATKAR

Major Professor: Geert-Jan Boons
Committee: Robert J. Woods
Kelly W. Moremen
James H. Prestegard

Electronic Version Approved:

Maureen Grasso
Dean of the Graduate School
The University of Georgia
August 2006

DEDICATION

To my wonderful wife, Aarti. Without your support this endeavor was not possible.

To Aai (my mother) and Baba (my father), for all your hardwork to take me to this stage.

ACKNOWLEDGEMENTS

I wish to express my deepest gratitude to my wife, Aarti for all her love and encouragement during my tenure as a graduate student. I know, I can count on her for anything. I also want to thank our daughter, Pooja, as I always enjoyed relaxed moments while being with her.

I would like to thank Professor Geert-Jan Boons for giving me such a wonderful opportunity of working on a multidisciplinary project, and allowing me to pursue my goals. Thank you for being considerate throughout my presence here in the University of Georgia.

My special thanks go to Professor Robert J. Woods who trained me to be a computational chemist. Your encouraging support and mentorship transformed me into an independent scientist. Thank you for giving me the freedom of using the laboratory resources without any reservations.

I wish to thank the administrative staff in the CCRC, for guiding me through different issues. I also wish to thank Carolyn and Shielah for being wonderful administrative assistantants and helping me out on various occasions. I would like to thank members from Woods' group and Boons' group. In particular, I thank Austin, for all those "lunch time" discussions on possibly every subject on the earth.

Finally, many thanks go to the Department of Chemistry and Complex Carbohydrate Research Center for this opportunity.

TABLE OF CONTENTS

	Page
ACKNOWLEDGEMENTS	v
CHAPTER	
1 INTRODUCTION	1
2 INHIBITION OF GOLGI α -MANNOSIDASE II WITH MANNOSTATIN A ANALOGS: SYNTHESIS, BIOLOGICAL EVALUATION AND STRUCTURE ACTIVITY RELATIONSHIP STUDIES	40
3 THE STRUCTURAL BASIS OF THE INHIBITION OF GOLGI α - MANNOSIDASE II BY MANNOSTATIN A AND THE ROLE OF THE THIOMETHYL MOIETY IN LIGAND-PROTEIN INTERACTIONS	62
4 CATALYTIC MECHANISM OF GOLGI α -MANNOSIDASE II: A QUANTUM MECHANICAL STUDY	94
5 CONCLUSIONS.....	163
REFERENCES	173

CHAPTER 1
INTRODUCTION

Carbohydrates, also known as saccharides (Greek: sakcharon, sugar), are essential components of all living organisms and the most abundant class of biomolecules. It has been long known that carbohydrates serve as an energy source. However, increasing research in the field of carbohydrates has revealed that these structures are involved in diverse biological processes including cell-cell adhesion, protein folding, protein trafficking and signal transduction.¹ Despite the involvement of carbohydrates in several biological processes, there are relatively few carbohydrate-based therapeutics,^{2, 3} likely due to fears that such agents will suffer from poor oral bioavailability and high clearance rates (which may be of benefit in some applications) and, most notably, the lack of a detailed understanding of the biological phenomena in which carbohydrates are involved.⁴ For example, an increasing number of carbohydrate processing enzymes are being identified and validated as targets for therapeutic intervention.^{4,5} Inhibitors of these enzymes have garnered much attention and are currently used for the treatment of diabetes, viral infections and Gauchers disease.⁶⁻¹⁰ However, efforts to design more potent and/or selective inhibitors often are limited due to a dearth of knowledge pertaining to the catalytic mechanisms and the mechanism of inhibition by natural inhibitors of these targets.

The research presented in this dissertation focuses on one such enzyme that has been validated as a target for cancer therapy namely Golgi α -mannosidase II (GMII). We have employed a computational approach in conjunction with experimental techniques to understand the mechanism of inhibition of GMII by inhibitors containing in particular cyclopentitol moieties, such as mannostatin A (chapter 2 and 3), and to determine the mechanism of the hydrolysis reaction catalyzed by GMII (chapter 4).

1.1 Carbohydrate Processing Enzymes

The biological processes in which carbohydrates are involved are often mediated through biological recognition of specific oligosaccharide structures that are synthesized in the form of glycoconjugates via several biosynthesis pathways. A glycoconjugate is a compound in which one or more monosaccharide or oligosaccharide units (the glycone) are covalently linked to a noncarbohydrate moiety. These glycoconjugates include glycolipids, glycoproteins and glycopeptides. Glycoconjugate biosynthesis requires conversion of monosaccharide building blocks with the help of carbohydrate processing enzymes. Such carbohydrate processing enzymes can be classified into two major classes based on the function they perform specifically, Glycosyl hydrolases (glycosidases) and Glycosyl transferases. Glycosidases are involved in cleaving a linkage between two specific monosaccharide units, whereas glycosyl transferases are involved in formation of such linkages. Huge numbers of these processing enzymes exist, and each enzyme is usually involved in the cleavage or formation of a specific linkage. The following sections present a more detailed review of the general mechanism, mechanistic studies that have been reported in recent years, and the clinical importance of glycosidases. As the subject of this research is glycosidases, the ensuing discussion is largely restricted to glycosidases.

1.2 Glycosyl Hydrolases

Glycosidases are a group of enzymes that catalyze the hydrolysis of specific glycosidic linkages through a nucleophilic substitution reaction at the anomeric carbon of a donor sugar moiety (known as glycone), which is characterized by displacement of the

leaving group (the aglycone, generally also a sugar moiety) by an acceptor molecule (water).

Currently, there are about 6000 known glycosidases, which have been classified into 89 families based on their primary structure. Updated information on the classification is available on the Internet at <http://afmb.cnrs-mrs.fr/CAZY>. In addition to the classification based on the primary structure, glycosidases can also be broadly classified according to the stereochemistry at the anomeric carbon atom in the substrate as well as the corresponding hydrolyzed product. For example, GMII is an α -retaining enzyme, which indicates that the configuration at the anomeric carbon in the natural substrate of GMII is α . This configuration is retained in the hydrolyzed product.

The glycosidic bond, particularly that between two glucose residues, is the most stable of all linkages within naturally occurring biopolymers, with half-lives for the spontaneous hydrolysis of cellulose and starch in the range of 5 million years.¹¹ Glycosidases, which are responsible for the hydrolyses of these materials therefore face a challenging task, yet they accomplish this with rate constants of up to 1000 s^{-1} (or enhancement of 10^{17} fold in the rate of the reaction), earning them a reputation as some of the most proficient catalysts.¹² Hydrolysis of the glycosidic bond can occur with one of two possible stereochemical outcomes, specifically an inversion or retention of anomeric configuration (Figure 1.1). This is achieved by two different mechanisms, originally proposed by Koshland¹³ based on chemical mechanisms of similar uncatalyzed reactions. While the general concept of these mechanisms remains acceptable, several details have been revealed and refined in recent years.^{12, 14-16}

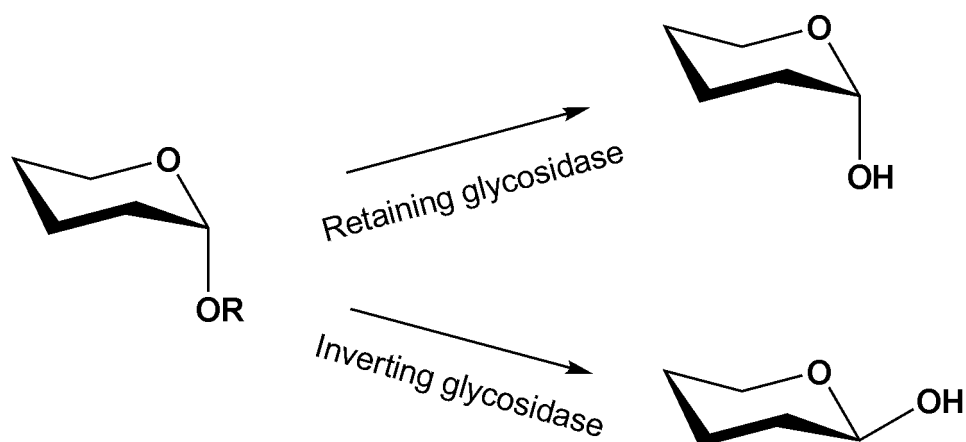


Figure 1.1 Stereochemical outcome of a hydrolysis reaction catalyzed by an α -glycosidase.

1.3 General Catalytic Mechanism of Inverting Glycosidases

The catalytic mechanism of an inverting glycosidase is believed to be a single step substitution reaction at the anomeric carbon¹³ which involves displacement of the aglycone with the incoming water molecule. Similar to the acid-catalyzed hydrolysis of glycosides¹⁷, this reaction is believed to proceed via an oxacarbenium ion-like transition state (Figure 1.2). Two conserved carboxylic acid residues in the active site are necessary for the reaction to proceed. One residue acts as general acid and the other as a general base, thereby protonating the aglycone and assisting its departure, and deprotonating the incoming water molecule, respectively. Since the subject of this research is an α -retaining enzyme, inverting enzymes and their mechanism will not be discussed further.

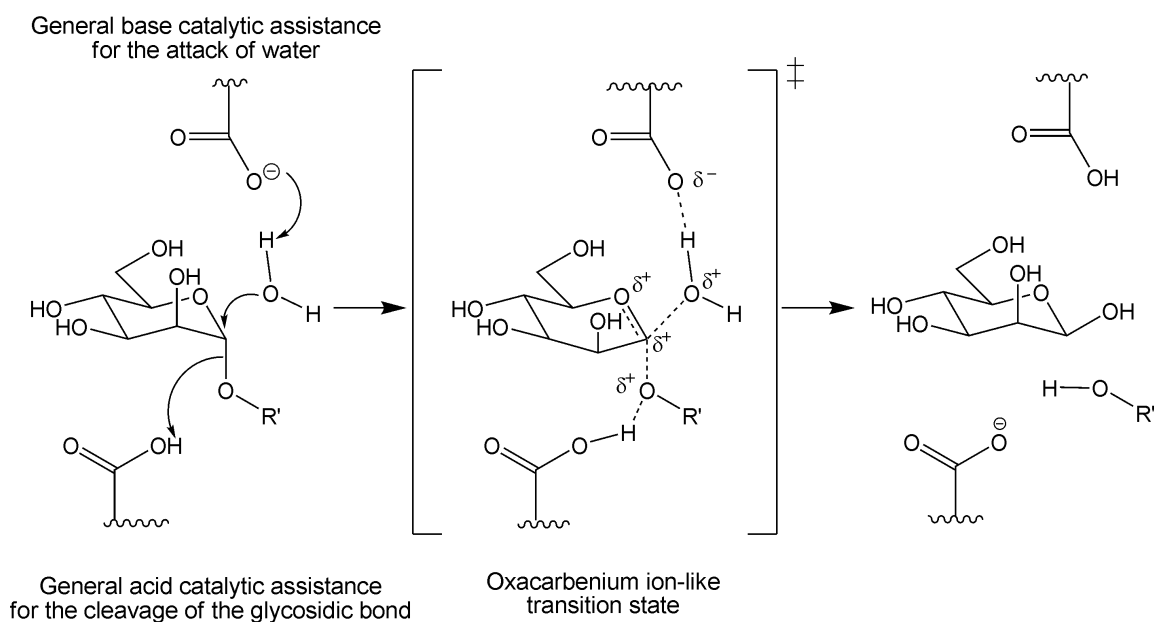


Figure 1.2. Proposed single step mechanism for an inverting α -glycosidase.

1.4 General Mechanism of Retaining Glycosidases

The original catalytic mechanism proposed by Koshland¹³ for retaining glycosidases was a two-step process (also known as the double displacement mechanism) involving two displacement reactions at the anomeric center (Figure 1.3). In the first step, referred to as the glycosylation step, a catalytic nucleophile (generally an aspartate or glutamate residue) attacks the anomeric carbon of the glycone from the β -face. The aglycone departure is assisted by a general acid-base catalytic residue (usually another aspartate or glutamate residue) which protonates the aglycone. This nucleophilic substitution results in the formation of a covalently linked glycosyl-enzyme intermediate with an inversion of the anomeric configuration. The second step, referred to as the deglycosylation step, is a nucleophilic attack by a water molecule at the anomeric center

of this glycosyl-enzyme intermediate. In this step, the conjugate base of the general acid-base residue deprotonates the water molecule, facilitating the attack. This reaction also results in the inversion of the anomeric configuration. The overall reaction thus proceeds with a net retention of the anomeric configuration.

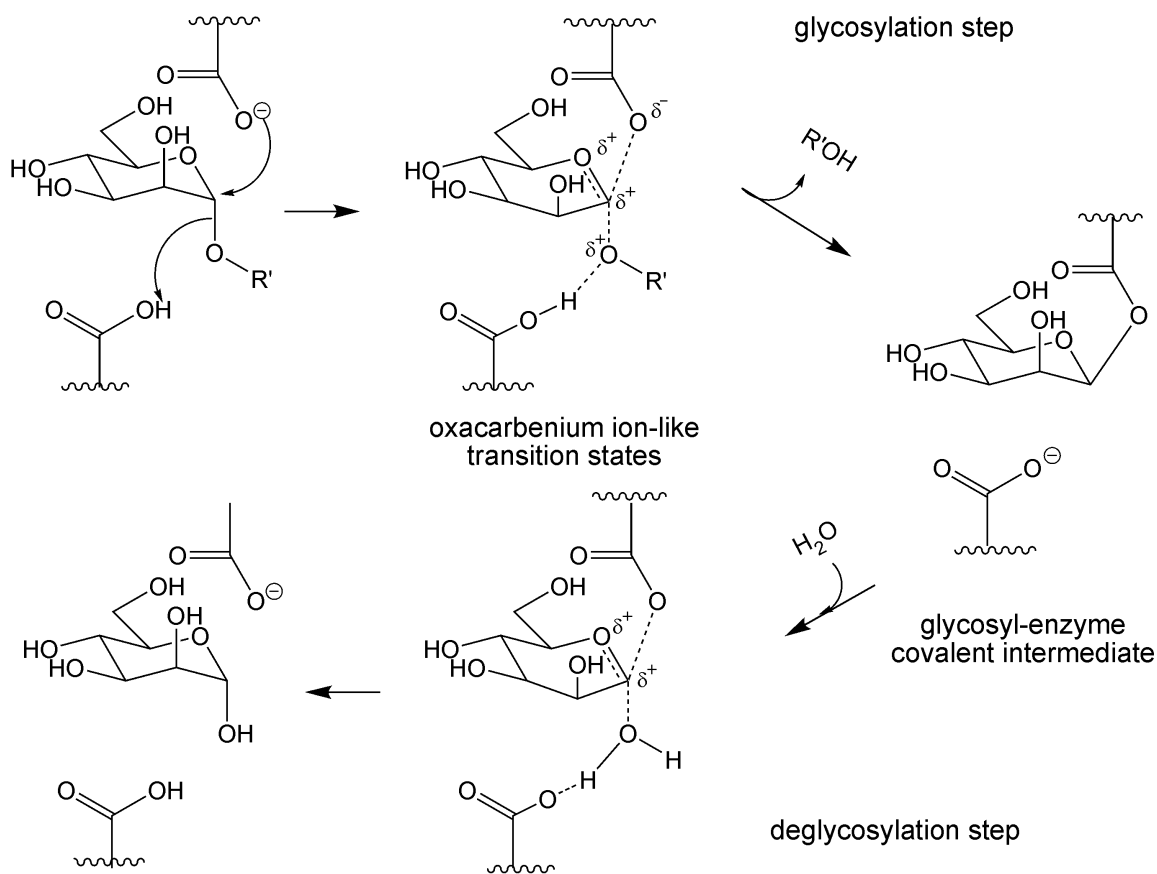


Figure 1.3. Proposed double displacement mechanism for a retaining α -glycosidase.

While many essential features of the general mechanism of action of retaining glycosidases are known,^{12, 16, 18, 19} several methods have contributed to the refinement of mechanistic details in recent years. These methods include kinetic isotope effects, crystal structure analysis of wild type and mutated glycosidases and of their complexes with

ligands, and the structure and kinetics of the transition state mimics. Many of these mechanistic studies have been carried out on β -glycosidases, largely due to the availability of good, easy to work with model enzymes and relative ease of synthesizing the substrates required for these glycosidases as compared to their α -counterparts. Despite our increasing understanding of these mechanisms some questions remain unanswered, and include the following:

1. Which conformational change is induced in the substrate by an individual glycosidase *en route* to the transition state (distortion towards chair, half-chair, boat, skew-boat or envelope)?
2. Which conformation is adopted at the transition state and the covalent intermediates? Is this conformation the same in all glycosidases?
3. Some glycosidases have a metal ion in the active site. Does this metal ion take part in the mechanism or it is necessary only for structural stability of the ligand-protein complexes?

Several studies in recent years have attempted to address these questions. The following sections present a general review of literature on mechanistic studies of glycosidases.

1.5 Distortion of Substrates upon Binding with Glycosidases

Almost all biological processes involve recognition of a ligand by a specific receptor. While the nature of interaction largely depends on the shape and size of the ligand as well as the binding pocket, such an interaction usually results in conformational changes in the ligand and/or receptor that result in what is known as the Michaelis

complex. Primary drivers of such induced conformational changes are different interactions of functional groups in the ligand with protein residues. While these conformational changes arrange the substrate in a conformation which otherwise is not accessible, they also reduce the activation energy for the reaction by preorganizing the substrate in a conformation that lies closer to the transition state on the potential energy surface.

It is known that glycosyl hydrolases distort the substrate to arrive at the Michaelis complex structure. First proposed for the hen egg white lysozyme,²⁰ such substrate distortion has also been unambiguously observed in high-resolution X-ray structures of Michaelis complexes for two structurally unrelated endoglucanases (from glycosyl hydrolase families 5 and 7^{21, 22} and hexosaminidase (family 20)).²³

Ducros et al. recently reported the X-ray structure of the Michaelis complex for a family-26 β -Mannase, which is a retaining endo- β -(1-4)-mannose. In these studies the mechanism based inactivator of mannaes 2,4-dinitrophenyl 2-deoxy-2-fluoro- β -mannotrioxide was used to probe the reaction coordinate of the reaction. Surprisingly, the Michaelis complex displayed 1S_5 conformation of the substrate,²⁴ which is different than enzymes that work on gluco-configured substrates. This result suggested a different conformational itinerary for the mannosidases as compared to glucosidases.

1.6 The Oxacarbenium Ion-like Transition State

The transition state for both the glycosylation and deglycosylation steps of retaining glycosidase catalysis is believed to closely resemble the oxacarbenium ion. In the case of the oxacarbenium ion, the positive charge developed on the sugar is

delocalized between the anomeric carbon and the *endo*-oxygen (Figure 1.4). This introduces a partial double bond character in the bond between the anomeric carbon and the ring oxygen, thus forcing atoms C-5, O-5, C-1 and C-2 to be in one plane. Belief in this kind of transition state has been supported by α -deuterium kinetic isotope effects (α -DKIE) measured with several β -glycosidases.²⁵⁻²⁹ For example, in the case of *Agrobacterium* β -glucosidase, in both the glycosylation and deglycosylation steps the ratio of the rates of hydrolysis of the normal substrate to that of the substrate deuterated at the anomeric carbon (k_H/k_D) was found to be positive.²⁹ This indicated a transition state with increased sp^2 character at the anomeric center when compared to the ground state. Moreover, the same study suggested that the transition state for the glycosylation step is ‘dissociative’, meaning that there is significant cleavage of the bond between the anomeric carbon and anomeric oxygen.

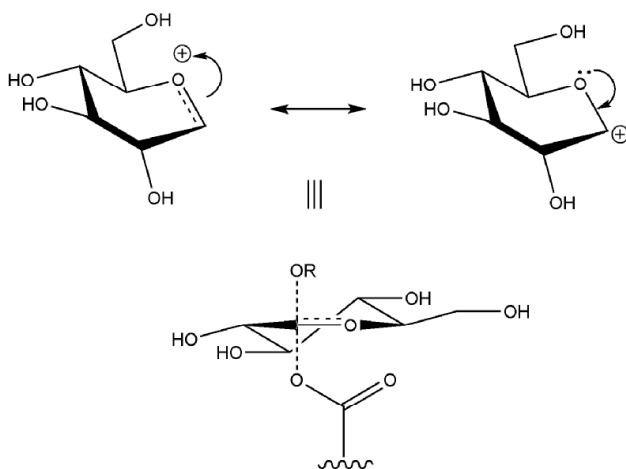


Figure 1.4. Proposed structure of the oxa-carbenium ion-like transition state for the hydrolysis reaction catalyzed by α -retaining glycosidases, where C-5, O-5, C-1, and C-2 atoms are in one plane.

In addition to this, fluorinated sugars have also been used as substrates to validate the hypothesis of delocalization of positive charge. Placement of fluorine at the 2- or 5-

position has been shown to reduce the rate of hydrolysis significantly for β -retaining enzymes.^{30, 31} These modifications destabilize the positive charge development on the anomeric carbon and the *endo*-oxygen (by inductive effects), thereby making it less susceptible to the attack from the nucleophile. It was also proposed that these modifications might affect the conformational properties of the glycone, possibly resulting in a loss of potential interactions of the glycone with the residues in the active site.³²

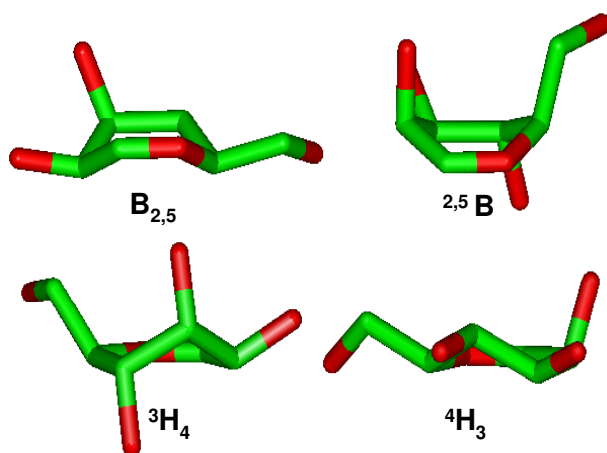


Figure 1.5. Possible conformations of the transition state for manno-pyranose ring, which display atoms C-5, O-5, C-1, and C-2 in one plane.

The suggested nature of the transition state leaves only a few conformational itineraries that the pyranosyl ring can follow *en route* to the transition state structure. An analysis of the pseudorotation wheel for the pyranose ring suggests that there are only four possible conformers which support the planarity of the C-5, O-5, C-1 and C-2 atoms: 4H_3 , 3H_4 , $^{2,5}B$ and $B_{2,5}$ (Figure 1.5). Indeed, crystallographic studies of family-5 and -7 retaining cellulases have suggested a 4H_3 half chair conformation at the transition state.²¹⁻
²³ Furthermore, a $B_{2,5}$ boat conformation was proposed as a transition state conformation for β -mannosides.

Linus Pauling suggested in the 1940s that the enzymes catalyze the reactions by binding tighter in the transition state conformation, leading to the suggestion that the transition state analogues should act as high-affinity inhibitors of enzymes. In the case of glycosidases, several inhibitors have been reported as transition state analogues. For example, D-manno-1,5-lactone³³⁻³⁵ and D-manno-1,5-lactam³⁶ are found to adopt a $B_{2,5}$ conformation, which is the suggested transition state conformation, and both are strong inhibitors of β -mannosidases. Thus, the knowledge of transition state structure would facilitate efforts aimed at the design of potent inhibitors that mimic transition state conformation.

1.7 The Glycosyl-Enzyme Covalent Intermediate

Similar to the transition state, the nature and conformation of the glycosyl-enzyme covalent intermediate (CINT) is also a subject of extensive research. The earliest explanation of the nature of CINT was based on the crystal structure of hen egg-white lysozyme²⁰, which suggested that the CINT must exist as an ion-pair. A more recent study also suggests that nucleophilic catalysis is unlikely without major conformational changes within the active site of the lysozyme.³⁷

α -Deuterium kinetic isotope effect (α DKIE) has also been used to probe the nature of CINT. The use of α DKIE is based on the expectation that if the intermediate formed is a covalent intermediate, the anomeric carbon should be sp^3 hybridized. Since the transition state on either side of CINT is oxa-carbenium ion-like with more sp^2 character than the ground state, the anomeric carbon must be covalently linked with the catalytic nucleophilic residue. Indeed, in studies in which α DKIE was measured for the

deglycosylation step, kH/kD was found to be greater than unity¹⁵, a finding consistent with a covalent intermediate.

Efforts to isolate covalent intermediates have also been successful using substrate mimics in the presence of wild type as well as mutant enzymes. One of the strategies employed is to use 2- and 5-fluorosugars as mechanism-based deactivator.^{30, 31, 38} As discussed above, these substrate mimics reduce the rate of hydrolysis of CINT. If the difference in the rates of glycosylation and deglycosylation reaction is significant, the covalent intermediate accumulates and can be isolated.

1.8 Glycosidases in the N-glycan Biosynthesis Pathway and Their Biological Roles

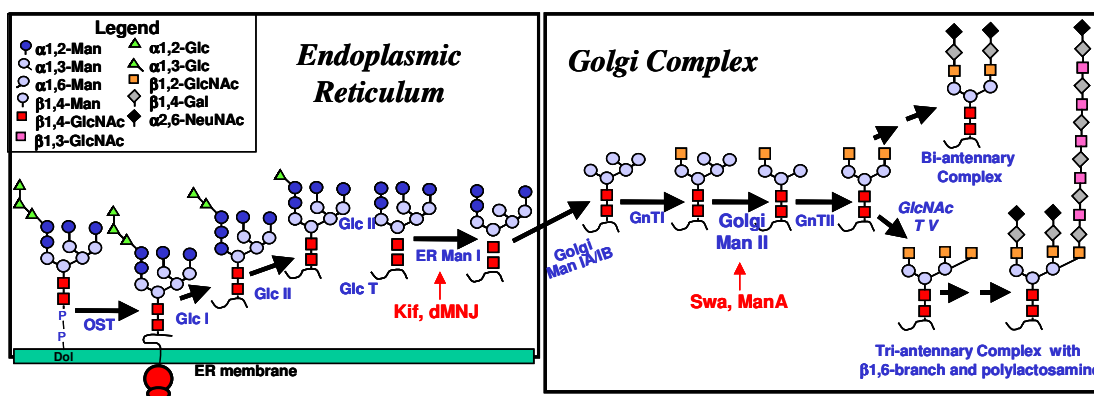


Figure 1.6. Biosynthesis of glycoproteins that possess N-linked glycans. As the nascent glycoprotein enters the endoplasmic reticulum (ER), a preformed oligosaccharide known as the dolichol-phosphate precursor (DPP) is attached co-translationally to some Asn residues that are part of the consensus sequence Asn-Xaa-Ser/Thr. The biosynthesis of this precursor, its attachment to Asn residues and the subsequent steps of its processing in the ER and the Golgi, are performed by a series of glycosidases and glycosyltransferases.

The biosynthesis of N-linked glycans is a complex process that occurs in secretory pathway of eukaryotic cells and requires the participation of glycosyl

transferases as well as glycosidases. The enzymes involved in the maturation of mammalian N-linked glycans are found in the ER and Golgi complex, where they act upon newly synthesized glycoproteins to generate an array of complex structures from a common oligosaccharide precursor.³⁹ The synthesis and maturation of N-linked oligosaccharides occurs in four stages in the membranes of the ER and Golgi complex.

In the first stage, a dolichol-linked $\text{Glc}_3\text{Man}_9\text{GlcNAc}_2$ oligosaccharide precursor is synthesized and transferred en bloc to the Asn-X-Ser/Thr sequons on newly synthesized polypeptides through the action of the oligosaccharide transferase.⁴⁰ The second stage involves trimming of the transferred oligosaccharide resulting in the removal of all three glucose residues and six of the nine original mannose residues to generate the $\text{Man}_3\text{GlcNAc}_2$ core structure present on complex type oligosaccharides. The third stage of maturation involves synthesis of GlcNAc branches on the $\text{Man}_3\text{GlcNAc}_2$ core by the action of a collection of GlcNAc transferases. The final stage involves elaboration of these branches with unique capping structures, which are characteristic of complex type oligosaccharides.^{1, 41} This final modification of the N-glycans results in extremely diverse oligosaccharide structures which are implicated in the adhesion of cells, either by direct interaction with lectins associated with the extracellular matrix or the surfaces of other cells, or indirectly by influencing the protein-protein interaction of cell adhesion molecules at points of focal contact.

While it is clear from the pathway depicted in Figure 1.6 that glycosidases are essential to the production of substrates required for Golgi glycosyl transferases, glycosidases in the ER are also involved in quality control. As shown in Figure 6, N-linked oligosaccharide chains are co-translationally added to proteins in the ER lumen as

Glc₃Man₉GlcNAc₂ precursors. The outer and two inner glucoses are trimmed by ER α -glucosidases I (Glc I) and II (Glc II), respectively. Incorrectly folded glycoproteins are recognized by the enzyme UDP-Glucose:glycoprotein glucosyltransferase (GT) which reattaches a single glucose to the *N*-linked oligosaccharide chain.⁵ Monoglucosylated glycans are then recognized by the lectin-like ER chaperones calnexin (CNX) and calreticulin (CRT), which promote correct folding by inhibiting aggregation and preventing premature oxidation and oligomerization. The reattached glucose is then removed by Glc II. Depending on the folded state of the glycoprotein, it either continues down the maturation pathway in the Golgi apparatus or enters a reglucosylation/deglucosylation cycle until it is fully folded and can exit the ER. Inhibitors of these enzymes are known to cause delays in the folding and intracellular transport of glycoproteins and are thus compounds of interests in various therapies.⁵ Similar to Glc I and Glc II, recent studies have shown that class I α -mannosidase located in the ER plays an important role in the degradation of misfolded glycoproteins.⁵

1.9 Association of the β 1,6-Branch with Malignancy

The complexity of N-glycan structures is largely based on the cell-specific expression of a collection of glycosyl transferases, which specify the extension of oligosaccharide structures onto the trimmed Man₃GlcNAc₂ core, structure derived from ER and Golgi α -mannosidase action.¹ Linkage specific GlcNAc transferases establish the branching pattern of the Man₃GlcNAc₂ core resulting in common bi-, tri- or tetra-antennary complex type structures that are further extended with either simple or highly complex branched or linear terminal capping structures. Among the most extended and

complex termini are the polylectosamine-containing (repeating Gal β 1,4GlcNAc β 1,3-) structures that are preferentially added to a single β 1,6GlcNAc branch from the tri-mannosyl core. These structures are high-affinity ligands for extracellular lectins such as galectin 1 and 3, and act as the scaffold for elaboration of branched termini, such as Le^x, Le^y and sialyl-Le^x antigen sequences.

One of the rate limiting factors in polylectosamine expression on N-glycans is the synthesis of the β 1,6GlcNAc branch on the Man₃GlcNAc₄ core. The reaction is catalyzed by the Golgi glycosyltransferase GlcNAc transferase V (Gn TV).⁴²⁻⁴⁴ In mammalian tissues, β 1,6GlcNAc branched structures on the plasma membrane are largely restricted to cells that are capable of invasion, including endothelial cells and activated lymphocytes.^{45, 46} In transformed cells and human cancer cells, including carcinoma of the breast, colon and skin, a significant increase has been found in β 1,6GlcNAc branching.⁴⁷⁻⁵⁰ Since the extent of β 1,6-branching and polylectosamine structures correlates with disease progression, these structures are considered as markers of malignancy in many tissues.^{51, 52} The role of β 1,6-branching in metastasis and tumor progression was further addressed by the generation of Gn TV-deficient mice, which indicated that β 1,6GlcNAc branching catalyzed by Gn TV influences the migration of tumor cells and leucocytes, presumably by affecting their adhesion to the extracellular matrix, and that induction of β 1,6-branching contributed to the altered adhesion characteristics of metastatic cells.⁵³

1.10 Glycoprotein Processing Inhibitors as Anti-tumor Agents

While evidence for the correlation between β 1,6-branching, metastasis, tumor progression and Gn TV expression levels is compelling, no natural or synthetic inhibitors of Gn TV have been identified that are cell-permeable and effective in blocking oligosaccharide processing *in vivo*. Since selective and high inhibition of Gn TV has not yet been achieved, inhibitors, that act earlier in the N-glycan biosynthesis pathway and interfere with the formation of the precursor for β 1,6-branching, have been tested as anti-tumor agents.

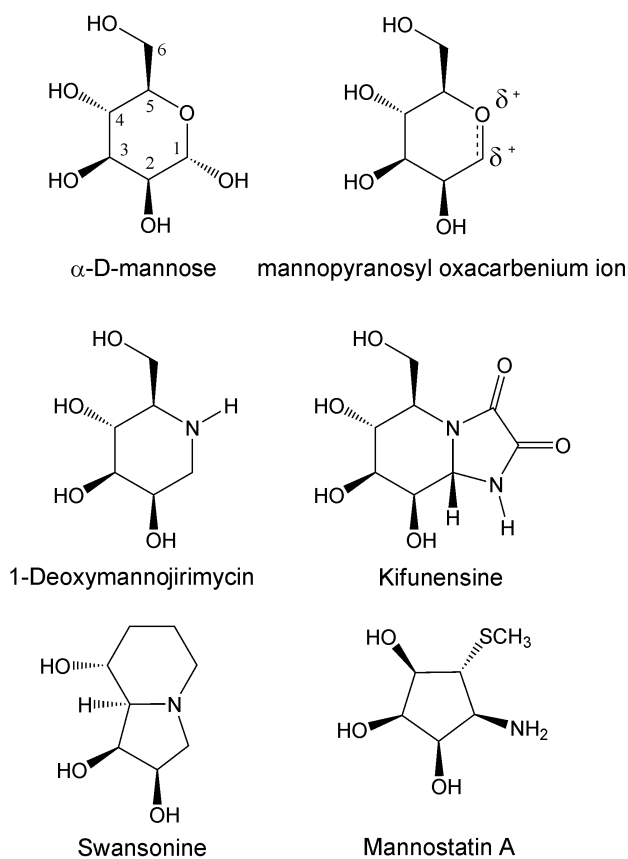


Figure 1.7. Glycoprotein processing inhibitors.

Among the known inhibitors, glucosidase inhibitors block the N-glycan processing at an early stage, resulting in the generation of glucosylated high-mannose type oligosaccharides. In addition, these inhibitors tend to be less effective due to multiple routes of early oligosaccharide processing in mammalian cells. The α -mannosidase inhibitors can be divided into two groups based on their selective action toward the two classes of α -mannosidases in mammalian cells.^{39, 54} Aza-sugar mannopyranose mimics such as kifunensine and deoxymannojirimycin inhibit class I mannosidases, resulting in extended high mannose structures.^{55, 56} In contrast, inhibition of class II mannosidases by presumed manno-furanoses transition state mimics such as swainsonine and mannostatins, results in the formation of hybrid-type structures.⁵⁵

Glucosidase and class I α -mannosidase inhibitors have some potential as inhibitors of β 1,6-branch formation because they can block N-glycan processing. However, accumulation of extended high-mannose structures by these compounds can also affect the function and intra cellular transport of some glycoproteins.^{54, 57-60} On the other hand, the class II inhibitors do not appear to influence the function or transport of glycoproteins and exhibit low toxicity in tissue cultures and animals, including mice and humans.⁶¹

Among the known class II α -mannosidase inhibitors, swainsonine, which was first isolated from the Australian plant *Swainsona canescens* and subsequently from additional plants in America^{55, 62}, is the most studied. Since swainsonine influences the maturation of glycoproteins, yielding hybrid-type rather than complex-type structures, it could be anticipated that the compound might influence cell adhesion characteristics and thus the metastatic behavior of transformed cells.⁶³ The low toxicity of the compound

was revealed when no changes in cell growth rates were found in transformed cells in culture. Furthermore, when transformed cells were introduced into animal models, swainsonine was found to possess strong immunostimulatory activity which resulted in a significant anti-cancer effect.^{63, 64} Swainsonine was shown to stimulate natural killer cells and lymphokine activated killer cells, and significantly blocked tumors in the lungs, liver, and spleen.^{64, 65} The compound was also shown to stimulate the anti-tumor activity of macrophages in a time- and dose-dependant manner.⁶⁶ Furthermore, in addition to stimulating bone marrow proliferation, swainsonine also shown to enhance bone marrow cellularity, engraftment efficiency, and colony forming units in mice.⁶³ Two phase I clinical trials have demonstrated that swainsonine has a low toxicity in humans and is well tolerated.^{63, 67}

Swainsonine and all other known GMII inhibitors have an additional serious side effect that precludes their use a therapeutic in that they also inhibit the broad specificity lysosomal α -mannosidase, resulting in the accumulation of mannose-containing oligosaccharides in tissues, serum and urine as a phenocopy of the hereditary lysosomal storage disease, α -mannosidosis.^{68, 69} This disease results in various clinical features such as coarse features, skeletal abnormalities, dilated cerebral ventricles, and severe mental retardation.^{70, 71} Thus, a preferable approach for therapy to inhibit tumor growth and metastasis is to develop alternate lead compounds that specifically inhibit GMII without affecting lysosomal α -mannosidase. It should be mentioned that despite the similarities between the two mannosidases in the sequence, response to inhibitors, and catalytic mechanism as retaining enzymes, GMII and lysosomal α -mannosidase have significant

differences in the aglycone specificity that can be utilized for selective inhibitor design.

72-74

1.11 The X-ray Structure of Swainsonine:GMII Complex

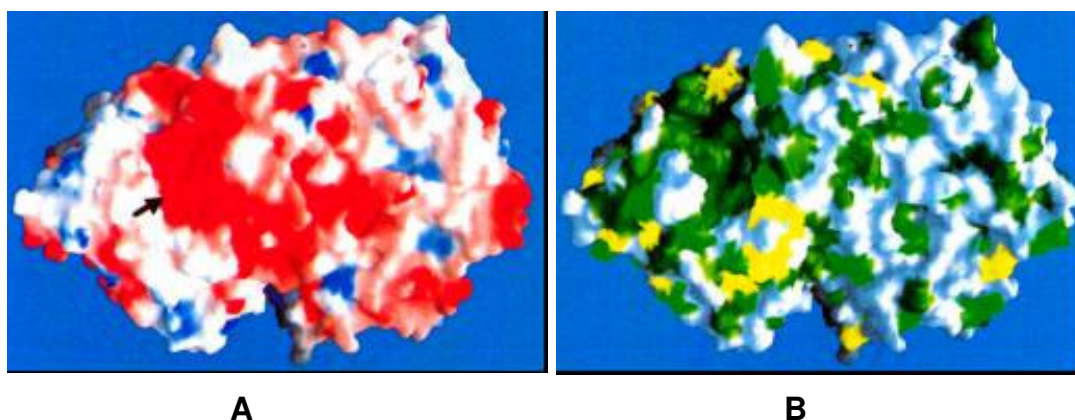


Figure 1.8. A. Molecular surface representation of the planer surface of dGMII (adopted from reference 75). The arrow indicates location of the active site region. B. Molecular surface of dGMII, colored for homology with the sequence of human GMII (dark green for identical, light green for conserved, yellow for similar and white for different residues).

Although the crystal structure of human GMII (hGMII) is not yet available, X-ray structures of GMII obtained from *Drosophila melanogaster* (dGMII) in absence of ligand and in complex with swainsonine and 1-deoxymannojirimycin (PDB codes 1HTY, 1HWW and 1HXK) have been described in detail by van den Elsen et. al.⁷⁵. This enzyme has high sequence identity when compared with human counterpart (41% identity and 61% similarity).⁷⁵ dGMII has also been shown to display comparable kinetic properties and inhibitor sensitivity as well as identical substrate specificity to hGMII.

dGMII is an oval-shaped molecule with two distinct faces. The N-terminal face of dGMII is convex, whereas the opposing face has a planar surface. The molecular surface of dGMII reveals an expanded pocket in the N-terminal α/β -domain, formed primarily by

acidic residues (Figure 1.8A). These same residues form the core of a large, surface-exposed patch of highly conserved amino acids, as compared to hGMII sequence (Figure 1.8B). The active site of the enzymes is located in a small cavity inside this region.

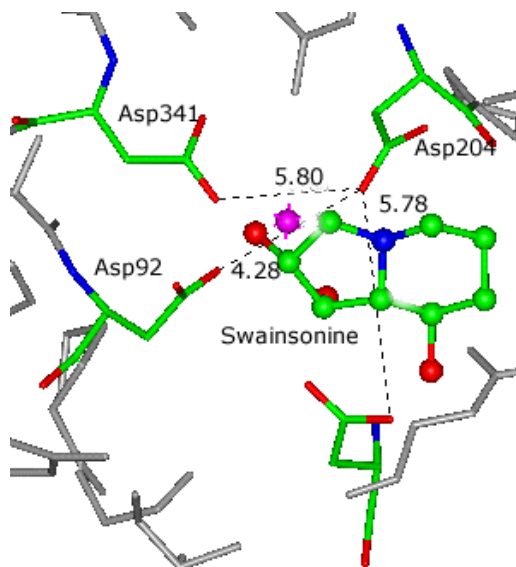


Figure 1.9. Active site region of dGMII with a bound swainsonine molecule. Distances between catalytic residues are represented by dotted lines.

From the structures of dGMII-inhibitor complexes, four acidic amino acid residues, specifically Asp92, Asp204, Asp341 and Asp472, were identified as candidates for catalytic side chains based on their proximity in the active site (Figure 1.9). Studies of the catalytic mechanism of Jack-bean α -mannosidase have identified an aspartate residue as a catalytic nucleophile.⁷⁶ Comparison of the highly conserved sequence region surrounding this aspartate in Jack-bean α -mannosidase with the same sequence region in dGMII suggests that Asp204 is the catalytic nucleophile that attacks the glycosidic linkage.⁷⁵ An identical finding was confirmed for another α -mannosidase belonging to family 38, the bovine lysosomal α -mannosidase.⁷⁷

As dGMII is a retaining α -mannosidase, the distance between the catalytic nucleophile and the base should be about 5.5 Å. Based on this expected distance, Asp341 and Asp 472 are likely candidates as the catalytic base. Geometrically Asp341 is well positioned to be the catalytic base, a notion that is also supported by the fact that the D341N mutant is catalytically inactive.⁷⁵

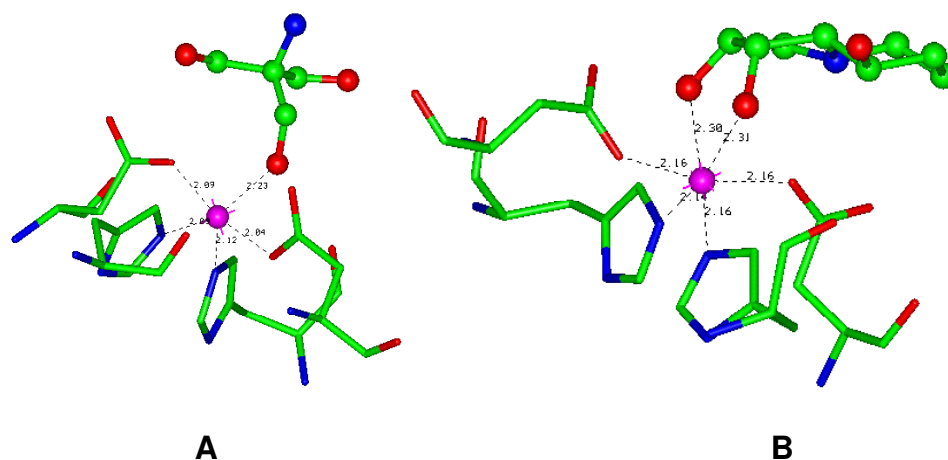


Figure 1.10. Binding site of dGMII showing Tris (A) and swainsonine (B) bound to the enzyme and coordination of zinc ion. Zinc ion coordinates with T₅ geometry in case of Tris molecule whereas, coordinates with T₆ geometry in the case of swainsonine.

The crystal structure of dGMII complexed with 2-amino-2-hydroxy methyl propane-1,3-diol (Tris) also revealed the presence of the enzyme-bound Zn⁺² ion⁷⁵ in the binding site. It was also observed that Zn⁺² ion binds to the enzyme in a T₅ square-based pyramidal geometry (Figure 1.10A) by coordinating to OD1 oxygens of Asp92 and Asp204, the NE2 nitrogens of His90 and His471 and the hydroxyl oxygen O2 of the bound Tris molecule. It was observed that, for dGMII-inhibitors complexes the coordination geometry of Zn⁺² ion changes to a less favored⁷⁸ hexavalent (T₆) state (Figure 1.10B). It was proposed that in the actual glycosidase reaction this change in

geometry might energetically facilitate the deglycosylation step by reverting to more stable T_5 geometry. Thus, zinc may contribute directly to the glycosidase mechanism.

1.12 Covalently Linked Glycosyl-Enzyme Intermediates of dGMII

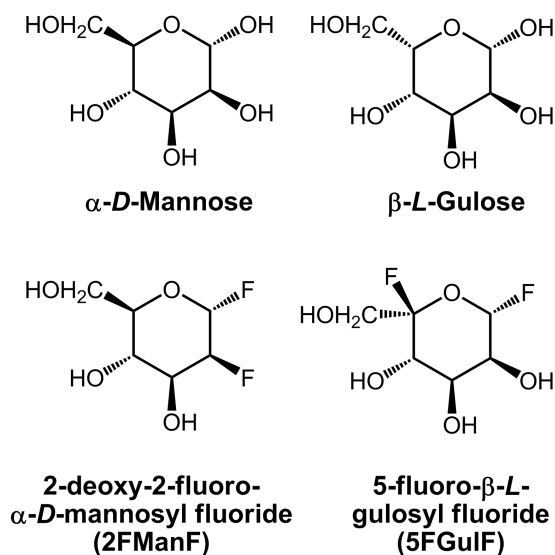


Figure 1.11. Substrates used to trap the glycosyl-enzyme covalent intermediate for dGMII.

In addition to the efforts to crystallize dGMII in presence of inhibitors, high resolution X-ray structures of glycosyl-enzyme covalent intermediates using fluorinated sugars have also determined (PDB Ids: 1QWN, 1QWU and 1QX1).³⁸ The authors employed both the wild type and D341A mutant enzyme and used mechanism-based deactivators 2-hydroxy-2-fluoro- α -D-mannosyl fluoride (2FManF) and 5-fluoro- β -L-gulosyl fluoride (5FGulF) for this purpose (Figure 1.11). Inspection of all three X-ray structures revealed a 1S_5 skew boat conformation of the sugar ring. In addition to moving the C-2 hydroxyl into a pseudo-equatorial orientation, the observed 1S_5 skew boat conformation also avoids a steric clash between this group and Asp204OD1.

Furthermore, in this conformation the leaving group was found to be anti-periplanar to the lone pair of the ring oxygen, a requirement for the departure of the leaving group according to Deslongchamps' anti-periplanar lone-pair hypothesis.⁷⁹ The electron density maps for all three structures showed the presence of a covalent linkage between the anomeric carbon and nucleophilic carboxylate oxygen of Asp204. Comparison of covalent intermediates with bound conformations of swainsonine and kifunensine revealed that covalent intermediates mimic best swainsonine. This is consistent with the notion that swainsonine mimics the transition state, as the reactive intermediate should itself mimic the transition state according to the Hammons postulate.

1.13 Role of Zinc in the Active Site

The active site of GMII is characterized by the presence of a Zn^{2+} ion coordinated by four protein side-chains, specifically His90, Asp92, Asp204, and His471. Zinc atoms are very common in metalloproteins and play a number of roles. There are number of intrinsic characteristics of zinc that are relevant to its role in proteins. With full d-orbital, it is quite stable electronically and not prone to redox changes. It can adapt to anywhere from 2 to 8 coordinates, though 4, 5 and 6 are the most common. Furthermore, it can adapt to its ligation state according to its environment, for example during the course of a reaction.

In the case of GMII, Asp204, which is one of the side-chains coordinating with zinc, is the nucleophilic side-chain in the catalytic mechanism. This coordination thus helps to maintain the deprotonated state of the catalytic nucleophile. Recently Kuntz et al. proposed that in addition to this, zinc is important for substrate binding and subsequent

conformational changes in the substrate. This hypothesis is based on the co-crystal structure of noeuromycin complexed with dGMII⁸⁰ and other crystallographic studies.^{38,}

75, 81, 82

1.14 Features of GMII Inhibitors

Most natural as well as synthetic potent inhibitors of GMII reported thus far display certain features that are common and essential for high inhibitory activity. These features include a *cis*-diol moiety, basic amine nitrogen and other functionalities, typically hydroxyl groups, which presumably mimic hydroxyl groups in the natural substrate. The *cis*-diol moiety is believed to mimic the C-2 and C-3 hydroxyl groups in the natural GMII substrate and coordinates with zinc in the active site. Indeed, the X-ray structure of swainsonine complexed with dGMII showed coordination of the vicinal hydroxyl groups with the Zn⁺² ion in the active site.⁷⁵ Similar coordination has also been reported in the case of other ligands.^{38, 75, 80-82} Furthermore, the synthesis and biological evaluation of a small number of mannosatin analogues has revealed that the basicity of the primary amine and neighboring *cis*-diol is essential for inhibitory activity.⁸³⁻⁸⁸ The possible role of methylthio and methyl sulfenyl functions in mannosatin A and B, respectively is intriguing. These features are unique to these natural mannosidase inhibitors. It has been proposed that these functionalities lie near the 4-hydroxyl group of mannosyl oxacarbenium ion but it is also conceivable that these moieties mimic the hydroxyl methyl group in the natural substrate.⁸⁹ If these sulfur containing functionalities play a role in the recognition and binding of the mannosatins by GMII, the extent to which these structural elements are important remains unclear.

1.15 Objective of the Dissertation

Although the mechanism of retaining glycosidases is common across a variety of different glycosidase families, the detailed atomic characteristics that drive the mechanism are diverse. An understanding of the details of these characteristics at an atomic level is necessary if one is to harness the therapeutic potential of glycosidases. While structural and mechanistic studies on dGMII:ligands complexes have provided a great deal of information, several aspects of the inhibition and catalytic mechanism are not yet clear. We have employed a computational approach in conjunction with experiments to address these issues. The specific aims of the project are:

1. *To enhance our understanding of the mechanism of inhibition of GMII by mannostatin A.* This project involved prediction of the binding mode of mannostatin A and its analogues in the active site of dGMII and subsequent validation of these predictions using X-ray crystallography. We have employed molecular docking in conjunction with molecular dynamics (MD) simulations for this purpose (chapters 2 and 3).
2. *To determine the role of the thiomethyl moiety in mannostatin A in binding.* We have used MD simulations, along with X-ray crystallography and biological evaluation, of some mannostatin A analogues in order to study the dynamics of the ligands and ligand-protein complexes, and to determine the role of the thiomethyl functionality (chapter 3).

3. *To determine the catalytic mechanism of hydrolysis reaction catalyzed by GMII.* We have applied a quantum mechanical (QM) methodology to determine the structures of all reactive species along the reaction coordinate (chapter 4).

The results obtained in this study will be instrumental in achieving the ultimate goal of designing and synthesizing more potent and /or selective inhibitors of GMII.

1.16 Overview of the Computational Methods Used in this Dissertation

Interactions between ligands and receptors are fundamental to all biological processes. A theoretical understanding of these interactions is of great significance in understanding the mechanism by which these biomolecules interact. The knowledge of a three-dimensional structure of the receptor, either in the absence or in the presence of a ligand, provides a great deal of information about the interactions critical for ligand binding. When the structure of a receptor is known, structure-based computational strategies can be employed to understand more about the inhibition and catalytic mechanism of the target protein. In the case of GMII, a plethora of structural data is available, which makes it possible to employ computational techniques such as molecular docking and MD simulations in order to understand more about the inhibition and the catalytic mechanism of GMII. The following sections present a general review of computational methods that have been used in this research.

1.16.1 Molecular Docking

The docking process involves sampling the coordinate space of the binding site and scoring each possible ligand pose. The pose with the best score is then taken as the

predicted binding mode of that compound. There are a large number of docking programs available and they differ in the sampling algorithms used, handling of the ligand and protein flexibility, and scoring functions they employ. Several commonly used docking methods are listed in Table 1 along with the type of sampling and scoring algorithms used. Some of these programs are commercial software packages and expensive to use. We have used AUTODOCK⁹⁰ for molecular docking, which has been successfully used in studies of several ligand-protein complexes.

The majority of the docking tools, including AUTODOCK, currently assume that the protein target is fixed in its crystal structure conformation.⁹¹ This is usually an inaccurate approximation, but a necessary one because of the increased complexity and consequently the computational cost that is required to accurately sample the flexibility of the binding site. In the case of GMII, X-ray structures with several ligands have revealed that there is only a minor change in the binding site upon ligand binding when compared with the X-ray structure of the native enzyme (PDB ID 1HTY⁷⁵). Thus, in order to predict the binding modes of mannostatin A and its analogues, we have ignored the flexibility of the GMII binding site.

Another important aspect of molecular docking is the conformational flexibility of the ligand. The conformation of a compound bound to a macromolecule may be different from its conformation in the unbound form. It is therefore crucial to consider the conformational flexibility of the compounds during the docking process. This can be achieved by pre-computing a set that contains several conformers of the compound to be docked. Several methods are available to generate large conformational databases rapidly and each conformation can be rigidly docked into the targeted binding site. Examples of

methods that work with conformational ensembles are Dock, Fred and slide. Alternatively, since the size of the conformational space for a ligand is directly proportional to the number of rotatable bonds present in the ligand, a variety of efficient algorithms have been employed to explore the conformational flexibility as the calculation proceeds. For example, the genetic algorithm has been successfully employed in GOLD, whereas the Lamarkian genetic algorithm has been used in AUTODOCK.

Table 1. Common programs used for molecular docking.

Method	Ligand flexibility sampling	Scoring function
Dock	Incremental build	Force field or constant score
FlexX	Incremental build	Empirical score
Slide	Conformational ensembles	Empirical score
Fred (Openeye Software)	Conformational ensembles	Gaussian score or empirical scores
Gold	Genetic algorithm	Empirical score
Glide (Schrodinger)	Exhaustive search	Empirical score
Autodock	Genetic algorithm	Force field
LigandFit (Accelrys)	Monte Carlo	Empirical score
ICM	Pseudo-Brownian sampling and local minimization	Mixed force field and empirical score
QXP	Monte Carlo	Force field

One limitation of AUTODOCK is that it does not take into account the flexibility of the rings in the cyclic ligand and only rotatable bonds are rotated in order to sample the conformational space for the ligand. However, five-membered rings, such as that in mannostatin A, are inherently flexible, making it necessary to consider the flexibility of the five-membered ring while docking. While MD simulations can be used to sample populated conformations in the solution, it is possible that the solution phase conformer is

different than the one which is biologically recognized. Therefore, we have employed quantum mechanical calculations to derive a set of different ring conformers of mannostatin A and its analogues. These pre-computed conformers were then docked individually into the active site of dGMII.

The molecular docking technique can also be used to estimate the free energy of binding for a particular ligand-protein complex. Currently, most structure-based docking methods employ an empirically derived free energy function that reproduces observed binding constants. Most of these approaches follow an expanded “master equation” to model the free energy of binding, adding entropic terms to the molecular mechanics equations:

$$\begin{aligned} \Delta G = & \Delta G_{vdW} + \Delta G_{h-bond} + \Delta G_{electrostatics} \\ & + \Delta G_{conformational} + \Delta G_{torsional} + \Delta G_{solvation} \end{aligned} \quad \text{Equation 1.1}$$

AUTODOCK implements a similar approach using the thermodynamic cycle of Wesson and Eisenberg.⁹² The scoring function used in AUTODOCK includes the following five terms:

$$\begin{aligned} \Delta G = & \Delta G_{vdW} \sum_{i,j} \left(\frac{A_{ij}}{r_{ij}^{12}} - \frac{B_{ij}}{r_{ij}^6} \right) \\ & + \Delta G_{h-bond} \sum_{i,j} E(t) \left(\frac{C_{ij}}{r_{ij}^{12}} - \frac{D_{ij}}{r_{ij}^{10}} \right) \\ & + \Delta G_{electrostatics} \sum_{i,j} \frac{q_i q_j}{\epsilon(r_{ij}) r_{ij}} \\ & + \Delta G_{torsional} N_{tor} \\ & + \Delta G_{solvation} \sum_{i,j} (S_i V_j + S_j V_i) e^{(-r_{ij}^2/2\sigma^2)} \end{aligned} \quad \text{Equation 1.2}$$

The five ΔG terms on the right hand side of equation 1.2 are coefficients empirically determined using linear regression analysis of a set of protein ligand complexes with known binding constants. The summations are performed over all pairs of ligand atoms, i , and protein atoms, j , in addition to all pairs of atoms in the ligand that are separated by three or more bonds.

The ‘*in vacuo*’ contributions include three interaction energy terms: a Lennard-Jones 12–6 dispersion / repulsion term; a directional 12–10 hydrogen bonding term, where $E(t)$ is a directional weight based on the angle, t , between the probe and the target atom; and a screened coulombic electrostatic potential. Each of these terms, including their parameterization, have been described.⁹³ A measure of the unfavorable entropy of ligand binding due to the restriction of conformational degrees of freedom is added to the ‘*in vacuo*’ function. This term is proportional to the number of sp^3 bonds in the ligand, N_{tor} .

For the calculation of the desolvation term, AUTODOCK employs the pair-wise, volume-based method described by Stouten et al.⁹⁴ since it is consistent with the pre-calculated affinity grid formulation used by AUTODOCK. In this method, for each atom in the ligand, fragmental volumes of surrounding protein atoms are weighted by an exponential function and then summed, evaluating the percentage of volume around the ligand atom that is occupied by protein atoms. This percentage is weighted by the atomic solvation parameter of the ligand atom to give the desolvation energy.

1.16.2 MD Simulations of Ligand-Protein Complexes

A fundamental appreciation for how biological molecules interact requires knowledge of their three-dimensional structure and dynamics. While experimental techniques such as X-ray crystallography provide a great deal of information, these techniques are unable to explore the dynamic nature of the interactions that are important for complex formation. MD simulation is a powerful method for exploring the dynamic nature of the interactions between biological molecules and conformational changes in the ligand and the macromolecule following ligand binding. Almost 30 years have passed since the report of the MD simulation of a protein, BPT1.⁹⁵ Since then this, computational technique has become an established tool in the study of biomolecules and is complementary to experimental techniques.

The biomolecular simulations find three major areas of application today.⁹⁶ First, MD simulations are used for exploring the conformational space of a ligand. This is an advantageous approach as it is possible to sample conformations that are populated in solution. Furthermore, the conformations generated in this manner can be docked individually into the binding site of the target protein and scored according to the predicted binding affinity. The second major application is the study of the interactions of the ligand with protein residues in a ligand-protein complex. In addition to capturing conformational changes in ligand and/or in the protein, such a simulation also reveals the dynamic nature of interactions that are critical for ligand binding. Knowledge of the X-ray structure of the target protein in the presence or absence of the ligand is beneficial for setting up an MD simulation of the ligand-protein complex. Finally, MD simulations can

also be used to estimate free energy changes for chemical processes such as ligand binding.

In this dissertation, we have employed the AMBER⁹⁷ suit of programs to perform MD simulations of mannostatin A and its benzylated analogue complexed with dGMII. We have also performed MD simulations of these ligands in an unbound state (chapter 3). The simulations have provided valuable insights into the dynamic nature of interaction that are important for the binding of mannostatin A and the conformational properties of mannostatin A in water. Furthermore, this study has also revealed the importance of the thiomethyl moiety for the binding of mannostatin A by GMII.

Mathematically, the MD simulation method is based on Newton's second law of motion stated in equation 1.3.

$$F = m \cdot a \qquad \text{Equation 1.3}$$

Where, F = the force exerted on the particle,

m = the mass of the particle, and

a = its acceleration

The MD simulation is a deterministic method whereby the knowledge of the total forces on a particular atom at time t can be used to determine the positions and velocities of that particle at any time $(t + \delta t)$. The result of a simulation is a trajectory that specifies how the positions and velocities of the atoms in the system vary with time. A general solution to this problem was proposed by Verlet in 1967.⁹⁸ AMBER implements a variation of this solution referred to as the leap-frog Verlet algorithm, (ref) which uses a

series of equations to describe atomic position (x), velocity (v) and acceleration with respect to time (t). Since acceleration is the rate of change of the velocity and velocity is the rate of change of displacement, the relationship between these variables can be summarized in the following equation.

$$a = \frac{dv}{dt} = \frac{d^2x}{dt^2} \quad \text{Equation 1.4}$$

Integrating equation 1.4 we get,

$$v = a \cdot t + v_0 \quad \text{Equation 1.5}$$

and,

$$x = v \cdot t + x_0 \quad \text{Equation 1.6}$$

Combining equation 1.6 with the expression for velocity (1.5), the following equation is obtained which gives the value of x at time t as a function of acceleration, a , initial position, x_0 , and initial velocity, v_0 .

$$x = a \cdot t^2 + v_0 \cdot t + x_0 \quad \text{Equation 1.7}$$

Furthermore, the force can also be expressed as the first derivative of the potential energy (E) with respect to the position, x . Therefore,

$$F = -\frac{dE}{dx_i} \quad \text{Equation 1.8}$$

Combining equations 1.4 and 1.8 we get,

$$m \cdot a = -\frac{dE}{dx} \quad \text{Equation 1.9}$$

Thus, the acceleration of each atom is given as,

$$a = -\frac{1}{m} \frac{dE}{dx} \quad \text{Equation 1.10}$$

The calculated value of acceleration is then used in equation 1.7 to determine the new position of the atom. Thus, initial positions and velocities of the atoms in the system determine their positions and velocities at all other times. Initial positions can be obtained from experimental techniques such as NMR or X-ray crystallography.

In the MD simulation, the potential energy of the system is defined as a sum of different energetic contributors as depicted in equation 1.11 below.

$$E_{total} = E_{bonds} + E_{angles} + E_{torsions} + E_{vdW} + E_{electrostatic} \quad \text{Equation 1.11}$$

More completely, this equation, also known as the force field equation, can be written as:

$$\begin{aligned}
E_{total} = & \sum_{bonds} \frac{k_i}{2} (D_i - D_{ref})^2 + \sum_{angles} \frac{k_i}{2} (\theta_i - \theta_{ref})^2 \\
& + \sum_{torsions} \frac{V_i}{2} (1 + \cos(n\omega_i - \gamma_i)) \\
& + \sum_{vdW} 4\epsilon_{ij} \left[\left(\frac{\sigma_{ij}}{r_{ij}} \right)^{12} - \left(\frac{\sigma_{ij}}{r_{ij}} \right)^6 \right] \\
& + \sum_{electrostatic} \left(\frac{q_i q_j}{4\pi\epsilon_0 r_{ij}} \right)
\end{aligned}
\tag{Equation 1.12}$$

In equation 1.12, the first two terms are simple harmonic and contribute energy penalties for any deviations the reference values. The third terms represents a description of the energy barrier for the torsion potential (V), multiplicity or number of minima during a 360° rotation (n), phase factor (γ), and torsion angle (ω). The van der Waal term is often described by a Lennard-Jones potential where the well depth is ε_{ij}, collision diameter is σ_{ij}, and inter-atomic distance is r_{ij}. The electrostatic term is a coulombic term that includes the charge on the interacting atoms (q_i, q_j) and the inter-atomic distance.

In addition to the above, it is essential to include solvent effects in the simulation of biomolecular systems. In most simulations, water is the solvent because almost all interactions, which involve biomolecules, take place in the presence of water. There are two methods by which solvent effects can be incorporated into the simulation. In the first method, the solvent is explicitly represented in the system of interest, whereas in the second method, also known as the continuum solvation method, the solvent is represented by a mathematical expression which describes the average effect of bulk solvent on the solute. This is done by approximating the dielectric constant in the solute and solvent

regions. For the purpose of this dissertation, we have used explicit solvation method to perform MD simulations on ligand-dGMII complexes.

The nature of the AMBER force field requires the use of water molecules parameterized with explicit partial charges. There are several empirical water models currently in use, which differ in their treatment of partial charges, overall geometry, and the ability to properly represent bulk properties. We have used the TIP3P water model⁹⁹ in our simulations, as it is an established model over last several years. In this model, the partial charges on the hydrogen atoms are balanced by the negative charge on the oxygen atom.

1.16.3 Modeling the Chemistry of the Active Site of GMII

Elucidation of the chemistry of a metalloprotein active site at an atomic level of detail has been an enduring challenge to bioorganic and bioinorganic chemistry. It has proven to be extremely difficult by experimental means alone to discriminate between alternative reaction mechanisms and reactive species, or to determine precisely the relative energies of these species.¹⁰⁰ In principle, accurate computational methods are capable of complementing experimental methods to answer these questions at an atomic level of detail.

The use of traditional *ab initio* quantum chemical methods in modeling the catalytic mechanisms of metalloproteins is limited in terms of the size of the system. The selection of model thus becomes critical as inclusion of large number of atoms can lead to intractable CPU times. On the other hand, a smaller model may not be sufficient to produce reasonable results as it lacks explicit effects of the protein residues on the active

site chemistry. In addition, the structurally and electronically diverse nature of transition metals makes it difficult to use computationally less intensive approaches such as semiempirical and force field based methods, as such systems have proven difficult to describe with a set of universal parameters.

Over the past few years, effective methods have emerged to address these problems. Two alternative approaches exist to make modeling of the metalloprotein active site computationally tractable. First, one can construct a purely QM model by truncating the active site core and capping the truncated regions with hydrogen atoms. This traditional approach has been used for many years with increasingly large models. The widespread use of the Density Functional Theory (DFT), which employs gradient-corrected and hybrid functionals, has demonstrated that transition metal systems can be treated in a reasonable, yet cost-effective manner. Advances in DFT-based algorithms, along with a dramatic reduction in the cost and performance of computer hardware, allow quantum chemical treatment of a system containing about 150-200 atoms. (ref)

Another approach is to retain the entire protein, but treat only a specified region in the active site at the QM level, and model the remaining protein via molecular mechanics. This approach, known as the combined quantum mechanical and molecular mechanical (QM/MM) approach, affords a strategy that takes into consideration the effects of protein environments while still keeping the CPU time reasonably low. The most difficult task in this approach is the partitioning of the system into QM and MM regions. It is not obvious how much of the system needs to be included in the QM region¹⁰¹. Variations in results are likely when the size and composition of the QM region is altered, because the description of the interactions described by the QM/MM potential function is different as

compared to the same interactions described by the purely QM semiempirical Hamiltonian approximation.¹⁰¹ Generally, the two subsystems can be separated by cutting the covalent bonds within the neighboring residues of amino acids included in the QM region. For example, a covalent bond, which links atom X and atom Y, can be cut in such a way that X is in the QM region and Y is in the classical region. The problem occurs at this frontier because the electron of X involved in the covalent bond is not paired with any other electron as in molecular mechanics electrons are not explicitly represented (Figure 12). Thus, this electron needs special treatment.

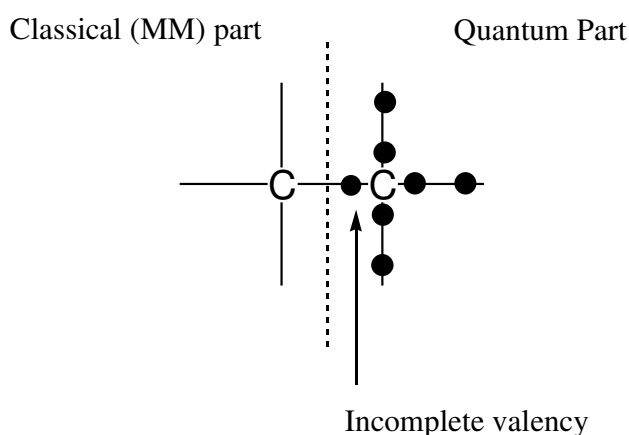


Figure 1.12. Example of the problem of cutting covalent bonds at the QM/MM interface: A covalent C–C bond at the frontier between a MM part and a QM part.

Several solutions have been proposed for this problem and can be divided into two broad categories¹⁰¹: those that add a pseudoatom to fill the valencies of the quantum frontier atom, (e.g. the link atom method¹⁰² and the connection atom method¹⁰³), and those that deal specifically with the frontier bond orbitals by trying to compute directly its main characteristics from known parameters (e.g. the local self consistent method¹⁰⁴ and the generalized hybrid orbital method.¹⁰⁵) Although link atoms are an approximate

approach to QM/MM partitioning of a covalently bonded system, they have been found to yield good results for a number of simulations of enzymatic reactions.¹⁰⁶⁻¹¹⁰

In order to characterize the catalytic mechanism of GMII, we have employed the DFT based quantum mechanical method. The general strategy used for this task included four major steps: 1. docking the substrate into the active site of GMII; 2. truncation of the active site to create a model of reasonable size; 3. perform a relaxed geometry scan along a pre-defined reaction coordinate; and 4. optimization of the approximate geometries of the intermediates predicted in the scan. We used the JAGUAR program¹¹¹ for all the optimizations because it can be run in parallel and is faster than other programs such as Gaussian.¹¹² The QM/MM implementation used in Jaguar is a program referred to as QSITE. The current version of QSITE does not allow the performing of a relaxed geometry scan. Hence, we have performed density functional calculations on models of differing size (chapter 4).

The results presented in this dissertation are significant not only for GMII, but also for other glycosidases belonging to glycosyl hydrolase family 38, in particular the lysosomal α -mannosidase. Since the binding site of the lysosomal enzyme is very similar to that of GMII, computational insights into the binding of GMII by mannosatin A and its analogues enhance our understanding of the inhibition mechanism of the lysosomal enzyme by mannosatin A. Thus, the research presented in this dissertation is a step forward in the search for potent and, more importantly, selective GMII inhibitors that can be used in cancer therapy.

CHAPTER 2

INHIBITION OF GOLGI α -MANNOSIDASE II WITH MANNOSTATIN A ANALOGS: SYNTHESIS, BIOLOGICAL EVALUATION AND STRUCTURE ACTIVITY RELATIONSHIP STUDIES^a

^a Li, B.; Kawatkar, S. P.; George, S.; Strachan, H.; Woods, R. J.; Siriwardena, A.;

Moremen, K. W.; Boons, G. J., *Chembiochem* **2004**, 5, (9), 1220-1227

Reprinted here with permission of the publisher.

2.1 Abstract

Mannostatin and aminocyclopentitretrol analogs, which have varying substitutions at the amino function, were synthesized. These compounds were tested as inhibitors of human Golgi- and lysosomal α -mannosidases. Modification of the amine of mannostatin had only marginal effects, whereas similar modifications of aminocyclopentitretrol led to significantly improved inhibitors. *Ab initio* calculations and molecular docking studies were employed to rationalize the results. It was found that Mannostatin and aminocyclopentitretrol could bind to Golgi α -mannosidase II in a similar mode as that of the known inhibitor swainsonine. However, due to the flexibility of the five membered rings of these compounds, additional low energy binding modes could be adopted. These binding modes may be relevant for the improved activities of the benzyl-substituted compounds. The thiomethyl moiety of mannostatin was predicted to make favorable hydrophobic interactions with Arg228 and Tyr727, possibly accounting for its greater inhibitory activity.

2.2 Introduction

Cells that have undergone oncogenic transformation often display abnormal cell surface oligosaccharides and these changes in glycosylation are important determinants of the stage, direction and fate of tumor progression.¹¹³ Inhibition of the mannose trimming enzyme human Golgi α -mannosidase II (hGMII), which acts late in the *N*-glycan processing pathway, provides one route to blocking the oncogene-induced changes in cell surface oligosaccharide structures.⁶³

HGMII selectively cleaves α 1-3 and α 1-6 mannosyl residues present in its natural substrate GlcNAcMan₅GlcNAc₂.⁷⁴ It is a retaining glycosylhydrolase, which employs a two-stage mechanism involving two carboxylic acids positioned within the active site to act in concert: one as a catalytic nucleophile and the other as a general acid/base catalyst.^{12, 14, 19, 114, 115} Protonation of the exocyclic glycosyl oxygen of the substrate leads to bond-breaking and simultaneous attack of the catalytic nucleophile to form a glycosyl enzyme intermediate. Subsequent hydrolysis of the covalent intermediate by a nucleophilic water molecule gives a α -mannose product with overall retention of configuration. Studies on retaining mannosidases with 5-fluoro pseudo-substrates and deuterium labeled substrates have shown that the transition states on either side of the covalent intermediate have marked oxocarbenium ion character.^{12, 14, 19, 114, 115} Potent inhibitors of glycosidases are thought to mimic oxocarbenium ion-like transition states and for example, the inhibitory activity of the natural product swainsonine has long been attributed to its 5-membered ring resembling a flattened six-membered ring, which had been forced to attain an oxocarbenium-like structure. In fact, the crystal structure of Swainsonine complexed with Golgi α -mannosidase II from *Drosophila melanogaster* shows the inhibitor to be tilted in such a way as to bring the equivalent of its anomeric carbon close to the presumed catalytic nucleophile.⁷⁵

Swainsonine has been much investigated as a consequence of its potent inhibitory properties. Clinical studies have shown^{61, 62, 64, 67} it to exhibit potent anti-tumor and anti-metastatic activity. An unfortunate side effect resulting from this compound is blockage in oligosaccharide catabolism arising from inhibition of a related catabolic α -mannosidase found in lysosomes.^{63, 67} It is clear that to develop a drug appropriate for

anti-metastatic therapy, an alternate lead compound is required, which is amenable to easy modification in a combinatorial manner to give compounds that specifically inhibit GMII without affecting the function of lysosomal α -mannosidase (LAM).

Mannostatins A and B, isolated from the soil microorganism *Streptoverticillus*, are some of the most potent inhibitors of class II α -mannosidases reported¹¹⁶ thus far, and provide interesting compounds for combinatorial modification to give more selective derivatives (Figure 2.1). They were the first non-azasugar type inhibitors to be discovered that possess an aminocyclopentitol structure. The inhibitors are of the reversible, competitive type and do not show the slow-binding phenomenon exhibited by Swainsonine and its analogs. The synthesis and biological evaluation of a small number of mannostatin analogs has revealed that the basicity of the primary amine and also the neighboring *cis*-diol are essential for inhibitory activity.^{83-88, 117} The thiomethyl moiety could, for example, be replaced by a hydroxymethyl group.^{117, 118} Most mannostatin derivatives have been tested as inhibitors for jack bean and almond mannosidases and structure-activity relationships for the more relevant Golgi and lysosomal enzymes are scarce.

Here, we report the synthesis of a range of mannostatin analogs, which have varying aromatic substitutions at the amino function. In parallel, a range of aminocyclopentitols, which are structurally simpler than mannostatin and have as an additional feature that they are non-chiral, were modified in a similar fashion. It was hoped that the aromatic substitutions of **1a** and **2a** would be able to make favorable interactions with aromatic residues in the binding site of the mannosidase enzymes. These two families of compounds have been tested for their ability to inhibit hGMII and

human LAM (hLAM) and the activities of the two series of compounds were compared. Computational studies have been performed to rationalize the data.

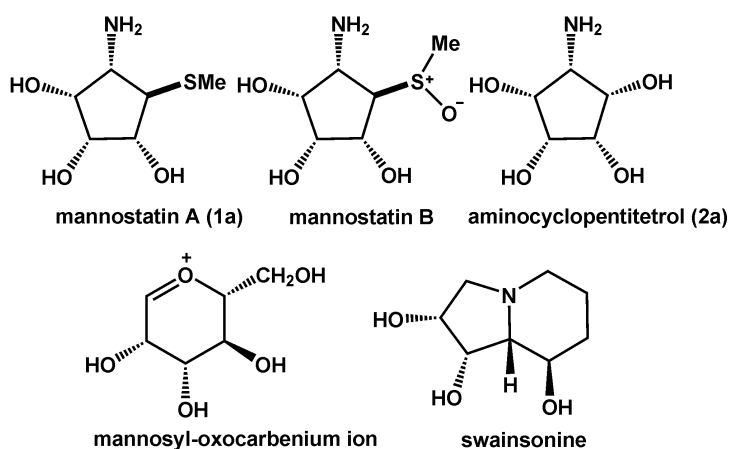


Figure 2.1. Aminocyclopentitol inhibitors of Golgi α -mannosidase II.

2.3 Synthesis and biological evaluation of mannosidase inhibitors

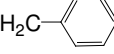
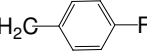
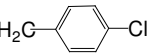
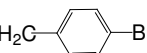
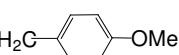
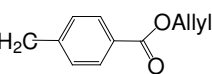
Optically pure mannostatin A (**1a**) and the *meso*-aminocyclopentitretol **2a** were prepared by a modified literature procedure.¹¹⁹ A key step of this approach involved an Aldol condensation of nitromethane with a dialdehyde derived from myo-inositol. The physical and spectroscopic data of the two compounds were in agreement with previously reported data. The amino functionalities of **1a** and **2a** were modified by reductive amination using a range of aromatic aldehydes. Conventional procedures involving Na(CN)BH₃ in combination with solvents such as Trimethyl Ortho Formate (TMOF)¹²⁰ or TMOF/methanol or DCM/methanol in the presence or absence of benzotriazole (BtH)¹²¹ resulted in mixtures of products. Alkylation of the amines with benzyl bromide

in the presence of CsOH¹²² gave, apart from the required product, a substantial amount of di-substituted amine. Fortunately, the addition of a methanolic solution of the hydrochloride salts of **1a** and **2a**, pretreated with methanolic sodium hydroxide (0.2 eq), to a slurry of an aromatic aldehyde (2.5 eq), Na(CN)BH₃ (1.0 eq), and molecular sieves 3Å followed by stirring for 18 hrs, gave the secondary amines **1b-g** and **2b-g** in reasonable to good yields.⁸⁴ The compounds were purified by Iatro bead column chromatography and in each case satisfactory compositional and spectroscopic data were obtained.

Recently, we described recombinant forms of human Golgi α -mannosidase II¹²³ and human lysosomal α -mannosidase.⁷³ For these enzymes, the rate of hydrolysis of different concentrations of 4-methylumbelliferone alone and in the presence of different concentrations of inhibitor was measured fluorometrically and K_i values were determined from Dixon plots. As can be seen in Table 2.1, mannostatin A (**1a**) is a markedly better inhibitor than the corresponding aminocyclopentitretol **2a**. Benzylation of the amino functionality of Mannostatin A gave compounds (**1b-g**) which were slightly less potent inhibitors of the Golgi mannosidase II than the lead compound and *N*-benzyl, *N*-(*p*-fluorobenzyl), *N*-(*p*-chlorobenzyl) and *N*-(*p*-bromobenzyl) and *N*-(*p*-methoxybenzyl) substitution caused similar reductions in inhibitory activity (3-5 fold). Modification of the amino functionality with allyl 4-hydroxymethylenebenzaldehyde (to form **1g**) had a larger impact with a 15-fold loss of activity being observed. Surprisingly, the chemical modifications had no significant effect on HLM indicating that they do not lead to either favorable or unfavorable interactions with the binding site.

The inhibition data for aminocyclopentitetrals (**2a-g**) displayed a different profile than for the mannostatin analogs and for each enzyme, the introduction of a substituted benzyl moiety resulted in an improvement of inhibitory activity. In the case of the hGMII, modification of the amino group of **2a** with substituted benzyl moieties led to small improvements in inhibitory activity (5-10 fold) whereas large increases in activity were measured (10-40 fold) with the lysosomal enzyme. Compound **2g**, having a *N*-(allyl 4-hydroxymethylenebenzoic acid) substitution proved to be the best inhibitor tested, displaying a 40-fold more favorable K_i value than parent **2a**. Surprisingly, this substituent caused the largest loss in inhibitory activity for Mannostatin A.

Table 2.1. Inhibition of human Golgi Mannosidase II (hGM II) and human Lysosomal Mannosidase (hLAM) by compounds **1a-g** and **2a-g** (K_i in μM).

R	(1a-g)		(2a-g)	
	hGMII K_i	hLAM K_i	hGMII K_i	hLAM K_i
a) H	0.21	0.09	50	6.6
b) 	0.88	0.11	10	0.45
c) 	0.53	0.17	6.0	0.33
d) 	0.91	0.10	8.1	0.67
e) 	0.51	0.05	7.6	0.33
f) 	0.52	0.10	6.6	0.48
g) 	3.22	0.14	4.4	0.16

Despite that the introduction of a substituted benzyl moieties resulted in a less favorable ratios of $K_i(\text{hGMII}) / K_i(\text{hLAM})$, the compounds described here provide important leads for the development of selective inhibitors of hGMII. This Golgi enzyme is able to recognize two potential aglycones during substrate cleavage: $\text{GlcNAcMan}_5\text{GlcNAc}_2$ to $\text{GlcNAcMan}_3\text{GlcNAc}_2$. Since the corresponding alternate substrate, $\text{Man}_5\text{GlcNAc}_2$, is >1000-fold less effective as a substrate, the Golgi enzyme must have an obligatory binding site for recognition of one branch of the aglycone for high affinity substrate interaction. There is no data to support that the broad specific lysosomal α -mannosidase is able to recognize an extended aglycone to any significant degree. Thus, by combinatorial extension of the benzyl derivatives with other chemical functionalities, the promise exists that favorable interactions may be established with the extended binding pocket for the aglycone of hGMII thereby accentuating the selectivity of this enzyme.

2.4 Computational studies

The mode of inhibition by an azasugar, such as swainsonine, has been rationalized by their resemblance to the mannosyl oxycarbenium ion; a putative intermediate in the hydrolysis of mannosidases.¹²⁴ There has, however, been some debate as to whether this model can be extended to the mode of inhibition of **1a**. It has been contended that in their lowest energy conformations, aminocyclopentitols, such as mannostatin, do not superimpose well onto the hypothetical oxycarbenium ion intermediate.^{84, 125} An alternative mode of inhibition has been proposed⁸⁴ that is based on the resemblance of **1a** to β -mannopyranosylamine.

Recently, crystal structures have been reported for dGMII obtained from *Drosophila melanogaster* (dGMII) in the absence and presence of the inhibitor swainsonine.⁷⁵ This enzyme has 41% sequence identity and 61% similarity with hGMII and most importantly, amino acids in catalytic domain are preserved. Furthermore, it has been shown that the two enzymes display similar kinetic and inhibitory properties.¹²⁶ Thus, it has been proposed that dGMII is a good model system for the analogous human enzyme.

Molecular docking of **1a** and aminocyclopentitretrol **2a** into the crystal structure of dGMII may provide an opportunity to study the mode of inhibition of these compounds. Furthermore, some of the inhibitory data summarized in Table 2.1 may be rationalized by comparing docking modes of the two compounds with their benzylated counterparts (**1b** and **2b**).

Five-membered ring systems, such as in compounds **1a** and **2a** are inherently flexible due to their ability to assume several twist and envelope conformations, which can interconvert with relative ease *via* pseudo-rotational itineraries.^{127, 128} Therefore it is necessary to consider all the possible low energy envelope conformers of **1a** and **2a** for the docking studies.

Conformational properties of isolated five-membered rings such as furanoses have been studied by geometry optimizations of the ten possible envelope conformations, using *ab initio* molecular orbital calculations.¹²⁹⁻¹³¹ Thus, the conformational properties of **1a** and **2a** were studied by optimizing the ten possible envelope conformers by constraining a specific endocyclic torsion angle to 0° and allowing all other parameters to be optimized at the B3LYP/6-31G* level. The hydroxyl

and amino groups of the resulting structures were placed in each of the three staggered orientations, which were re-optimized without any restraints at the same level of theory. The effects of solvation were approximated by single point calculations of gas phase and solution phase energies using the Poisson-Boltzmann treatment^{132, 133} in the Jaguar program¹¹¹ (Table 2.2). It was observed that for both compounds, many hydroxyl rotamers converged to a single structure. In the case of **1a**, thirty initial structures led to twenty unique structures, which represented only six envelope conformations (E_1 , 1E , E_2 , E_3 , 3E and 4E). In the case of **2a**, fifteen unique structures were obtained, which resembled nine envelope conformations (E_1 , 1E , E_2 , 2E , E_3 , 3E , E_4 , 4E and E_5). The fact that **2a** can adopt a larger number of envelope conformations indicates that its ring structure is more flexible than that of **1a**. The difference in ring flexibility is likely due to the differences in ring substitutions, which are known to determine pseudorotational itineraries of five membered rings.¹²⁸

Each of the low energy conformers of **1a** and **2a** was subsequently docked into the binding site of dGMII. The six envelope conformers of **1a** could be complexed in three different binding modes (Figure 2.2), with conformer 1E exhibiting the most favorable binding energy ($\Delta G = -9.1 \text{ kcal mol}^{-1}$). In this binding mode the five membered ring of **1a** stacks against the aromatic side chain of Trp95, a type of interaction seen in many carbohydrate-protein complexes.¹³⁴ The C-4 and C-5 hydroxyl oxygens of **1a** coordinate with the zinc ion in the active site resulting in T_6 -octahedral coordination geometry. Furthermore, the nitrogen of the exocyclic amino group of **1a** forms hydrogen bonds with the carboxylate oxygen of the putative general acid base residue Asp341 and with the hydroxyl oxygen of Tyr269. In addition, the thiomethyl moiety of **1a** makes

favorable hydrophobic interactions with Arg228 and Tyr727. In the crystal structure of dGMII with swainsonine⁷⁵, the Zn⁺² ion has T₆-octahedral coordination geometry complexing the hydroxyl oxygens O4 and O5. However, the bridgehead nitrogen of Swainsonine forms a hydrogen bond with the catalytic nucleophile Asp204. Thus, the two complexes may differ in the interactions of their amines with acidic residues in the binding site.

Table 2.2. Relative gas phase and solution phase energies (in kcal mol⁻¹) for envelope conformers of Mannostain A (**1a**) and aminocyclopentitol (**2a**). Energies for only those conformers are given which were docked in the active site of dGMII.

Low energy conformers of 1a	Relative energy (kcal mol ⁻¹)		Low energy conformers of 2a	Relative energy (kcal mol ⁻¹)	
	Gas phase	Solution phase		Gas phase	Solution phase
E ₁	0.0	0.0	E ₁	0.0	1.8
¹ E	2.8	1.5	¹ E	1.2	3.1
E ₂	8.6	4.6	E ₂	6.4	3.4
E ₃	5.2	1.7	² E	1.6	3.5
³ E	8.9	2.8	E ₃ ^a	6.4	3.4
⁴ E	5.4	0.5	³ E ^a	1.6	3.5
			E ₄ ^a	0.0	1.8
			⁴ E ^a	1.2	3.1
			E ₅	0.3	0.0

^aConformers E₃, ³E, E₄ and ⁴E are mirror images of conformers E₂, ²E, E₃ and ³E respectively with same relative energies. These conformers were also docked in the binding site of dGMII.

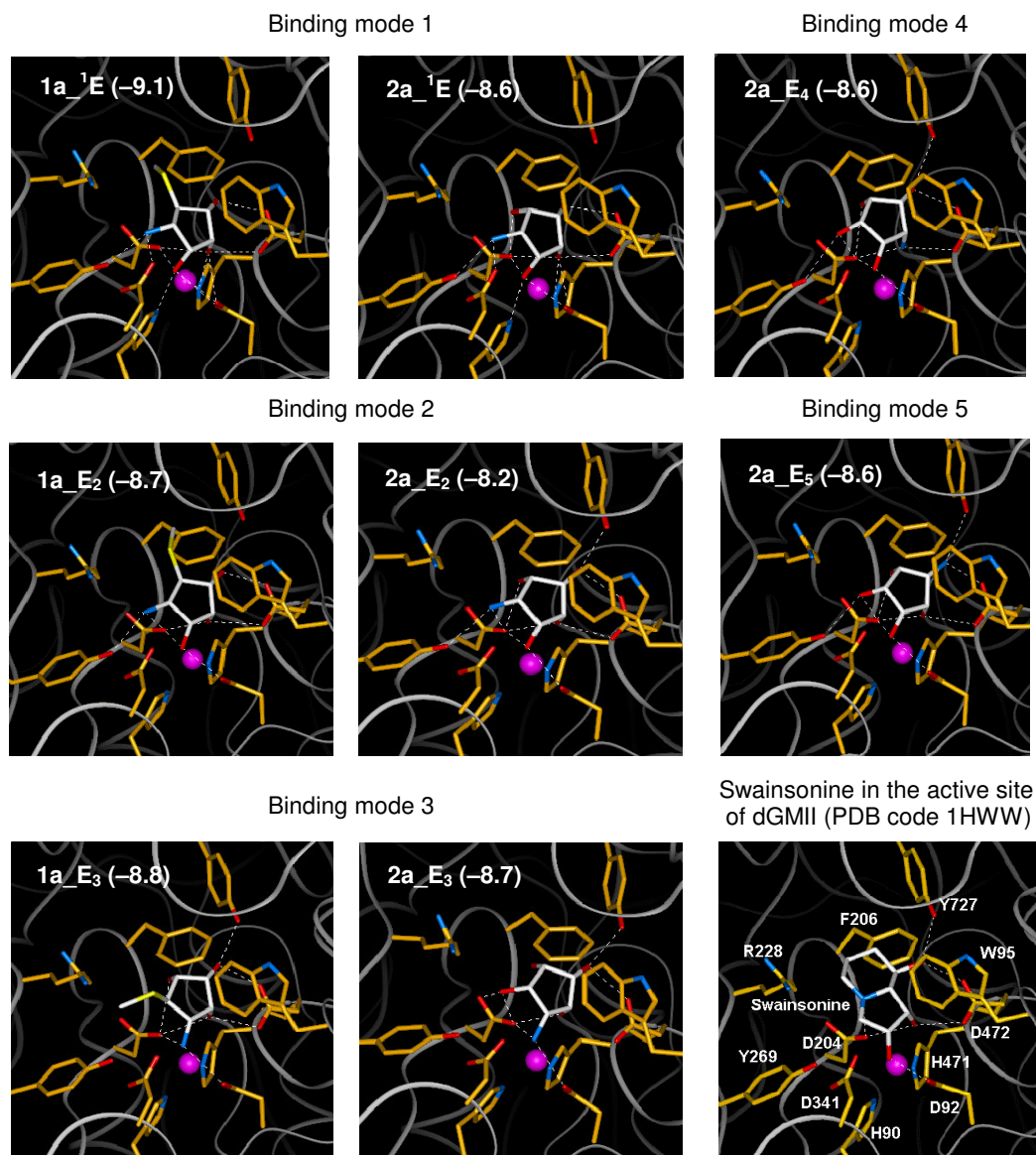


Figure 2.2. Different binding modes observed for conformers of **1a** and **2a**. White dashed lines indicate h-bond interactions and free energies of binding are given in the parentheses (in kcal mol⁻¹).

Conformers E₂ and ³E of **1a**, which were predicted to bind with only slightly smaller computed binding energies than ³E (–8.7 kcal mol⁻¹ and –8.8 kcal mol⁻¹, respectively), displayed a binding mode very similar to that of swainsonine. In this case, the exocyclic amine of **1a** formed a hydrogen bond with the catalytic nucleophile Asp204. Furthermore, The C-4 and C5-hydroxyl oxygens of **1a** coordinated with the zinc

ion in T_6 -octahedral coordination geometry. The somewhat lower computed binding energies may be due to loss of hydrogen bonding interactions of the C5-hydroxyl with amino hydrogens of His90 and His471, but may also reflect limitations in the computational method.

Conformers E_1 , E_3 and 4E displayed yet another complexation mode of **1a**. In this case, the amine of **1a** coordinated with zinc ion leading to T_5 coordination geometry. Pentavalent coordination is energetically more favorable than the hexavalent (T_6) coordination of zinc⁷⁸ and therefore may be an important contributor to the stabilization of these complexes. Further stabilization came from hydrogen bonds between the nitrogen of the amine with carboxylic oxygen of the catalytic nucleophile Asp204. The interactions between the thiomethyl group and Trp727 and Arg228 were lost in this binding mode, which may account for the slightly lower binding energies.

It has been suggested that the coordination of O4 and O5 of swainsonine with Zn^{+2} mimics a similar chelation of the C-2 and C-3 hydroxyls of mannosyl oxycarbenium ion. This coordination is an important determinant of the α -mannoside specificity of the enzyme. The binding of swainsonine is stabilized by an important hydrogen bond between N4 and the catalytic nucleophilic residue Asp204. In the case of the mannosyl oxycarbenium ion, its flattened ring structure may place the anomeric center in close proximity to nucleophile Asp204 for favorable interactions. Furthermore, Swainsonine, and probably the oxycarbenium ion, can make van der Waals stacking interactions with Trp95 and Phe206. The conformers E_2 and 3E of **1a** displayed a very similar binding mode, in which the exocyclic amino group formed a hydrogen bond with Asp204 and the C-4 and C-5 hydroxyls coordinated with the Zn^{+2} ion. However, due to

the flexibility of its five membered ring, mannostatin can bind in other low energy modes. For example, the small change in ring conformation of ¹E places the exocyclic amine in a position to form hydrogen bonds with Asp341 and Tyr269. Other ring conformers allowed the amine of **1a** to coordinate with the Zn⁺² ion in a favorable T₅ coordination geometry.

In addition to the three binding modes observed for **1a**, aminocyclopentitretrol **2a** could complex in two additional ways (Figure 2.2). All the five binding modes displayed very similar computed binding energies. Conformers ³E and E₄ of **2a** complexed in a unique mode, in which the amine and C2- hydroxyl coordinate with the zinc ion resulting in T₆ coordination geometry. The ring stacked against Trp95 and the amine formed hydrogen bonds with the catalytic nucleophile Asp204, Asp472 and Asp92. In the case of E₅, the amine formed hydrogen bonds with hydroxyls of Tyr727 and Asp472. This binding mode is further stabilized by coordination of C-2 and C-3 hydroxyls with the Zn ion. All the hydroxyls formed hydrogen bonds with Asp204 in addition to hydrogen bond interaction with Tyr269, Asp92 and Asp472.

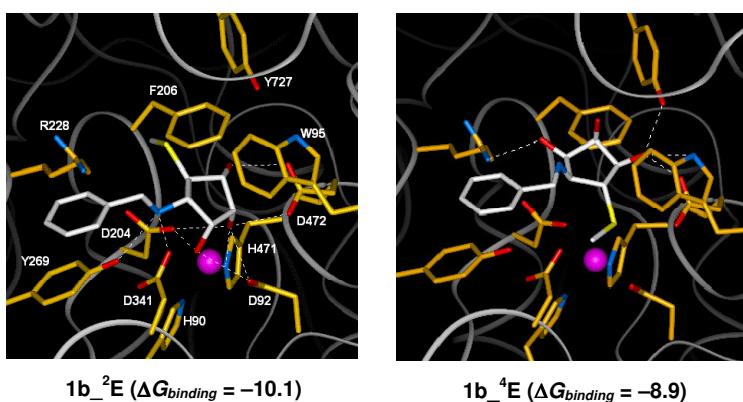


Figure 2.3. Binding modes observed for conformers of **1b**.

Mannostatin A is a significantly more potent inhibitor of GMII than aminocyclopentitretrol **2a** (Table 2.1). Overall, the computational studies show that **2a** is more flexible allowing additional binding modes. Furthermore, due to inversion of configuration at C-2 and replacement of the thiomethyl moiety with a hydroxyl, the hydrophobic interactions of thiomethyl moiety of **1a** cannot be made by **2a**. Although that the C-2 hydroxyl of **2a** can make hydrogen bonds with Asp204 and Asp341, it is unlikely that these interactions can compensate for the loss of hydrophobic interactions.

135, 136

Modification of the amine of mannostatin A with benzylic moieties did not improve the inhibitory potential of the resulting compounds (Table 2.1). In order to rationalize these observations, docking studies were also performed with compound **1b**. Thus, benzyl moieties were attached to the low energy conformations of **1a**. The resulting derivatives were docked in the binding site of dGMII to give three different binding modes. In case of conformer ¹E, typical interactions were observed, such as a hydrogen bond between the amine and general acid-base residue Asp341 and coordination of the C-4 and C-5 hydroxyls with the zinc ion. Furthermore, the phenyl ring of **1b** made van der Waal's interactions with the aromatic moiety of Tyr269. The orientation of both the phenyl rings was observed as similar to the preferred off-centered parallel-displaced arrangement with average $R_{\text{cen}} = 4.4 \text{ \AA}$, $\gamma = 19.9^\circ$ and $\theta = 41.5^\circ$ as reported by McGaughey et al.¹³⁷ The latter π - π stacking required, however, a tilting of the ring structure of **1b** disrupting a hydrogen bond between the C-5 hydroxyl and N ϵ 2 nitrogen of His90, which is observed in the complex with the parent compound. The phenyl ring in conformers E₂, E₃ and ⁴E of **1b** made similar stacking interactions with Tyr269. For all

three conformers, the amine formed a hydrogen bond with the catalytic nucleophile Asp204 and hydroxyl oxygen of Tyr269. As in ¹E the stacking interactions required a tilting of the five membered ring of **1b**, leading to loss of hydrogen bonds. Thus, the computational studies indicate that the favorable interactions made between the phenyl ring of **1b** and Tyr269 may be offset by loss of hydrogen bonds due to a tilting of the five membered ring of the inhibitor.

Conformers E₁ and ³E of **1b** display a very different binding mode than similar conformer of parent compound **1a**. Thus, in these cases the orientation of the inhibitor is flipped in the catalytic site allowing the thiomethyl to make hydrophobic interactions with Trp95. Nevertheless, stacking interactions of the phenyl ring of **1b** with Tyr269, and hydrogen bonds with Arg228 and Tyr727, further stabilizes these complexes.

Docking of the conformers of **2b** in the binding site of dGMII resulted in two binding modes, which mainly differ in the interactions of the amine with either Asp204 (E₁, E₂, E₃, ³E and E₅) or Asp341 (¹E, ²E, E₄ and ⁴E). A stacking interaction of the phenyl ring of **2b** with Tyr269 (average R_{cen} = 4.3 Å, γ = 13.0° and θ = 41.5°) plays an important role for positioning the inhibitor in the binding site of the enzyme. In the case of conformers E₃, ³E, E₄, ⁴E and E₅, the ring structure of **2b** was tilted to allow the stacking interactions. As a result, the hydrogen bond patterns observed in **2a** were altered. However, conformers E₁, ¹E, E₂ and ²E did not require a tilt of the five membered ring and therefore no loss of hydrogen bonds was observed. In this case, the interactions made by the phenyl moiety might be responsible for the improved affinity of compounds **2b-g** for GMII.

Although, the molecular docking analysis predicted that each of the inhibitors had a significant affinity for the enzyme, the method could not distinguish between stronger and weaker binding. The benzylated analogs would be expected to pay a proportionally larger entropic penalty upon binding than that associated with the simpler, more rigid inhibitors. Autodock does not explicitly consider conformational entropy and so would be expected to overestimate the strength of binding of compounds **1b** and **2b**. While a quantitative ranking of affinities was not achieved, much information could be gained from inspection of the predicted binding modes.

2.5 Conclusions

A range of mannostatin analogs and structurally simpler aminocyclopentitretols has been synthesized, which have varying benzylic moieties at their amino function. It was observed that mannostatin A (**1a**) is a markedly better inhibitor than the corresponding aminocyclopentitretol **2a**. Furthermore, the substitutions of the aminocyclopentitretols led to significant improvements of inhibitory activity for both hGMII and hLAM whereas similar substituents of mannostatin A had only a marginal effect. Computational studies have been performed to provide a rationale for these observations. First, the conformational properties of mannostatin and aminocyclopentitretol were studied by geometry optimizations of the ten possible envelope conformations, using *ab initio* molecular orbital calculations. Subsequently, the low energy conformers of each compound were docked in the binding site of dGMII and the results compared with interactions of swainsonine observed in a crystal structure with the same enzyme. It has been shown that mannostatin A and aminocyclopentitretol could

bind to GMII in a similar mode as swainsonine. Probably, the latter compounds mimic the mannosyl oxycarbenium ion, which is a putative intermediate in the hydrolysis of mannosidases. Thus, it appears that mannostatin and aminocyclopentitretrol can inhibit GMII in a similar fashion. However, due to the flexibility of the five membered rings of **1a** and **2a**, additional low energy binding modes could be adopted. It is conceivable that the ring structure of **1a** and **2a** is flexible in the binding site of GMII allowing transitions between different binding modes. The thiomethyl moiety of mannostatin could make favorable hydrophobic interactions with Arg228 and Tyr727. These interactions are not present in complexes with aminocyclopentitretrol (**2a**) providing a rationale for the lower inhibitory potential of this compound. It was also observed that the five membered ring of **2a** is significantly more flexible than that of **1a** allowing additional binding modes. Attachment of benzyl moieties to mannostatin led to stacking interactions with the aromatic moiety of Tyr269. These π - π interactions required, however, a tilting of the ring structure of **1b** resulting in a disruption of the hydrogen-bonding network observed. Due to the greater flexibility of aminocyclopentitretrol (**2a**), attachment of the benzyl moiety led to conformers that could make the stacking interactions without disrupting hydrogen bonds. This observation may provide a rationale for the improved activities of benzyl-substituted aminocyclopentitretrol.

It is to be expected that further combinatorial extension of the benzyl derivatives will lead to compounds that can interact with the extended binding pocket for the aglycone of HGMII thereby accentuating the selectivity of this enzyme. In this respect, the different binding modes computed for both compounds may provide an important opportunity for the design of targeted libraries.

2.6 Experimental Section

2.6.1 General procedure for reductive amination

A solution of NaOH in MeOH (0.1M, 0.2eq) was added under Argon at room temperature to a solution of compound 1a or 2a in CH₃OH to give a solution having pH 7. To this solution was added a methanolic solution of benzaldehyde (2.5M, 1.0eq) and 3 Å MS. A methanolic solution of NaCNBH₃ (1.75M, 0.6eq) was added, and after 20hrs, the reaction was diluted with CH₃OH and filtered through Celite. The solution was acidified to pH=1 with 1N HCl and concentrated *in vacuo*. The residue was purified by flash chromatography (Iatrobeads; eluent: CH₃CN:HOAc:H₂O, 10:0.5:1 v/v to give the expected product.

2.6.2 Inhibition studies

Assays of the hLAM were assembled at 4°C in a reaction volume (50µL) containing 4-methylumbelliferyl α-D-mannopyranoside (SIGMA)(3 mM), sodium acetate (100 mM), pH 4.5, and purified recombinant hLAM expressed and purified from HEK293 cells (methods to be published separately). Assays for the hGMII were prepared in a similar reaction volume containing 4-methylumbelliferyl α-D-mannopyranoside (SIGMA)(2.5 mM), sodium acetate (83.3 mM) at pH 5.6, ZnCl (83.3 µM) and purified recombinant HGMII expressed and purified from HEK293 cells (methods to be published separately). Reactions were incubated for one hour at 37°C and stopped with the addition of sodium carbonate (150 µL) to a final concentration of 150 mM. Fluorescence was quantitated on a Spectramax Gemini XS fluorescence reader. All fluorescence values are compared to a 4-methylumbelliferone standard curve. Inhibitors were prepared as stock

solutions in water (1-10 mM depending on the amount of compound) and IC₅₀ data were obtained in triplicate over a concentration range of 10 nM – 1 mM and plotted as percent inhibition versus inhibitor concentration. Ki determinations were performed under similar conditions as IC₅₀ determinations, with the exception that 4-methylumbelliferyl α -D-mannopyranoside concentrations were also varied from 160 μ M - 3 mM. Dixon plots were used to transform the kinetic data into Ki values.

2.6.3 Computational studies

All the geometry optimizations were performed with Gaussian 94 program¹³⁸ using density functional theory (B3LYP¹³⁹⁻¹⁴¹) and 6-31G*¹⁴² basis set. The low energy unique conformers of **1a** and **2a** were determined by optimizing ten possible envelope conformers (¹E, E₁, ²E, E₂, ³E, E₃, ⁴E, E₄, ⁵E and E₅, the abbreviated nomenclature used here is similar to the one suggested for furanose ring system¹⁴³), by constraining a specific torsion angle to 0° and allowing all other parameters to optimize at BLYP/6-31G* level of theory. The hydroxyl and amino groups of the resulting structures were placed in three different orientations to give different rotamers which were reoptimized without any restraints at B3LYP/6-31G* level. The solvation effects on the energies of the resulting conformers were approximated using the Poisson-Boltzmann treatment^{132, 133} provided in the Jaguar program.¹¹¹ The unique envelope conformers obtained were docked in the binding site of dGMII.

Preparation of ligand and receptor molecules for docking – The crystal structure of drosophila GMII complexed with Swainsonine (PDBid: 1HWW) was used as a model for macromolecule in docking experiments. The protein target, dGMII and the ligands were prepared for docking using AutoDock Version 3.0.5.^{90, 144} Charges were assigned using

the Kollman algorithm.¹⁴⁵ Atomic solvation parameters and fragmental volumes were determined using Addsol programs available in AutoDock. AutoTors was used to define torsional angles in the ligand. Polar hydrogen charges of Gasteiger type¹⁴⁶ were assigned and the non-polar hydrogens were merged with the carbons. The macromolecule was kept rigid in all the docking simulations.

Docking simulations – Grid maps for docking simulations were generated with 40 grid points (with 0.375 Å spacing) in x, y and z direction, by Autogrid program. The center of the grid was positioned at the Zn⁺² ion (Zn1102). Lennard-Jones parameters 12-10 and 12-6 (supplied with the program package) were used for modeling H-bonds and van der Waals interactions, respectively. The distance dependant dielectric permittivity of Mehler and Solmajer¹⁴⁷ were used for the calculations of the electrostatic grid maps. The genetic algorithm (GA) and Lamarckian genetic algorithm with the pseudo-Solis and Wets modification (LGA/pSW) methods were used with the default parameters. For all the simulations, the populations in the genetic algorithm were 50 and each simulation comprised of 2.5×10^5 energy evaluations. Each docking experiment consisted of a series of 100 simulations.

The π - π stacking interactions between the phenyl ring in 1b and 2b conformers and the phenyl ring in Tyr269 were evaluated by determining the average distance between the centroids of the two phenyl rings (R_{cen}), the angle between the planes of the two rings (γ) and the normal-centroid angle (θ) as discussed in reference 44.

2.7 Acknowledgements

The authors are grateful for financial support for this work by NCI of NIH (5UO1CA91295).

CHAPTER 3

THE STRUCTURAL BASIS OF THE INHIBITION OF GOLGI α -MANNOSIDASE II BY MANNOSTATIN A AND THE ROLE OF THE THIOMETHYL MOIETY IN LIGAND-PROTEIN INTERACTIONS^a

^a Kawatkar, S. P.; Kuntz, D. A.; Woods, R. J.; Rose, D. R.; Boons, G. J., *J. Am. Chem. Soc.* 2006, 128, 8310-8319.

Reprinted here with permission of the publisher.

3.1 Abstract

The X-ray crystal structures of mannose trimming enzyme *Drosophila* Golgi α -mannosidase II (dGMII) complexed with the inhibitors mannostatin A (**1**) and an *N*-benzyl analog (**2**) have been determined. Molecular dynamics simulations and NMR studies have shown that the five-membered ring of mannostatin A is rather flexible occupying pseudo-rotational itineraries between 2T_3 and 5E , and 2T_3 and 4E . In the bound state, mannostatin A adopts a 2T_1 twist envelope conformation, which is not significantly populated in solution. Possible conformations of the mannosyl oxacarbenium ion and an enzyme-linked intermediate have been compared to the conformation of mannostatin A in the co-crystal structure with dGMII. It has been found that mannostatin A best mimics the covalent linked mannosyl intermediate, which adopts a 1S_5 skew boat conformation. The thiomethyl group, which is critical for high affinity, superimposes with the C-6 hydroxyl of the covalent linked intermediate. This functionality is able to make a number of additional polar and non-polar interactions increasing the affinity for dGMII. Furthermore, the X-ray structures show that the environment surrounding the thiomethyl group of **1** is remarkably similar to the arrangements around the methionine residues in the protein. Collectively, our studies contradict the long held view that potent inhibitors of glycosidases mimic an oxacarbenium ion like transition state.

3.2 Introduction

Glycosidases are enzymes that catalyze the cleavage of glycosidic bonds and play critical roles in a number of biological processes. Inhibitors of these enzymes have garnered much attention and are currently used for the treatment of diabetes, viral

infections and Gauchers disease.⁶⁻¹⁰ Furthermore, inhibition of the mannose trimming enzyme human Golgi α -mannosidase II (GMII; mannosyl-oligosaccharide 1,3-1,6- α -mannosidase II; E.C. 3.2.1.114), which acts late in the *N*-glycan processing pathway, provides a route to blocking the oncogene-induced changes in cell surface oligosaccharide structures.^{61, 63, 113, 148} GMII selectively cleaves $\alpha(1-3)$ and $\alpha(1-6)$ mannosyl residues present in its natural substrate GlcNAcMan₅GlcNAc₂.¹⁴⁹ It is a retaining Family 38 glycosylhydrolase, which employs a two-stage mechanism involving two carboxylic acids positioned within the active site which act in concert: one as a catalytic nucleophile and the other as a general acid/base catalyst.^{12, 14, 19, 114, 115} Protonation of the exocyclic glycosyl oxygen of a substrate molecule leads to bond-breaking and simultaneous attack of the catalytic nucleophile to form a glycosyl enzyme intermediate. Subsequent hydrolysis of the covalent intermediate by a nucleophilic water molecule gives an α -mannose product with overall retention of configuration. Studies with 5-fluoro pseudo-substrates and deuterium labeled substrates have shown that the transition states on either side of the covalent intermediate have marked oxacarbenium ion character.^{12, 14, 19, 38, 114, 115} Furthermore, X-ray crystal structures of the wild type and a mutant *Drosophila melanogaster* GMII (dGMII) in which the acid/base catalyst has been removed, with fluorinated sugar analogs have revealed that the glycosyl enzyme intermediate adopts a distorted ¹S₅ skew boat conformation.³⁸ In this conformation, the leaving group is placed anti-periplanar to the lone pair of the ring oxygen, a requirement for the departure of the leaving group according to Deslongchamp's anti-periplanar lone-pair hypothesis.⁷⁹ Furthermore, steric clashes between the *syn*-hydrogens at C-3 and C-5 and the attacking water are minimal in the ¹S₅ skew boat conformation.

Potent inhibitors of glycosidases are believed to mimic oxacarbenium ion-like transition states.^{12, 14, 19, 114, 115} The inhibitory activity of the natural product swainsonine has long been attributed to the resemblance of its 5-membered ring to a flattened six-membered ring mannosyl oxacarbenium ion. In fact, the crystal structure of swainsonine complexed with dGMII shows the inhibitor to be tilted in such a way as to bring the equivalent of its anomeric carbon close to the presumed catalytic nucleophile.⁷⁵

Mannostatins A and B, which were isolated from the soil microorganism *Streptovercillus*, are some of the most potent inhibitors of class II α -mannosidases reported thus far (Figure 3.1).¹¹⁶ They were the first non-azasugar type inhibitors to be discovered that possess an aminocyclopentitol structure. The inhibitors are of the reversible, competitive type and do not show the slow-binding phenomenon exhibited by swainsonine and its analogs. Mannostatin A effectively blocked the processing of influenza viral hemagglutinin in cultured MDCK cells and caused the accumulation of hybrid type protein linked oligosaccharides, which is in agreement with blocking Golgi mannosidase II.¹⁴⁸ The synthesis and biological evaluation of a small number of mannostatin analogs has revealed that the basicity of the primary amine and the neighboring *cis*-diol are essential for inhibitory activity.^{83-88, 117}

While interest in mannostatin A continues to grow, the mode of inhibition of this compound is not well understood. In this respect, its carbocyclic structure represents a significant departure from common alkaloid-based glycosidase inhibitors, and it is unclear whether mannostatin resembles either D-mannose or the mannosyl oxacarbenium ion.

We have now determined the X-ray crystal structure of dGMII in complex with

mannostatin A (**1**) and an N-benzyl analog (**2**). We have analyzed in detail key molecular interactions, in particular, the interaction of the thiomethyl ether with the protein to determine the structural basis for inhibition. Furthermore, molecular dynamics simulations of both the unbound mannostatin A and its complex with the enzyme have been performed to obtain information about the solution phase conformational properties and dynamic features of the enzyme-inhibitor interactions. Finally, possible conformations of the mannosyl oxacarbenium ion and the covalent-linked saccharide intermediate have been compared to the conformation of mannostatin A observed in the co-crystal structure.

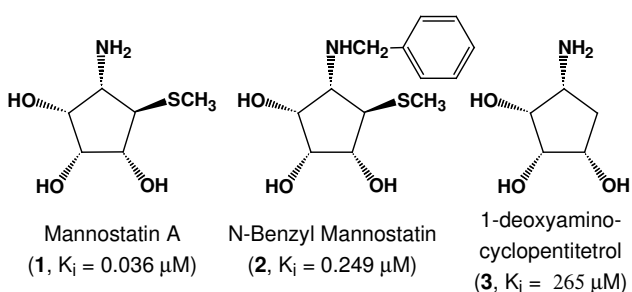


Figure 3.1. Cyclopentitol inhibitors of Golgi α -Mannosidase II. The inhibition constants in the parentheses indicate that the compound **3**, which lacks the thiomethyl moiety, is much less potent compared with compounds **1** and **2**.

3.3 Results and Discussion

Optically pure mannostatin A (**1**), *N*-benzyl mannostatin A (**2**) and 1-deoxyaminocyclopentitretol (**3**) were prepared by literature procedures.^{84, 87, 119} The rate of hydrolysis of different concentrations of 4-methylumbelliferyl α -D-mannopyranoside alone and in the presence of different concentrations of inhibitor was measured fluorometrically and K_i values were determined from Dixon plots. As can be seen in Figure 3.1, mannostatin A is a more potent inhibitor than its *N*-benzylated counterpart.

On the other hand, 1-deoxyaminocyclopentitol **3**, which lacks the thiomethyl ether, is a poor inhibitor indicating that the thiomethyl moiety of **1** makes important interactions with the binding site of the enzyme.

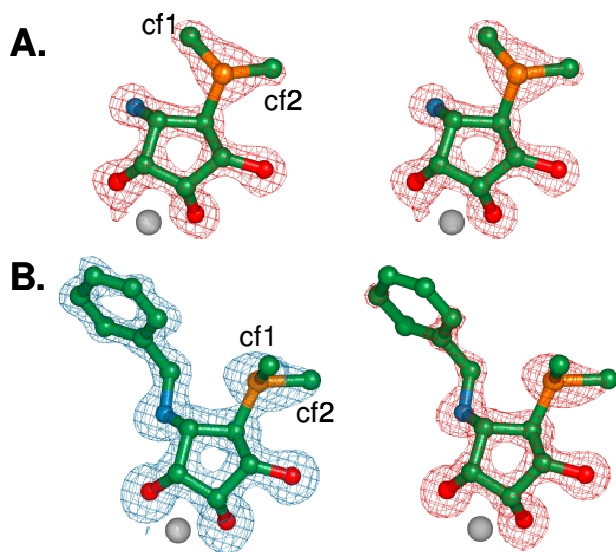
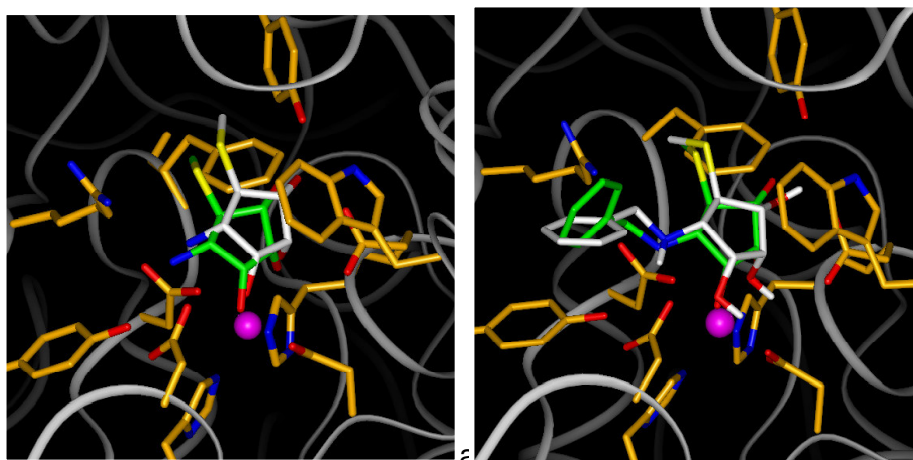


Figure 3.2. Stereoviews of electron density of bound inhibitors: Simulated annealing omit maps (Fo-Fc). A. Mannostatin A **1**, contoured at 5 sigma B. N-benzyl mannostatin **2** contoured at 3 sigma (blue) or 5 sigma (red). This figure was created with Pymol. cf1 and cf2 refer to the two possible conformations of C7 which fit into the observed density.

In order to rationalize the inhibition data, X-ray crystal structures of compounds **1** and **2** complexed with dGMII were solved at 1.3 Å. Data collection and refinement statistics are reported in supplemental data Table 1S. The quality of the density around the bound inhibitors is shown in Figure 3.2. The X-ray crystal structure of dGMII complexed with compound **1** did not show any significant changes in the backbone structure compared to the free enzyme (RMSD = 0.129 Å vs. PDB 1HTY). The five-membered ring of the inhibitor adopts a 2T_1 twist envelope conformation (phase angle, $\phi = 201^\circ$), which is stacked against the aromatic ring of Trp95, a type of interaction seen in

many carbohydrate-protein complexes.¹⁵⁰⁻¹⁵² Important close contacts between the inhibitors and dGMII are detailed in Table 1.

Gratifyingly a good agreement was obtained between the X-ray structures and the predicted docking mode from the docking studies (Figure 3.3).¹⁵³ There are a number of contacts, which have been observed in previous dGMII crystal structures.^{38, 75, 80, 82} The 3,4 *cis*-diol of **1** is complexed with a Zn²⁺ ion in the active site of dGMII resulting in T₆ coordination geometry, while the 2- hydroxyl forms hydrogen bonds with Asp472 and Tyr727. Furthermore, the amine of **1** forms hydrogen bonds with catalytic acid residues Asp204 and Asp341, and Tyr269. The binding of the inhibitors within the context of selected active site residues is shown in Figure 3.4.



ocking mode for mannostatin A and its N-benzylated analogue (green: X-ray structure, white: predicted binding mode). A good agreement was obtained for the binding mode of the five membered ring. However, in the case of benzylated analogue, the phenyl ring assumes different orientation than the one predicted by molecular docking experiments.

Data from SAR experiments (referred to above) has pointed to the importance of the amine and *cis*-diols in the inhibitory activity of mannostatin A and the crystal structure beautifully illustrates how these groups interact with the protein. Similar modes of

interaction, with almost identical distances, were seen in the crystal structure of dGMII complexed with swainsonine (Table 3.1) although only a single interaction with the amine group is observed in that case.

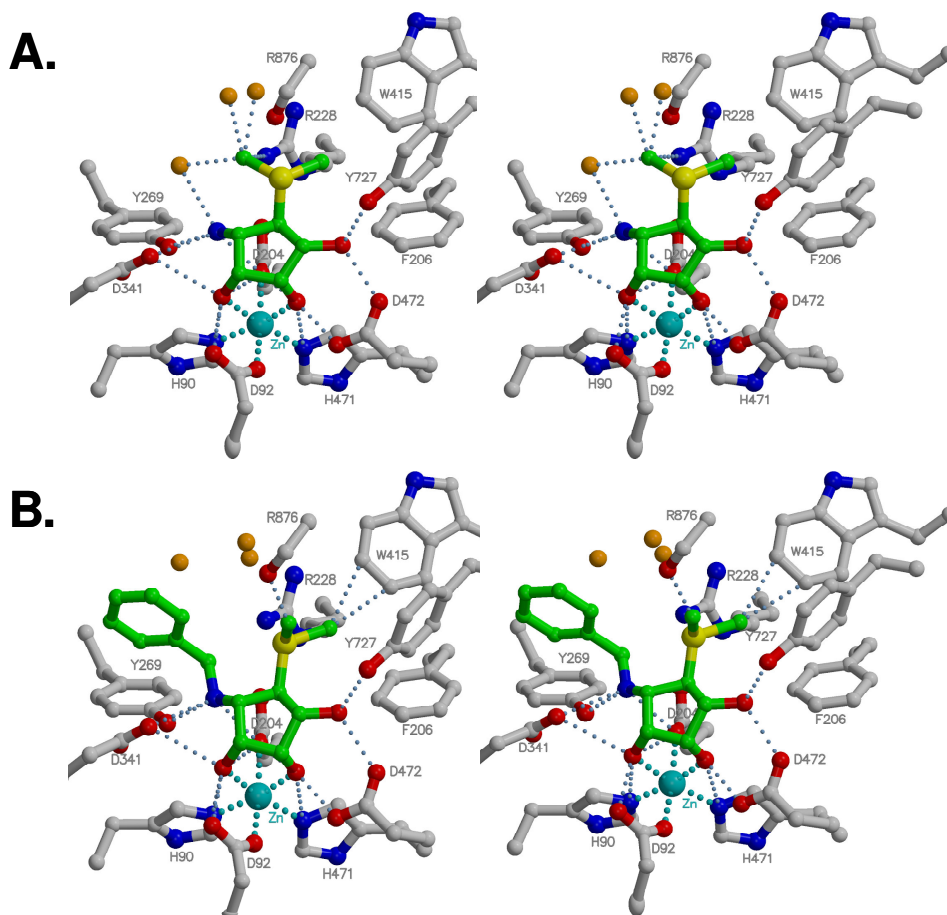


Figure 3.4. Stereoview of the interaction of Mannostatin A (**1**, A) and N-Benzyl Mannostatin (**2**, B) with residues in the active site of dGMII. Interactions closer than 3.2 Å are indicated. The interactions with zinc are indicated in cyan. Water molecules appear as orange balls. Distances are presented in Table 1.

The thiomethyl moiety of **1** and **2** is a feature that is not observed in any other glycosidase inhibitors and the data summarized in Figure 3.1 indicate that this structural feature is critical for potent inhibition. It must be noted that the thiomethyl moiety is structurally similar to the side chain of a methionine residue. It has been

proposed that the sulfur atom and ϵ -CH₃ group of methionine residues are involved in several different interactions important for protein stability.¹⁵⁴⁻¹⁵⁸ For example, aryl-sulfur interactions have been proposed favorable because of the observed proximity of the methionine residue to the aromatic side chains in protein X-ray structures and small molecules X-ray structures. In general, these interactions are either hydrophobic or electrostatic, of the types S-CH₃---Ar or S---H-Ar, respectively. In addition, the sulfur atom, possessing an empty *d*-orbital is also known to be involved in S---X (X = O and N) interactions.¹⁵⁸ Such an interaction is stabilized by the orbital interaction between the lone pair on O or N and the anti-bonding orbital of the sulfur atom. The strong dipole of the methionine residue also makes it an ideal hydrogen bond acceptor. However, an analysis of the NH---S and OH---S hydrogen bonds in proteins suggests that the sulfur atom in methionine has only a weak character of a hydrogen bond acceptor.^{156, 159}

In the context of dGMII at least one third of the methionines occur in a hydrophilic or surface environment, and a number bear a striking resemblance to the environment of the thiomethyl group of the inhibitors. In Figure 3.5, three different methionine residues whose methyl carbon occupies environments similar to **1** are presented, along with their respective distances from water (or a backbone carbonyl in the case of Met769). In two cases (Met264 and Met769) alternative conformations of the thiomethyl group are seen, similar to the situation observed with the inhibitors, while Met224 shows a single strong conformation that places the methyl group in close proximity to waters. In Met264 both conformers are in a hydrophilic environment. In Met769, one orientation places the methyl group in close proximity to 2 waters and the backbone oxygen of Pro684, while the other orientation results in the terminal methyl

group finding itself in a more hydrophobic environment, similar to what is observed for **1**. It should be noted that all the waters that are in close proximity to methionine have other strong hydrogen bond partners and the methionine residues do not appear to be their principal form of interaction with the protein.

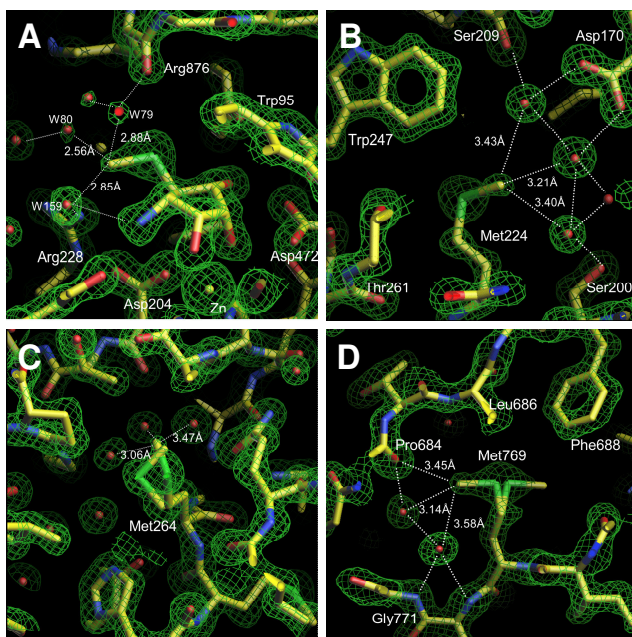


Figure 3.5. Comparison of the density of Mannostatin A cf1 with methionine residues of dGMII found in similar environments. Possible water interactions are shown with dotted lines. Distances between the thiomethyl group and proximal waters are indicated. The electron density ($2F_o - F_c$) is contoured at 1.5 -2 sigma. The figures are generated in O. **A.** Mannostatin A cf1 **B.** Methionine 224 **C.** Methionine264, showing both conformers **D.** Methionine769, showing both conformers.

The sulfur atom of the thiomethyl moiety of **1** seems to form a nonbonded S---O type of interaction with the main chain carbonyl oxygen of Arg876. Statistical analysis of protein structures performed by Iwaoka et al¹⁵⁸ suggests that most S---O interactions are between the sulfur atom in the methionine residue and backbone carbonyl oxygens or side chain carboxylate oxygens. An analysis of the spatial placement of sulfur with

respect to the oxygen revealed that the interaction between the π -orbital on the carbonyl oxygen and the antibonding σ^* orbital of S-C bond is largely responsible for this observation. *Ab initio* calculations with small molecules indicate that these interactions could result in stabilization of up to 2.5 kcal mol⁻¹ when these atoms are separated by 3.3 Å.¹⁵⁸ It is, however, important to note that these calculations have been performed in vacuo and therefore the binding energies may be different in an aqueous environment due to solvation effects. In the **1**-dGMII complex the sulfur atom is located at 3.49 Å from the Arg876O, suggesting that the interaction observed between the sulfur atom in the thiomethyl moiety and the carbonyl oxygen of Arg876 must be reasonably strong.

Table 3.1. Distances between different inhibitor atoms and protein atoms as observed in the complexes of swainsonine (PDB id 1HWW), **1** and **2** with dGMII.

Protein Atom	Swainsonine		Inhibitor Atom	1		2	
	Inhibitor Atom	Distance (Å)		Distance (Å)	Distance (Å)		
H90 NE2	O-2	2.97	O-4	3.07	3.11		
D92 OD1	O-1	3.04	O-3	2.92	2.99		
D92 OD2	O-2	2.54	O-4	2.55	2.51		
	O-1	2.83	O-4	2.82	2.91		
D204 OD2	O-2	2.97	O-3	2.92	2.95		
	N-4	2.75	N	2.77	2.9		
R228 NH2			C-7 (cf1)	3.11	5.08		
			S	4.01	3.54		
Y269 OH	N-4	4.17	N	2.78	2.96		
D341 OD2			N	2.99	3		
W415 CH2			C-7 (cf2)	3.36	3.17		
W415 CZ3			C-7 (cf2)	3.57	3.17		
H471 NE2	O-1	3.12	O-3	3.1	3.02		
D472 OD1	O-8	2.56	O-2	2.59	2.62		
D472 OD2	O-1	2.6	O-3	2.53	2.57		
Y727 OH	O-8	2.64	O-2	2.72	2.68		
R876 O	-----	-----	C-7 (cf1)	4	2.5		
			S	3.49	4.14		
			N	3.03			
WATERS			C-7 (cf1)	2.56, 2.85, 2.88			

The most striking structural feature of these inhibitor complexes is the fact that the C-7 carbon (i.e. the methyl group in the thiomethyl functionality) can occupy two possible positions (Figures 3.2 and 3.4). Both these positions are clearly visible in the electron density maps (Figure 3.2) and, in the case of **1**, have B-factors of 5.2 Å² and 6.8 Å² (conformer 1 (cf1) and conformer 2 (cf2), respectively) suggesting that cf1 conformer might be slightly favored.

The methyl group obviously forms favorable interactions in each of these positions, but the exact nature of the interactions is somewhat ambiguous and arguments can be made for both hydrophobic and hydrophilic bonds. In the case of the cf1 conformation of **1**, the methyl carbon is 4.3 Å from the CZ carbon in Arg228. The interaction between the methyl and Arg228 could be a C–H---cation type interaction where the C–H acts as donor. A statistical analysis of 1154 protein structures for C–H---π interactions revealed that such interactions are possible in proteins and are mostly intrahelical interactions¹⁶⁰ which could be classified as weak hydrogen bonds and which play an important role in the secondary structure stabilization. It was also found that the terminal methyl in methionine residue is one of the prominent donors for such interactions. The thiomethyl group of **1** can act as a donor to form such interaction with Arg228. There have been several theoretical studies, which estimate stabilization energies in other types of C–H---π interactions. However, to the best of our knowledge, energetic evaluation of the interaction between an aliphatic C–H and guanidinium moiety of an arginine has not been reported. Nevertheless, the relatively close proximity of the

guanidinium moiety as observed in the **1**-dGMII complex, indicate that there is strong possibility of formation of C–H--- π type of interaction between the two functionalities.

It is tempting to speculate that the polarizable methyl group may hydrogen bond with neighboring water molecules. Three water molecules (W79, W80 and W159) are present at less than 3.2 Å from the methyl carbon in the cf1 conformation, while a fourth (W80) is 3.3 Å away. W159 also makes a strong hydrogen bond with the amino group of **1** and two other waters. Waters 78-80 show relatively weak electron density while W159 is quite well defined. Iwaoka *et al*¹⁵⁸ showed that a single C–H---O hydrogen bond from the methyl group to a backbone oxygen was weakly stabilizing and one could surmise that 3 such weak hydrogen bonds to water would have an additive effect.

On the other hand, there are arguments for hydrophobic interactions being the predominant binding force.^{161, 162} In this respect, it has been shown that methionines display mainly hydrophobic character,¹⁶¹ at least in the context of artificial hairpin peptides where their measurements were made. In fact, it could be that the water molecules are actually stabilizing the cf2 conformations rather than the cf1 conformation by binding to sulfur. In the cf2 conformation, sulfur can form a hydrogen bond with these water molecules via the lone pair electrons. Moreover, W79 is hydrogen bonded to Arg876O (2.7 Å) and W80 is hydrogen bonded to W79 and W81 suggesting that there may not be any interaction between the methyl in **1** cf1 and the water-sulfur cf2 interaction is what is visible in the electron density.

The X-ray crystal structure shows that in the cf2 conformation the thiomethyl ether of **1** makes two arene-sulfur interactions with Phe206 and Tyr727. In protein structures, methionine is often found in close proximity of aromatic side chain residues

indicating that arene-sulfur interactions are important for protein structure stabilization.¹⁵⁴⁻¹⁵⁷ In general, arene-sulfur interactions are either hydrophobic of the S-CH₃---Ar type or electrostatic of the S---H-Ar type. *Ab initio* calculations of a dimethyl sulfide-benzene complex has predicted a stabilization energy of -1.6 kcal mol⁻¹ when methyl hydrogens point towards the centroid of an aromatic ring and when the distance between the sulfur atom and the centroid of the benzene ring (R_{cen}) is 5.8 Å.¹⁶³ In an alternative model, where both methyl groups are at the edges of the aromatic ring and the sulfur is 4.9 Å from the centroid of the aromatic ring, a stabilization energy of -2.5 kcal mol⁻¹ was calculated.¹⁶³ Furthermore, mutational experiments with β -hairpin model peptides¹⁶¹ have indicated that arene-sulfur interactions are primarily hydrophobic in nature contributing up to -1 kcal mol⁻¹ of stabilization energy.

Interestingly, the X-ray crystal structure shows that the thiomethyl functionality of **1** cf2 complexes with Phe206 of dGMII through a hydrophobic SCH₃---Ar type interaction. In this case, the sulfur atom is placed slightly off-centered from the aromatic ring ($R_{\text{cen}} = 5.8 \text{ \AA}$) similar to a mode predicted by *ab initio* calculations. The Tyr727 also makes a hydrophobic interaction with the thiomethyl group but in this case the methyl group is placed at the edge of the aromatic ring ($R_{\text{cen}}=5.3 \text{ \AA}$) similar to the second mode of interaction predicted by *ab initio* calculations.¹⁶⁴ Contact analysis shows that the thiomethyl group also makes van der Waals contacts with Trp415 and Arg876.

In the case of the **2**-dGMII complex, the methyl carbon in the thiomethyl functionality (C-7) also occupies two positions, the cf2 position is similar between **1** and **2** but the cf1 has moved. (Figure 3.4B). In the cf1 conformation, the methyl carbon is close to the backbone carbonyl oxygen of Arg876 and the sulfur atom seems to interact

with NH₂ of Arg228, which is at 3.5 Å from the sulfur atom, via the lone pairs of the sulfur atom. This interaction has been studied in protein structures before and the structural preferences observed for this interaction suggest a contribution from the $n(\text{S}) \rightarrow \sigma^*(\text{NH})$ orbital interaction to the stability.¹⁵⁸ Theoretical studies have shown that such interaction can contribute up to 2 kcal mol⁻¹ to the stability with 3.6 Å separation between the two atoms.¹⁵⁸ In the alternate cf2 conformation, this interaction may be weakened by the geometric position of the methyl group. However, this loss in the interaction may easily be compensated by the interaction between the sulfur atom and the Arg876O, which is also observed in **1**-dGMII complex and has been explained earlier. In addition to this interaction, the thiomethyl moiety is also involved in sulfur- π type interactions with Phe206 and Tyr727 in the same way as in the case of **1**. Additionally in the case of **2** cf2 the C-7 is perfectly centered at a distance of 3.17 Å with CH₂ and CZ3 of Trp415. The close contacts between the thiomethyl group and water molecules observed in **1**-dGMII complex are not seen in the **2**-dGMII complex; there is no equivalent to W159 whose position has been taken up by the phenyl ring and the W79 equivalent (W361) has moved to 4 Å from the sulfur, and the W80 equivalent (W360) is now 3.8 Å away. There is now an intramolecular interaction between the phenyl ring and sulfur (see below), which displaces the water interactions.

It is important to note that additional modified derivatives of mannostatin (**1**) need to be synthesized and biologically evaluated to determine whether the polar or non-polar interactions of the thiomethyl moiety are responsible for its enhanced activity.

Docking studies¹⁵³ had indicated that the aromatic substituent of **2** would be able to make a parallel, off-centered π - π stacking interaction with phenyl ring of Tyr269 and

therefore, it was expected that **2** would be a better inhibitor than **1**. The unexpected finding that **2** is a poorer inhibitor than **1** can, however, be rationalized by careful examination of the crystal structure of dGMII with **2** (Figure 3.4). In both **1** and **2**, the five-membered rings are identically positioned in the binding site of dGMII (Figure 3.4B). The distance between the centroid of the aromatic ring of compound **2** and Tyr269 is 5.7 Å at an angle of 118° between the planes made by the aromatic rings, indicating that no edge to face binding interactions are made which require a distance of 5.0 Å and angle of 90°. The unexpected orientation of the aromatic ring of **2** can be rationalized by an intramolecular S---H---Ar type hydrogen bond between the thiomethyl moiety and the phenyl ring with P = 0.3 Å and L = 5.0 Å (where P is the vertical and L is the horizontal distance between the sulfur atoms and the centroid of the aromatic ring). *Ab initio* calculations have indicated that this special arrangement of phenyl ring and the sulfur atom can contribute up to -1.5 kcal mol⁻¹ of bonding energy.¹⁶⁵ These calculations do, however, not take into account entropic and solvation effects.

3.4 MD Simulations of Free Ligands

Cyclopentane rings, such as in compounds **1-3**, are inherently flexible due to their ability to assume several twist and envelope conformations (Figure 5), which can interconvert with relative ease *via* pseudo-rotational itineraries.^{127, 128} Since ring substitutions may affect these pseudo-rotational itineraries,¹²⁸ compounds **1-3** may have different conformational properties. These differences may, in part, account for differences in the inhibition constants.

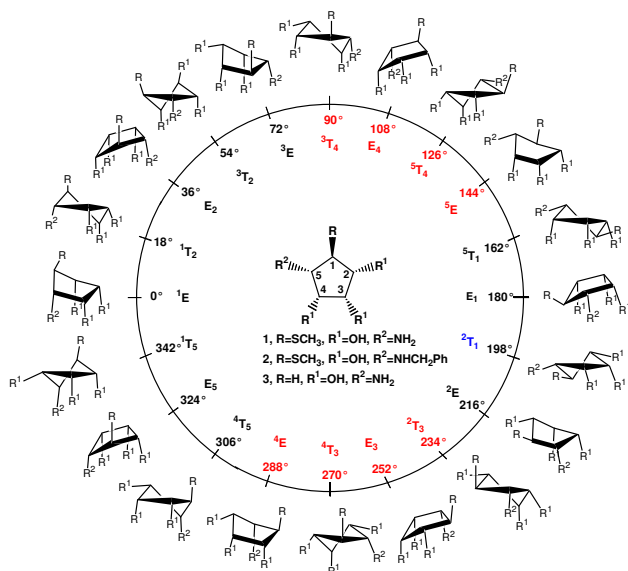


Figure 3.6. Pseudo-rotational itinerary for compounds **1-3**. Different envelope (E) and twist (T) conformers shown in the figure are uniquely defined by the value of phase angle (ϕ) of puckering. The phase angles for compounds **1-3** were computed using the carnal module in the AMBER suite of programs by employing Cremer and Pople's parameters. The bound conformation of **1** (blue) lies outside the preferred solution phase conformational families (red) as sampled in MD simulation of free ligand.

The conformational properties of **1** were probed by a 5-ns MD simulation of just the ligands in explicit water starting from the conformation of **1** observed in the X-ray crystal structure with dGMII. The most populated conformational family (80% occupancy) occupies pseudo-rotational itineraries between 3T_4 and 5E ($\phi = 90-144^\circ$) whereas a second and minor conformational family (20% occupancy) represents conformers between 2T_3 and 4E ($\phi = 234-288^\circ$) (Figures 3.6 and 3.7A). The 2T_1 conformer observed in the crystal structure was not populated and, thus, it appears that **1** is complexed in a high-energy conformation. The bound conformation of **1** is probably stabilized by a coordination of 3- and 4-oxygens with Zn⁺² ion and a hydrogen bond between the amine nitrogen and Asp204, which arrange atoms C-3, C-4 and C-5 in single plane resulting in an almost perfect 2T_1 ($\phi = 198^\circ$) conformation. This conformation also

allows interactions of the thiomethyl moiety with the aromatic residues of Phe206 and Tyr727.

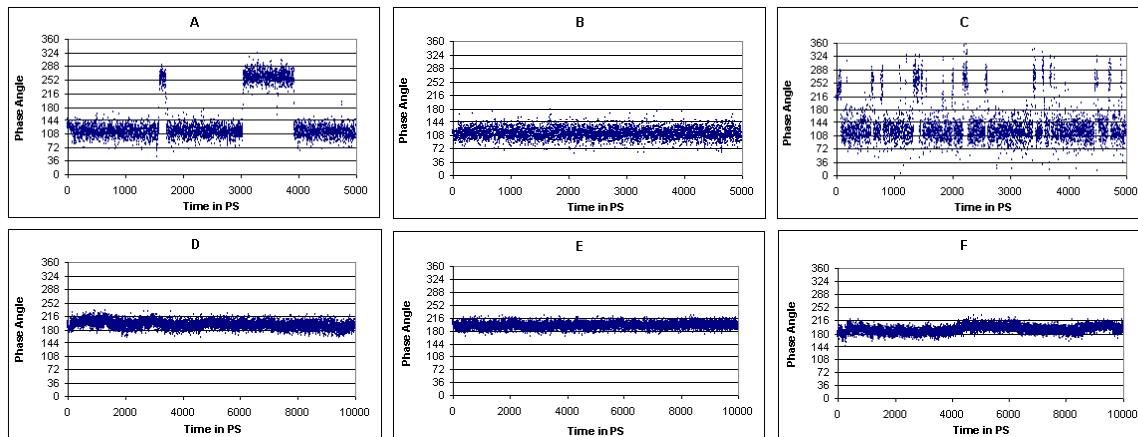


Figure 3.7. Plots of phase angles (ϕ) as a function of time in the MD simulation trajectories. A: **1** in water, B: **2** in water, C: **3** in water, D: **1** bound to dGMII, E: **2** bound to dGMII and F: **2** bound to dGMII with the phenyl ring in **2** making parallel off-center type of interaction with the phenyl ring in Tyr269. MD trajectories for ligands in a box of TIP3P water molecules (top row) indicate that compound **1** populates two clusters (A): the first consists of conformers 3T_4 , E_4 , 5T_4 and 5E ($\phi = 90\text{-}144^\circ$) and the second consists of conformers 2T_3 , E_3 , 4T_3 and 4E ($\phi = 234\text{-}288^\circ$). Compound **2** populates only one conformational cluster (B) with conformers 2T_3 , E_3 , 4T_3 and 4E . In the case of **3**, the interconversion barrier is reduced resulting in frequent conversion between different conformers (C). It can be noted that the bound conformation (2T_1 , $\phi = 201^\circ$) of the five-membered ring in **1** and **2** is different than the conformers populated in the 5-ns MD simulations and remains in the same conformational family comprising of E_1 , 2T_1 and 2E conformers ($\phi = 180\text{-}216^\circ$) during the 10 ns trajectory (bottom row, D and E). Although, the alternate orientation of the phenyl ring in **2** induces some flexibility in the five-membered ring, during the entire simulation the five-membered ring is restricted to the same conformational family (F), indicating that this arrangement of phenyl ring is also possible.

The MD simulation of **2** (Figure 3.7B) showed only the cluster of conformers between 3T_4 and 5E ($\phi = 90\text{-}144^\circ$) indicating that the benzyl substituent increases the barrier for interconversion between conformational states. Interestingly, the intramolecular S---H---Ar interaction between the thiomethyl moiety and the phenyl ring

was not stable and after 200 ps the distance between the phenyl and sulfur was already 7 Å. Although the removal of the thiomethyl group of compound **3** decreased the interconversion barrier as evident from the frequent interconversions between the two clusters of conformers (Figure 3.7C), it populated the same conformational clusters as **1**.

In order to validate the computational results, proton-proton J-coupling constants for compounds **1-3** were calculated over the entire trajectory using a Karplus type equation¹⁶⁶ and the resulting values compared with experimental data from NMR solution experiments (Table 3.2). Gratifyingly, a good agreement was obtained between the computed and experimental *J*-values. The best agreements were obtained for compound **3**, which is aided by a more effective statistical sampling of the two conformational states in **3**.

Table 3.2. Computed and experimental homonuclear *J*-coupling constants (in Hz) for compounds **1-3**. The coupling constants were calculated using a Karplus type equation proposed by Haasnoot et.al. (reference 48) over the entire 5-ns trajectory from MD simulations of ligands in a box of TIP3P water molecules. The values in the parentheses indicate the experimental values.

	1	2		3
			$J_{\text{Hb-H1}}$	1.5 (1.5)
$J_{\text{H1-H2}}$	6.2 (7.5)	5.0 (6.3)	$J_{\text{Ha-H1}}$	7.9 (7.6)
$J_{\text{H2-H3}}$	6.3 (4.8)	6.2 (5.1)	$J_{\text{H1-H2}}$	7.5 (6.2)
$J_{\text{H3-H4}}$	4.8 (4.1)	4.8 (4.3)	$J_{\text{H2-H3}}$	5.9 (5.6)
$J_{\text{H4-H5}}$	5.1 (6.3)	5.0 (6.1)	$J_{\text{H3-H4}}$	5.2 (5.6)
$J_{\text{H5-H1}}$	7.0 (7.0)	8.0 (7.9)	$J_{\text{H4-Ha}}$	7.6 (7.6)
			$J_{\text{H4-Hb}}$	6.0 (5.7)

3.5 MD Simulations of Protein-bound Ligands

While the X-ray crystal structures of **1** and **2** complexed with dGMII provided a great deal of insight into the binding modes of the inhibitors, MD simulations offer

additional information about the dynamic properties of the complexes. These simulations also allow an unambiguous analysis of hydrogen bonding patterns and occupancies and make it possible to determine the dynamic nature of H- π type, sulfur- π type hydrogen bonds and π - π type stacking interactions.

MD simulations of the complexes of **1** and **2** with dGMII only provided stable complexes when started with inhibitors in which the amino groups were protonated. This observation supports the notion that protonation of an amine of a glycosidase inhibitor is crucial for binding.¹⁶⁷ Furthermore, this behavior is in agreement with previously published SAR studies indicating the necessity of the amino group for inhibitory activity of the compounds.^{83-88, 117} During the entire simulations no significant changes were observed in the protein backbone compared to the X-ray structure suggesting that MD simulations did not induce any conformational changes in the backbone. In addition to this, during the entire 10-ns simulation the cyclopentane rings of compounds **1** and **2** exhibit little flexibility as only one a small region of the pseudorotation wheel was occupied (E_1 , 2T_1 , 2E : $\phi = 180$ - 216° , Figure 3.7D and 3.7E). This conformational family is different than the conformational states sampled in the simulations of ligands in explicit water, indicating that the cyclopentane rings do not revert to their low energy conformation.

Analysis of hydrogen bonding patterns and occupancies provides information about which interactions are the most important ones for complexation. Typically, the strongest hydrogen bonds have the highest occupancies, the smallest standard deviations and the shortest heavy atom separations. For compound **1**, very strong hydrogen bonds were observed between the 2-hydroxyl oxygen and Asp472 OD1-OD2, 3-hydroxyl

oxygen and Asp472 OD2 and 4-hydroxyl oxygen and Asp341 OD1 (Table 3.3). Moderately strong hydrogen bonds were assigned between 4-hydroxyl oxygen and Tyr269 OH, the amine nitrogen and Asp204 OD1-OD2, and Tyr269 OH and Asp341 OD1-OD2. The 2-hydroxyl oxygen also accepted a proton from Tyr727 to form a moderate hydrogen bond. In addition, the methyl group in the thiomethyl ether remained in cf2 conformation during the entire 10-ns period. The interactions between the thiomethyl moiety and the aromatic rings of Phe206 and Tyr727 were observed during the entire simulation further supporting the notion that these are important for ligand binding.

Table 3.3. Hydrogen bonding interactions between **1** and **2**, and dGMII over the 10-ns trajectories, computed using the carnal module in AMBER 7.0. The first value is the average distance between the specified atoms in Å, the values in parentheses indicate the percent occupancies.

Donor atom	Acceptor atom	1	2	2 ^a
R228NH2	S	3.8 (5)	3.9 (0.1)	3.8 (32)
Y727OH	O-2	3.0 (40)	3.1 (74)	3.2 (51)
O-2	D472OD1	3.2 (100)	3.0 (100)	3.0 (98)
O-2	D472OD2	2.6 (100)	2.9 (100)	2.9 (100)
O-3	D472OD1	3.9 (0.6)	3.8 (29)	3.9 (14)
O-3	D472OD2	2.5 (100)	2.5 (100)	2.5 (100)
O-4	Y269OH	3.7 (54)	3.8 (0.2)	3.8 (1.5)
O-4	D341OD1	2.5 (100)	3.6 (90)	3.6 (93)
O-4	D341OD2	3.8 (7)	2.6 (100)	2.6 (100)
N	D204OD1	3.6 (33)	3.6 (97)	3.6 (83)
N	D204OD2	3.2 (49)	3.4 (97)	3.4 (81)
N	Y269OH	2.9 (52)	2.9 (91)	3.0 (96)
N	D341OD1	3.0 (43)	3.1 (100)	3.4 (99)
N	D341OD2	3.5 (43)	3.4 (99)	3.3 (99)

The properties of the hydrogen bonds of the complex of **2** with dGMII were very

similar compared to those of **1**. Furthermore, the intramolecular hydrogen bond between the thiomethyl moiety and phenyl ring was maintained throughout the simulation. In order to investigate in more detail the importance of the intramolecular S---H---Ar interaction of **2** in the complex with dGMII, a MD simulation was performed whereby the phenyl ring of **2** was stacked against Tyr269 (Figure 3.7F). Interestingly, the π - π stacking interaction was found to be stable (data not shown) with average $R_1 = 3.3 \text{ \AA}$ and $R_2 = 2.1 \text{ \AA}$, where R_1 is the vertical and R_2 is the horizontal distance between the centroids of the phenyl rings. Theoretical study on benzene dimer indicates that this geometrical arrangement of the aromatic rings results in the stabilization energy of up to $-1.5 \text{ kcal mol}^{-1}$.¹⁶⁸ Furthermore, the conformation of the cyclopentane ring and hydrogen bonding and other interactions were unchanged. This result is in agreement with our previous modeling studies,¹⁵³ even though this interaction is not observed in the crystal structure. This discrepancy between the crystal structure and the modeling study may be a result of the fact that the docking program used does not explicitly consider conformational entropy.

3.6 Overlay studies

The mode of inhibition of GMII by azasugars such as swainsonine has been rationalized by their resemblance to the mannosyl oxacarbenium ion, a putative intermediate in the hydrolysis of glycosides. However, extension of this model to the aminocyclopentitols, such as mannostatin, has been a subject of debate.^{84, 89, 125, 169} Previous attempts to predict the precise binding mode of mannostatin A and its analogs resulted in multiple binding models that differed in the conformation of the five-

membered ring of these inhibitors.¹⁵³ The X-ray structures of dGMII complexed with inhibitors **1** and **2** offers a unique opportunity to compare the three dimensional arrangement of the functional groups of **1** and **2** relative to that of the mannosyl oxacarbenium ion.

Previously, it has been reported that the mannosyl oxacarbenium ion can adopt at least two conformations in which C-4 is either above (flap-up) or below (flap-down) the plane of the C-2, C-1, O-5 and C-5 atoms.^{89, 169} Optimized geometries of both the conformers were obtained by quantum mechanical calculations at the DFT/B3LYP/6-31G* level of theory. It was found that the flap-up conformer was more stable than flap-down conformer by 4.4 kcal mol⁻¹, which is in agreement with previous calculations.¹⁶⁹ Subsequently, the two conformers of the oxacarbenium ion were superimposed on the conformation of mannostatin A observed in the X-ray crystal structure. The zinc coordinating C-3, C-4 *cis*-diol of **1** mimics the C-3, C-2 *cis*-hydroxyl of the oxacarbenium ion and therefore the O-3, C-3, C-4 and O-4 of **1** were superimposed onto O-3, C-3, C-2 and O-2 of the oxacarbenium ion conformers (Figure 7).

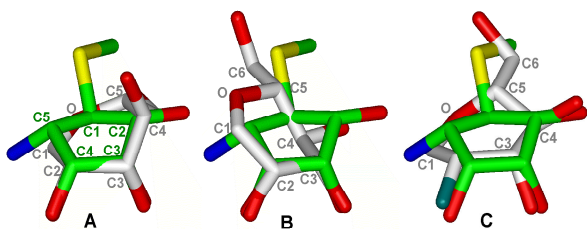


Figure 3.7. Superimposition of Mannostatin A (**1**) in bound conformation onto the flap-up (A) and flap-down (B) oxacarbenium ion, and covalent intermediate (C, PDB ID 1QX1). Mannostatin A mimics best the covalent intermediate.

In the case of the flap-up conformer, the cyclopentane ring of compound **1** seems to mimic the sugar ring with C-2, C-3 and C-4 carbon atoms lying very close to C-4, C-3

and C-2 carbon atoms in the sugar ring and the C-1 carbon is positioned very close to the ring oxygen. The zinc-coordinating 3- and 4-oxygen atoms in **1** display a nearly perfect overlap with corresponding hydroxyl oxygens with RMS deviation of 0.16 Å. The C-5 carbon is located above the anomeric carbon of the oxacarbenium ion placing the amino nitrogen in the region of the exo-cyclic anomeric oxygen of the substrate. The protonated form of this amine at physiological pH raises the possibility that in this arrangement the amine nitrogen mimics the positive charge on the exo-cyclic anomeric oxygen, which develops during the formation of the oxacarbenium ion. In the case of the inhibitor, swainsonine, the amine nitrogen is positioned very close to the ring oxygen suggesting that it probably mimics the positive charge on the ring oxygen in the transition state. The C-2 hydroxyl and thiomethyl moiety of **1** do not seem to mimic any functionality of the oxacarbenium ion. However, these moieties are involved in multiple interactions with protein residues enhancing the affinity of **1** for dGMII.

Attempts to superimpose **1** with the flap-down conformer were less successful. The C-3 and C-4 carbon atoms lie near the C-3 and C-2 atoms in the oxacarbenium ion, respectively, while all the other carbons are at a considerable distance. Moreover, the 3- and 4-hydroxyl groups display poorer overlap with the corresponding hydroxyl groups in the oxacarbenium ion with greater RMS deviation of 0.33 Å, compared to 0.16 Å in the flap-up conformer. The amine group now points away from the β -face of the oxacarbenium ion. It has been proposed that β -mannanase catalyzed hydrolysis proceeds through a transition state in which the oxacarbenium ion adopts a $B_{2,5}$ conformation.²⁴ Therefore, the geometries of the mannosyl oxacarbenium ion in the $B_{2,5}$ and $^{2,5}B$ conformation were optimized and the resulting structures superimposed on the bound

conformation of **1**. In each case, only the C-3, C-4 diol of **1** coordinating with Zn overlaid well with the C-2, C-3 diol of the mannosyl oxacarbenium ions (results not shown) demonstrating that **1** does not mimic a TS in the boat conformation.

Interestingly, the overlay of **1** with a covalently trapped fluorinated sugar analog,³⁸ which mimics the covalently linked reaction intermediate and is found in a distorted ¹S₅ skew boat conformation, shows a good correspondence with all three hydroxyls of **1**. Furthermore, in this overlay the sulfur is in a close proximity to the C-6 hydroxyl of the covalently linked sugar analog (Figure 7C). The thiomethyl group of **1** makes, however, additional polar and non-polar interactions with protein residues compared to the equivalent C-6 hydroxyl, thereby enhancing the affinity of compound **1** for dGMII. The amine is in close proximity to C-1 of the covalently linked intermediate and therefore is ideally positioned to interact with the catalytic nucleophile (Asp204).

Thus, the overlay studies indicate that mannostatin mimics best the enzyme-linked mannosyl intermediate, which has been proposed to adopt a ¹S₅ skew boat conformation. This conformation has been implicated in the reaction mechanism of α- as well as β-retaining glycosidases. For example, the three-dimensional structure of a β-mannanase from *Pseudomonas cellulosa* (endo β-retaining mannosidase) was determined at various points along its reaction pathway.²⁴ Interestingly, the conformation of the Michaelis complex of the β-mannanase was identical to that of the fluorinated sugar analog linked to dGMII.

The five-membered ring of swainsonine is believed to resemble the flattened six-member ring of the mannosyl oxacarbenium ion. However, superimpositions of swainsonine onto the two mannosyl oxacarbenium ion conformers and the enzyme

trapped intermediate showed that the best overlay is obtained with the latter intermediate (overlays shown in the supplementary material). It is generally believed that potent glycosidase inhibitors mimic an oxacarbenium-ion like transition state. The results of our studies highlight that they may also mimic reaction intermediates such as the Michaelis complex or enzyme-linked intermediate.

In his superimposition study,⁸⁹ Winkler reported that Mannostatin A mimics the flap-up conformer with the functional groups present in mannostatin A mimicking different hydroxyl groups in the oxacarbenium ion. Winkler used the X-ray structure of Mannostatin A tetraacetate for these superimposition studies.¹⁷⁰ It must be noted that conformation of the five-membered ring in Mannostatin B tetraacetate is 3T_4 ($\phi = 93.5^\circ$), which is different than the bound conformation of the cyclopentane ring (2T_1) in both the X-ray structures reported here. Moreover, 2- and 3-hydroxyl groups in mannostatin A were superimposed onto the zinc-coordinating 3- and 2-hydroxyl groups in the oxacarbenium ion, respectively. However, from the X-ray structure of **1**-dGMII complex, it is revealed that 3- and 4-hydroxyl groups in **1** coordinate with the Zn^{2+} ion and thus mimic the zinc-coordinating cis-diol in the actual substrate. The important role of the zinc ion in the catalytic mechanism of dGMII has recently been discussed.⁸⁰

3.7 Conclusions

Glycosidases are enzymes that play crucial roles in the biosynthesis of glycoproteins. Inhibitors of these enzymes have garnered much attention as lead compounds for drug discovery for diseases such as viral- and bacterial infections, diabetes, Gauchers disease and cancer. In many cases, the mode of inhibition by these

compounds is not well understood, complicating efforts to design and synthesize more potent- and/or selective inhibitors. As a result, only a very small number of glycosidase inhibitors have been successfully developed as therapeutics.

The studies reported here indicate that mannostatin A mimics the covalently linked mannosyl intermediate, which has been shown to adopt a 1S_5 skew boat conformation. In particular, the zinc-coordinating 3- and 4-hydroxyls of **1** display a good overlap with the corresponding *cis*-diol of the mannosyl residue. Furthermore, the amine nitrogen of **1** is positioned close to the C-1 carbon of enzyme-linked mannosyl intermediate and therefore can interact with the carboxylic acid of the catalytic nucleophile Asp204. The thiomethyl group of mannostatin A, which is required for high affinity binding, showed a good overlay with the C-6 hydroxyl of the covalently linked intermediate. This functionality is, however, able to make a number of additional interactions increasing the affinity for dGMII. The thiomethyl moiety of **1** is structurally similar to the side chain of methionine residues. Interestingly, the environment surrounding the thiomethyl group of **1** is remarkably similar to the arrangements around the methionine residues in the protein structure. While this observation supports the importance of interactions made by the thiomethyl moiety in methionine with respect to protein folding and secondary structure stability, it also supports the role of thiomethyl moiety in mannostatin A binding. Another important finding is that the methyl carbon of the thiomethyl moiety of **1** in the complex with GMII adopts two different conformations. In both conformations, the sulfur interacts with the backbone oxygen of Arg876 through the π -orbital on the carbonyl oxygen and the antibonding σ^* orbital of the S-C bond. In *cf1* conformation, the polarizable methyl group is in a hydrophilic environment

interacting with three water molecules and the π -system of the Arg228 side chain. The side chains of methionine residues 224 and 264 are in similar hydrophilic environments. On the other hand, the methyl group of the cf2 conformation is in a hydrophobic environment where it forms C–H--- π type interactions with the phenyl rings of Phe206 and Tyr727. In the protein structure, similar interactions have been observed for the Met769.

The MD simulations and NMR studies of the uncomplexed inhibitor showed that the five-membered ring can adopt two different conformational families. In the bound state, however, it is restricted to a single conformation, which is different from the conformations observed for the free ligand. This finding is surprising because it is generally believed that potent inhibitors are complexed in their ground state conformations. Probably, the flexibility of five membered rings renders the energy barrier for the conformational change relatively low.

Compound **2** was designed in such a way that its benzyl moiety can interact with aromatic residues of the binding site of the enzyme thereby increasing its affinity. However, it was found that this compound has a slightly reduced affinity indicating that the benzyl group cannot make favorable interactions with the enzyme. The unexpected finding could be rationalized by careful examination of the crystal structure of dGMII with **2**. Thus, the five-membered ring of compounds **1** and **2** were identically positioned in the binding site of dGMII. The distance between the centroid of the aromatic ring of compound **2** and Tyr269 was such that no edge to face binding interactions could be made. The unexpected orientation of the aromatic ring of **2** could be rationalized by an

intramolecular S---H---Ar type hydrogen bond between the thiomethyl moiety and the phenyl ring.

3.8 Experimental Procedures

Compounds **1-3** were prepared by reported procedures.^{84, 87, 119} Inhibition constants were determined as detailed in Li *et al.*¹⁵³

3.8.1 Crystallization, Data Collection and Structure Refinement

Measurement of inhibition, crystallization, data collection and structural refinement were carried out essentially as outlined by Kuntz *et al.*⁸² with the exceptions noted below. Inhibitors were dissolved at 100 mM in water (**1**) or methanol (**2**). Crystals of dGM2 were grown up overnight, washed with phosphate buffered reservoir solution and soaked with 10 mM **1** for at least 3-6 hrs. **2** was co-crystallized with dGMII in Tris-buffered reservoir solution without phosphate washing.⁸¹ Crystal quality was assessed on our home source and data was collected on Beamline F1 at the Cornell High Energy Synchrotron Source. Approximately 400 frames with 0.5 degree oscillation/frame were collected for each dataset. Each of the structures was refined independently. The last stage involved addition of alternate conformations and low quality waters followed by energy minimization and individual B-factor refinement. The quality of the final model was assessed using a number of structure validation programs including MolProbity, WhatIf, and hetze.

3.8.2 Molecular Dynamics Simulations

The sander¹⁷¹ module of AMBER 7.0⁹⁷ in conjunction with PARM99 parameter set for proteins, was utilized in molecular dynamics simulations. A modified GLYCAM¹⁷²

parameter set for glycosides and glycoproteins was used for all three ligands. The X-ray crystal structures were protonated using the leap module in AMBER and were solvated by a 25 Å droplet of TIP3P⁹⁹ waters around the Zn⁺² ion. Initially the solvent positions were optimized by energy minimization followed by energy minimization of whole system. This was followed by MD simulations at 300 K for 10-ns. In each simulation the system was heated gradually to 300 K in 100-ps and then held at 300 K for the entire simulation. For all simulations, protein residues within a sphere of 10 Å (with Zn⁺² ion as the center of the sphere), all waters and ligands were allowed to move. All other atoms were frozen to their positions in the crystal structures.

Simulations of free ligands were performed for 5-ns, under periodic boundary conditions at constant pressure. These simulations followed similar protocols for energy minimizations as used for the simulations of protein-bound ligands. The initial conformations of ligands in these simulations were kept same as observed in the crystal structure. In order to determine hydrogen bond occupancies, hydrogen bonding interactions were assumed to be present if the participating heavy atoms were 4 Å apart and the angle between the heavy atoms and the donating hydrogen was 60°. All MD simulations used an integration time step of 2 fs and scaling of 1-4 electrostatic and van der Waal interactions by standard values of 1/1.2 and 1/2.0, restraint of all hydrogen-containing bonds through the SHAKE algorithm¹⁷¹ and a cutoff of 8-Å for all non-bonded interactions. The MD trajectories were analyzed using the carnal module in AMBER 7.0. The phase angles of puckering were computed using Cremer and Pople's parameters.¹⁷³

3.8.3 Geometry optimization of flap-up and flap-down conformers of mannosyl oxocarbenium ion and superimposition

All the geometry optimizations were performed with Gaussian 98 program¹¹² using density functional theory (B3LYP¹³⁹⁻¹⁴¹) and 6-31G* basis set.¹⁴² The optimized conformers of flap-up and flap-down oxocarbenium ions were determined by constraining the dihedral angle made by C-2, C-1, O-5 and C-5 to 0° and allowing all other parameters to optimize at BLYP/6-31G* level of theory. The hydroxyl groups of the resulting structures were placed in three different orientations representing three rotamers and the conformers were reoptimized without any restraints at B3LYP/6-31G* level. For flap-up conformer two- and for flap-down conformer three unique conformers were identified with different orientations of hydroxy oxygen atoms. For each conformer, the C-2, C-1, O-5 and C-5 were in one plane with a distance between C1 and endocyclic oxygen of 1.27 Å, indicating oxocarbenium-like character. The lowest energy conformation of flap-up and flap-down conformers was used for superimposition with inhibitors **1** and **2**. The covalent intermediate geometry was obtained from PDB 1QX1. The superimpositions were performed using Insight II 2000.

3.9 Acknowledgement

The authors wish to thank the staff of CHESS for data collection time and support. The authors are also grateful for financial support for this work by NCI of NIH (5U01CA91295) and the Canadian Institutes of Health Research.

3.10 Supporting Information

Protein coordinates and structure factors are available from the Protein Data Bank. The PDB IDs are 2F7O (Mannostatin A) and 2F7P (benzylated Mannostatin A).

CHAPTER 4

CATALYTIC MECHANISM OF GOLGI α -MANNOSIDASE II: A QUANTUM

MECHANICAL STUDY

4.1 Abstract

A high-level quantum mechanical (QM) investigation of the hydrolysis reaction catalyzed by Golgi α -mannosidase II (GMII), which acts late in the *N*-glycan biosynthesis pathway, has been conducted. In all, four models have been studied, which differ in the number of atoms and the overall charge. Best results were obtained for the model, which contained explicit water molecules. These calculations indicate that in the transition state of the glycosylation reaction, the mannopyranose ring adopts a conformation that lies between an ideal $B_{2,5}$ boat conformation and 1S_5 skew boat conformation. It has also been shown that the transition state conformation of the sugar ring resembles oxacarbenium ion. In the case of deglycosylation step, the sugar ring adopts a conformation between $B_{2,5}$ and 0S_2 skew boat conformation. The glycosyl-enzyme covalent intermediate displays a conformation close to $B_{2,5}$ boat conformation, and is in excellent agreement with the X-ray structure of trapped covalent intermediate. Finally, the bound conformations of swainsonine and mannosatin A have been compared. These superimposition studies support long held view that swainsonine and mannosatin A are transition state mimics.

4.2 Introduction

Glycosidases are enzymes that catalyze the cleavage of glycosidic bonds and play critical roles in a number of biological processes. Inhibitors of these enzymes have garnered much attention and are currently used for the treatment of diabetes, viral infections and Gauchers disease.⁶⁻¹⁰ Furthermore, inhibition of the mannose trimming enzyme human Golgi α -mannosidase II (GMII; mannosyl-oligosaccharide 1,3-1,6-

α -mannosidase II; E.C. 3.2.1.114), which acts late in the *N*-glycan processing pathway, provides a route to blocking the oncogene-induced changes in cell surface oligosaccharide structures.^{61, 63, 113, 148} GMII selectively cleaves $\alpha(1-3)$ and $\alpha(1-6)$ mannosyl residues present in its natural substrate GlcNAcMan₅GlcNAc₂.¹⁴⁹ It is a retaining Family 38 glycosylhydrolase, which employs a two-stage mechanism (Figure 4.1) involving two carboxylic acids positioned within the active site which act in concert: one as a catalytic nucleophile and the other as a general acid/base catalyst.^{12, 14, 19, 114, 115} Protonation of the exocyclic glycosyl oxygen of a substrate molecule leads to bond-breaking and simultaneous attack of the catalytic nucleophile to form a glycosyl enzyme intermediate. Subsequent hydrolysis of the covalent intermediate by a nucleophilic water molecule gives an α -mannose product with overall retention of configuration. Studies with 5-fluoro pseudo-substrates and deuterium labeled substrates have shown that the transition states on either side of the covalent intermediate have marked oxacarbenium ion character.^{12, 14, 19, 38, 114, 115} Furthermore, X-ray crystal structures of the wild type and a mutant *Drosophila melanogaster* GMII (dGMII) in which the acid/base catalyst has been removed, with fluorinated sugar analogs have revealed that the glycosyl enzyme intermediate adopts a distorted ¹S₅ skew boat conformation.³⁸ In this conformation, the leaving group is placed anti-periplanar to the lone pair of the ring oxygen, a requirement for the departure of the leaving group according to Deslongchamp's anti-periplanar lone-pair hypothesis.⁷⁹ Furthermore, steric clashes between the *syn*-hydrogens at C-3 and C-5 and the attacking water are minimal in the ¹S₅ skew boat conformation.

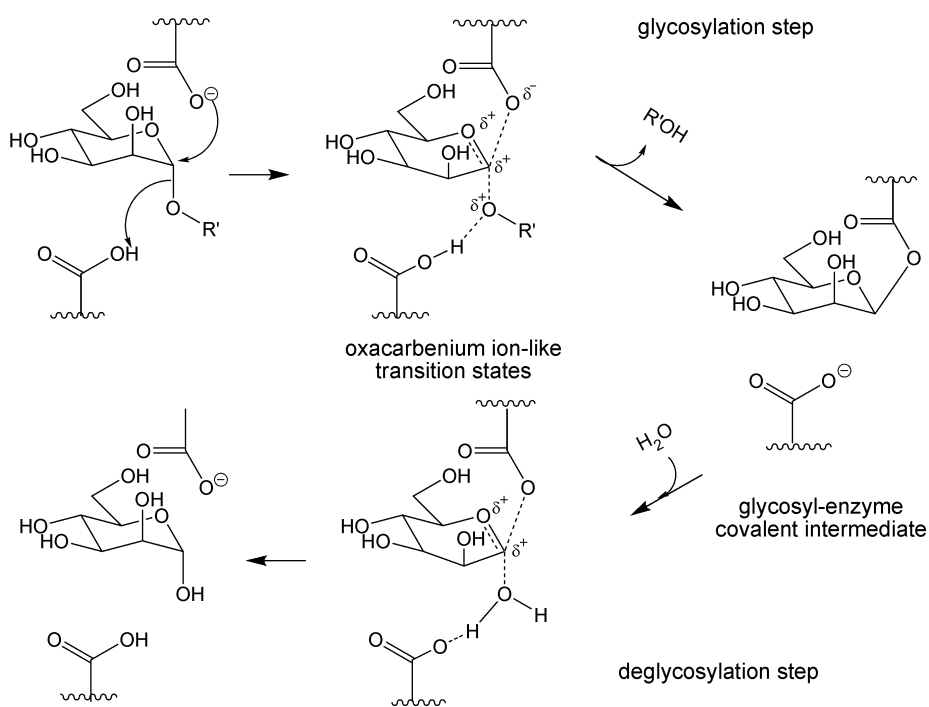


Figure 4.1. General double displacement mechanism proposed for retaining mannosidases.

Potent inhibitors of glycosidases are believed to mimic oxacarbenium ion-like transition states.^{12, 14, 19, 114, 115} The inhibitory activity of the natural product swainsonine has long been attributed to the resemblance of its 5-membered ring to a flattened six-membered ring mannosyl oxacarbenium ion. In fact, the crystal structure of swainsonine complexed with dGMII shows the inhibitor to be tilted in such a way as to bring the equivalent of its anomeric carbon close to the presumed catalytic nucleophile.⁷⁵ While similarities between swainsonine and mannostatin to the trapped covalent intermediates have recently been shown,¹⁷⁴ it is still unclear which conformation is adopted by the mannopyranose ring at the transition state, and whether potent inhibitors of GMII mimic the transition state.

In principle, computational methods are capable of determining enzymatic catalytic mechanisms to an appropriate level of detail when used in complement with experiments. However, formidable problems have had to be overcome in order to elucidate the mechanism using computational methods. The central role of transition metal atom in the active site chemistry demand use of *ab initio* quantum mechanical methods is the desired level of accuracy is to be achieved. While significant progress has been made in semiempirical methods and force field methods, these methods are system-specific and often require parameterization of the system under consideration.¹⁰⁰ The diverse nature of transition metals (structurally and electronically) makes it difficult to describe any system containing a transition metal atom with a set of universal parameters.^{175, 176} Furthermore, the number of atoms that can be treated by *ab initio* methods, although has increased substantially in recent years, is still limited. The selection of model thus becomes critical as inclusion of large number of atoms can lead to intractable CPU times. On the other hand, smaller model may not be sufficient to produce reasonable results as it lacks explicit effects of the protein residues on the active site chemistry.

Over past few years, effective computational methods have emerged to address these problems. The widespread use of density functional theory (DFT)^{177, 178} deploying gradient-corrected and hybrid functionals has demonstrated that transition metal systems can be treated in a reasonably accurate, yet cost-effective fashion (for review see reference¹⁰⁰ and references there in). Advances in DFT-based algorithms, along with dramatic reductions in the cost/performance of computational hardware, allow on the order of 150 – 200 atoms to be modeled at a quantum chemical level. Progress has also

been made specifically in the treatment of transition metals, including areas such as construction of an improved initial guess.¹⁷⁹ While the accuracy of DFT methods is best established for organic systems, a substantial number of comparisons have been made between theory and experiment (see reference¹⁰⁰ and references there in). Furthermore, it has been shown that Becke's three-parameter hybrid exchange functional¹³⁹ gives notable improvements in metal-ligand bond energies. Similar trend was observed in benchmark calculations using small organic molecules.¹⁰⁰

4.3 Computational Procedure and Models Used

In this work, we have investigated the mechanism of the hydrolysis reaction catalyzed by GMII using QM methods. The general strategy employed for this purpose includes four major steps: 1. docking the substrate into the active site of GMII; 2. truncation of the active site to create a model of reasonable size; 3. performing a relaxed geometry scan along a pre-defined reaction coordinate; and 4. optimization of the approximate geometries of the intermediates predicted in the scan. Tvaroska et al. have successfully used this strategy to determine the catalytic mechanism of glycosyl transferases.¹⁸⁰⁻¹⁸²

4.3.1 Docking of 1-methyl mannopyranoside into the active site of dGMII

In this study, 1-methyl mannopyranoside was used as the substrate. The substrate was placed in ⁴C₁ conformation and was optimized at B3LYP/6-31G** level using Gaussian98 program.¹⁸³ The optimized structure of 1-methyl mannopyranoside was docked in to the active site of dGMII by the procedure explained as follows.

Preparation of ligand and receptor molecules for docking – The crystal structure of dGMII (PDB id: 1HTY⁷⁵) was used as a model for macromolecule in docking experiments. The protein target, dGMII and the ligands were prepared for docking using AutoDock 3.0.5.^{90, 144} Charges were assigned using the Kollman algorithm.¹⁴⁵ Atomic solvation parameters and fragmental volumes were determined using Addsol programs available in AutoDock. AutoTors was used to define torsional angles in the ligand. Polar hydrogen charges of Gasteiger type¹⁴⁶ were assigned and the non-polar hydrogens were merged with the carbons. The macromolecule was kept rigid in all the docking simulations.

Docking simulations – Grid maps for docking simulations were generated with 40 grid points (with 0.375 Å spacing) in x, y and z direction, by Autogrid program. The center of the grid was positioned at the Zn⁺² ion (Zn1102). Lennard-Jones parameters 12-10 and 12-6 (supplied with the program package) were used for modeling H-bonds and van der Waals interactions, respectively. The distance dependant dielectric permittivity of Mehler and Solmajer¹⁴⁷ were used for the calculations of the electrostatic grid maps. The genetic algorithm (GA) and Lamarckian genetic algorithm with the pseudo-Solis and Wets modification (LGA/pSW) methods were used with the default parameters. For all the simulations, the populations in the genetic algorithm were 50 and each simulation comprised of 2.5×10^5 energy evaluations. Each docking experiment consisted of a series of 100 simulations.

The docking experiments resulted in exclusively one docking mode. In this orientation, the mannopyranosyl ring is stacked against the aromatic ring of Trp95. This type of interaction is common for several carbohydrate-protein complexes and is an

important interaction for carbohydrate recognition.^{134, 150-152} The 2- and 3-hydroxyl groups are coordinated to Zn⁺² ion, whereas 4-hydroxyl group forms a hydrogen bond with the carboxylate oxygen atom of Asp472.

4.3.2 Selection of the model

In the case of quantum mechanical calculations, the selection of the model used is critical, as the size of the model affects the required time and the accuracy of calculations. However, the selection of residues to be included in the model is not obvious. We have used four models, which differ in the number of atoms and overall charge (Table 4.1) in this study.

Table 4.1. Different models used in the computational study of the catalytic mechanism of GMII.

	Model 1	Model 2	Model 3	Model 4
Number of atoms	76	130	160	150
Protein Residues	Asp92, Asp204, Asp341, Asp472, Trp95	Model 1 + Ile96 and Arg228	Model 2 + His90 and His471	Model 1 + Ile96, His90, His471 and 4 water molecules
Overall charge on the model	-1	0	0	-1
Zn coordination sphere	Asp92, Asp204 and <i>cis</i> -diol in the substrate	Same as Model 1	Asp92, Asp204, His90, His471 and <i>cis</i> -diol in the substrate	Same as Model 3
Level of theory	B3LYP/LACVP*	B3LYP/LACVP*	B3LYP/6-31G** (LACVP** for zinc)	B3LYP/6-31G** (LACVP** for zinc)

4.3.3 Performing a relaxed geometry scan

The catalytic mechanism was investigated using relaxed geometry scans, which include finding minimum-energy geometries while holding a particular coordinate fixed to various values. Typically, this coordinate is the distance between the atoms involved in the process of bond formation or bond breaking. In the case of GMII, each step of the double displacement reaction can be represented as a function of different reaction coordinates. For example, the glycosylation step can be represented as a function of two reaction coordinates (Figure 4.2): the distance between the nucleophilic oxygen of Asp204 and the anomeric carbon in the substrate, and the distance between the anomeric oxygen and the proton from the general acid Asp341. The first coordinate mimics the formation of bond between the anomeric carbon and the catalytic nucleophilic oxygen whereas the second coordinate mimics the protonation of the leaving group. During a relaxed geometry scan, these distances will be changed and corresponding potential energy is calculated. The potential energy of the system can then be represented as a function of the coordinates in a three-dimensional plot. Such a two dimensional, relaxed geometry scan would result in the prediction of the alternative reaction pathways. Such geometry scans are useful to locate the approximate geometries of the Michaelis complex, the product of the catalytic reaction and other reactive intermediates observed along the reaction pathway. The exact structures and energies can be obtained by optimizing the approximate geometries without any restraints on the distances that have been used as reaction coordinates.

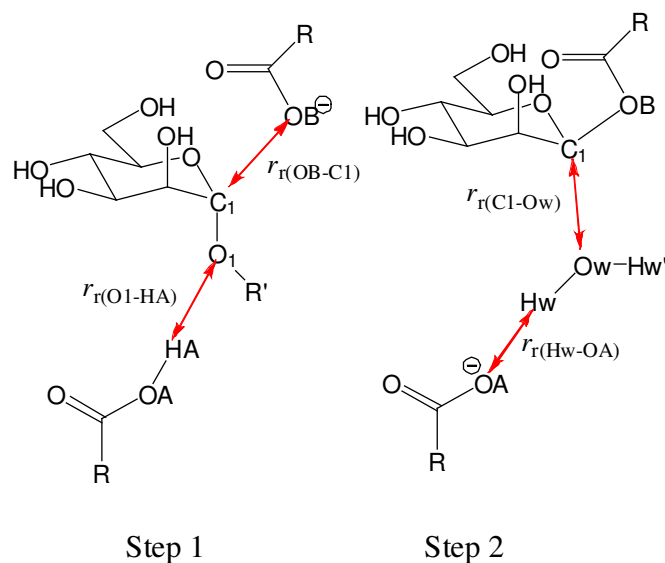


Figure 4.2. General representation of the relaxed geometry scans used in the investigation of the catalytic mechanism of GMII. Each step can be represented with the help of two reaction coordinates.

4.4 Model 1

4.4.1 Description of the Model and Computational Procedure

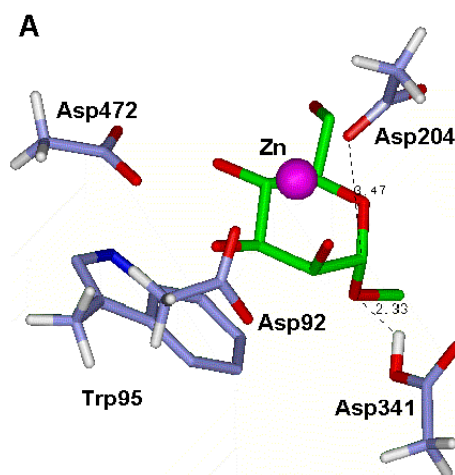


Figure 4.3. Model 1 used for the quantum mechanical study of the catalytic mechanism of GMII. The model consists of 76 atoms and the overall charge on the model is -1 . The model includes the substrate, 1-methyl mannopyranoside; Zn^{+2} ion; four aspartic acid residues (Asp92, Asp204, Asp341, and Asp472); and Trp95.

In this investigation, the structural model used to analyze computationally the catalytic mechanism of GMII consists of minimum essential residues, or their fragments that are involved in the reaction and are in direct contact with the substrate. The reaction site model, Model 1, consists of 76 atoms and contains: the substrate, 1-methyl mannopyranoside; Zn⁺² ion; four aspartic acid residues (Asp92, Asp204, Asp341, and Asp472); and Trp95 (Figure 4.3). The overall charge on the model is -1. All protein residues are truncated at the C β carbon atoms and are frozen at their positions in the X-ray structure of dGMII (PDB ID 1HTY). All C β atoms were represented by methyl groups. Furthermore, all atoms in Trp95 were frozen at the crystallographic position. Since Asp341 has been identified as the general acid-base catalyst in GMII,⁷⁵ this residue is protonated in the model and acts as general acid residue in the glycosylation step of the double displacement mechanism.

In the case of the glycosylation step, two distances were considered as the reaction coordinates: the distance (r_1) between the anomeric carbon and the catalytic nucleophilic oxygen Asp204 OD1, and the distance (r_2) between the anomeric oxygen and the proton from the general acid residue Asp341. The relaxed geometry scan was performed at DFT/B3LYP/LACVP* level of theory. During the scan, distance r_1 was decreased from 2.93 Å to 1.33 Å by 0.2 Å, whereas the distance r_2 was decreased from 1.69 Å to 0.89 Å by 0.2 Å. The approximate geometries obtained from this scan were further optimized at DFT/B3LYP/LACVP*. LACVP* uses 6-31G* basis for atoms up to Ar in the periodic table, whereas for zinc it uses effective core potential.

4.4.2 Results and Discussion

The glycosylation step of the double displacement reaction mechanism is described by means of a potential energy surface (PES) represented in the form of two-dimensional reaction coordinate contour diagram (Figure 4.4). The x-axis of the plot represents distance r_2 , which mimics the protonation of the leaving group. The y-axis of the plot represents distance r_1 , which mimics the formation of the covalent linkage between the anomeric carbon and the catalytic nucleophilic oxygen of Asp204.

The mannopyranose ring adopts a $B_{2,5}$ boat conformation at the Michaelis complex (MC). In this conformation, the 2- and 3-hydroxyl group coordinate with the Zn^{+2} ion in the active site. Furthermore, the anomeric oxygen forms a hydrogen bond with the proton from general acid Asp341 (1.7 Å), suggesting that this interaction may facilitate the protonation of the leaving group and its subsequent departure. The 4-hydroxyl group also forms a strong hydrogen bond with Asp472.

While it was possible to locate the Michaelis complex MC, it was not possible to identify the transition state and the glycosyl-enzyme covalent intermediate using the PES obtained from the geometry scan of Model 1. The PES displayed a plateau at about 45 kcal mol⁻¹, which ranged from $r_1 = 1.93$ Å to 1.43 Å and $r_2 = 1.29$ Å to 0.89 Å. Further approach of the catalytic nucleophile towards the anomeric carbon resulted in the higher potential energy (more than 48 kcal mol⁻¹). Furthermore, all attempts to optimize the transition state (TS1) and the glycosyl-enzyme covalent intermediate (CINT) failed. These calculations resulted in the Michaelis complex structure.

In order to confirm our results, we performed another PES scan where we changed r_1 from 1.93 Å to 1.43 Å by 0.05 Å and r_2 from 1.29 Å to 0.89 Å by 0.05 Å. This is the region where the first PES scan displayed a plateau. The analysis of the

refined PES (Figure 4) revealed three intermediates with identical energies (45.6 kcal mol⁻¹, 45.9 kcal mol⁻¹ and 46.6 kcal mol⁻¹). Optimization of all three intermediates resulted in the Michaelis complex.

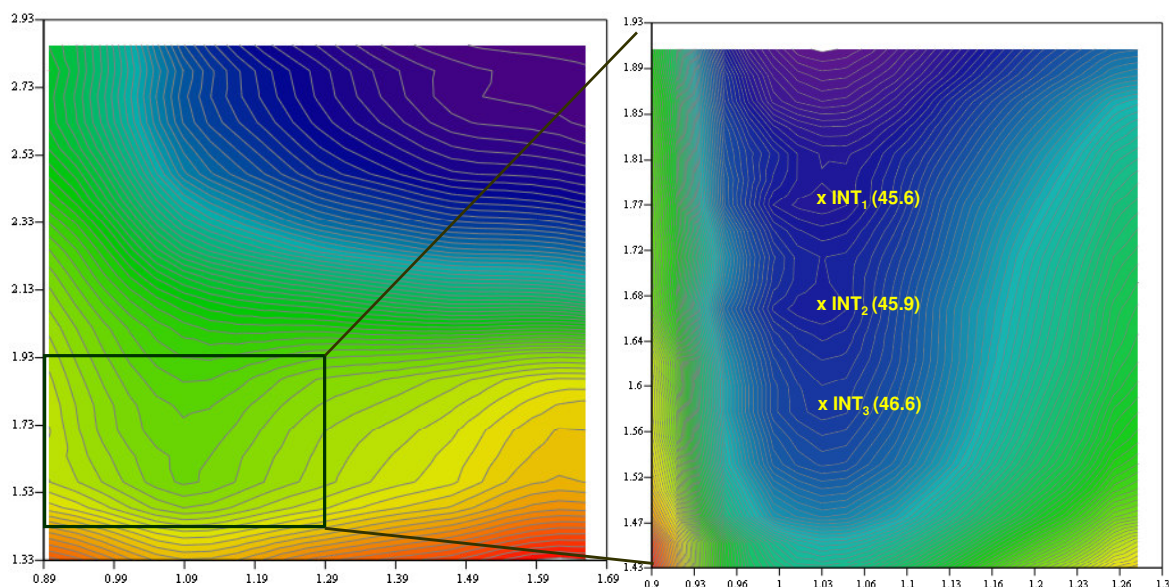


Figure 4.4. Potential energy surface obtained from the two-dimensional scan of Model 1 at DFT/B3LYP/LACVP* level (purple – lowest energy region, orange – highest energy region). Initial PES scan resulted in single reaction pathway. However, the approximate locations of the transition state and the glycosyl-enzyme covalent intermediate could not be identified. A refined scan resulted in three intermediates of identical energies. These intermediates converged to the structure of the Michaelis complex following the optimization at the same level.

The fact that the identification of approximate location of TS1 and CINT was not possible on the PES obtained from Model 1 suggests that Model 1 probably is an insufficient model to determine the catalytic mechanism of GMII. Furthermore, the potential energy (~ 45 kcal mol⁻¹) in the region, where the transition state is expected, is high for an enzymatic catalytic reaction. This may be the result of the lack of flexibility in the model. The model consists of protein residues that are truncated at the C β carbon

atoms and frozen at their crystallographic positions. In reality, the backbone of the protein is relatively stable than the side chain atoms. Thus, truncating the protein residues at C β carbon atoms and freezing them at their crystallographic positions may not reproduce the protein environment required for the reaction.

4.5 Model 2

4.5.1 Description of the Model and Computational Procedure

In order to increase the flexibility of protein residues, we increased the size of the model. In Model 2 (Figure 4.5), all protein residues were truncated at the C α carbon atoms. The C α carbon atoms of all residues were represented by a methyl groups and were frozen at the crystallographic positions. In addition to this, we also included Arg228 and Ile96 in the model. Arg228 is located close to 6-hydroxyl group, suggesting a possible hydrogen bond between the two moieties. Such an interaction may also affect the orientation as well and the conformation of the mannopyranosyl ring in the binding site. Furthermore, all atoms in Trp95 in Model 1 were fixed to their crystallographic positions. This was done to avoid movement of Trp95 from its original position that may result from the conformational changes in the substrate. However, a careful analysis of the X-ray structure of dGMII revealed that Ile96 is positioned just above the aromatic ring of Trp95. This arrangement probably locks Trp95 in such a way that it remains stacked against the mannopyranosyl ring in the substrate during the course of the reaction.

The reaction coordinates chosen for the PES scan were same as that in the PES scan of Model 1. All optimizations were performed at DFT/B3LYP/LACVP* level of

theory. During the PES scan for the glycosylation step, r_1 was changed from 3.28 Å to 1.48 Å by 0.2 Å. The second reaction coordinate r_2 was decreased from 2.15 Å to 0.85 Å by 0.2 Å.

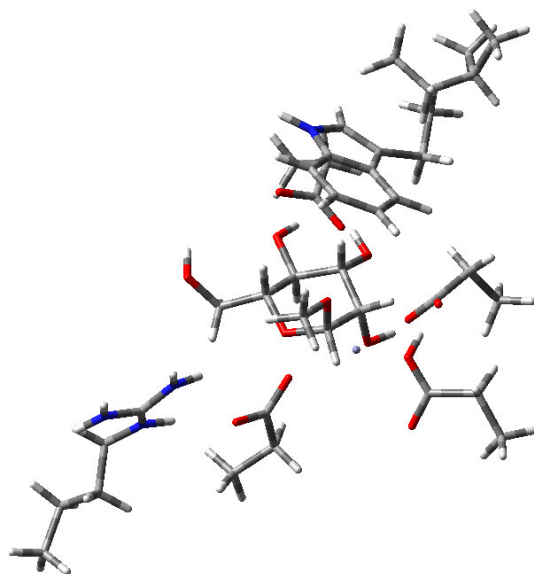


Figure 4.5. Model 2 used for the quantum mechanical study of the catalytic mechanism of GMII. The model consists of 130 atoms and the over all charge on the model is 0. The model includes the substrate, 1-methyl mannopyranoside; Zn^{+2} ion; four aspartic acid residues (Asp92, Asp204, Asp341, and Asp472); Trp95; Ile96 and Arg228.

4.5.2 Results and Discussions

Unlike Model 1, the PES scan of Model 2 displayed approximate location of MC, CINT and two transition states located very close to each other (Figure 4.6). In the case of Model 2, the sugar ring adopts $B_{2,5}$ conformation in the Michaelis complex MC. Similar conformation was also observed in the case of Model 1. All interactions made by different functionalities in the substrate are similar to those observed in Model 1. The inclusion of Ile96 proved to be important, as this residue seem to facilitate the stacking

interaction of the substrate with Trp95, by avoiding the movement of Trp95 away from the sugar ring. Arg228, however, does not form a hydrogen bond with 6-hydroxyl group.

Unlike Model 1, it was possible to identify two transition states for the glycosylation step. Both transition states, when optimized further, converged to a single structure (TS1), suggesting that there is only one reaction pathway. However, the calculated reaction barriers are very high ($61.5 \text{ kcal mol}^{-1}$) for either structure. The transition state conformation is slightly twisted $B_{2,5}$ boat conformation and lies between an ideal $B_{2,5}$ and an ideal 1S_5 skew boat conformation. In this conformation the distance r_1 is 1.97 \AA . Furthermore, the glycosidic bond is completely cleaved in the transition state suggesting the dissociative nature of the transition state as proposed by experimental studies.²⁹

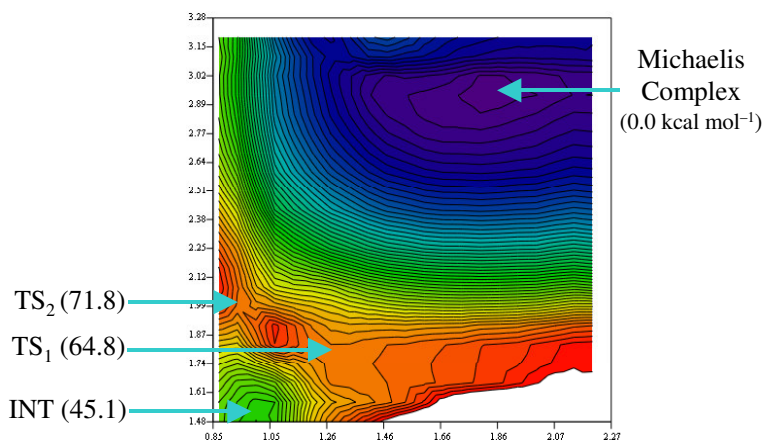
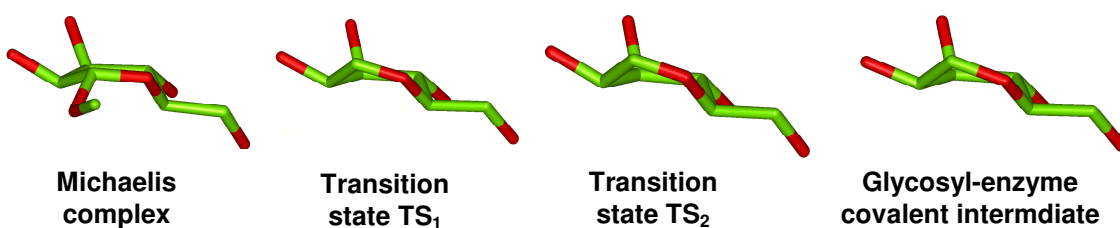


Figure 4.6. Potential energy surface obtained from the two-dimensional scan of Model 2 at DFT/B3LYP/LACVP* level (purple – lowest energy region, white – highest energy region)

region). The Y-axis of the plot represents the distance between the anomeric carbon and the catalytic nucleophile, whereas the x-axis represents the distance between the proton from general acid catalyst and the anomeric oxygen. The approximate locations of the Michaelis complex, glycosyl-enzyme covalent intermediate and two transition states that are close to each other could be identified. However, computed reaction barriers were very high. Optimized structures of the mannopyranose ring in the Michaelis complex, transition states and the covalent intermediates are shown at the top. Optimization of two transition state structure converged into a single structure suggesting that only one reaction pathway is possible. This pathway is a function of the distance between the anomeric carbon and the catalytic nucleophile.

Interestingly, in the optimized structure of TS₁, the carboxylate oxygen of Asp472 abstracts the proton from 3-hydroxyl group following a strong ionic linkage formation between the Zn⁺² ion and the 2-hydroxyl oxygen. This may be the result of an incomplete coordination sphere for the Zn⁺² ion. In the X-ray structure of dGMII complexed with swainsonine, the Zn⁺² ion is coordinated to Asp92, Asp204, His90 and His471. In addition to this, the *cis*-diol moiety in swainsonine coordinates with the Zn⁺² ion resulting in T6 geometry of coordination for the Zn⁺² ion. In the case of Model 2, the histidine residues, which coordinate with the Zn⁺² ion, were not included. This may result in larger partial charge on zinc and stronger attraction between the Zn⁺² ion and the functionalities coordinating with zinc. Such an interaction would result in tighter binding of the substrate, which may prevent the substrate from leaving the binding site following the hydrolysis reaction. The optimized structure of CINT, which is 41.4 kcal mol⁻¹ higher in energy than the MC, displayed similar proton abstraction.

The PES scan for Model 2 revealed that increase in the size affected the energy profile when compared with Model 1. While it was possible to identify the transition state for the glycosylation step and the glycosyl-enzyme covalent intermediate on the two-dimensional PES for Model 2, the reaction barrier and the reaction energy were too high for the reaction to be feasible under physiological conditions. Furthermore, abstraction of

proton from 3-hydroxyl oxygen by Asp472 suggests that complete coordination sphere of the Zn^{+2} ion must be included in the calculations.

4.6 Model 3

4.6.1 Description of the Model and Computational Procedure

This model consists of His90 and His471 in addition to all residues in Model 2 (Figure 4.7). Introduction of these two histidine residues completes the coordination sphere for the Zn^{+2} ion. Furthermore, we performed one-dimensional relaxed geometry scan where we chose the distance between the anomeric carbon and the nucleophilic oxygen as the reaction coordinate. This decision was based on the fact that the PES for both models previously studied did not display multiple reaction pathways for the glycosylation reaction. The observed reaction pathway in either case could be represented as the function of the distance between the anomeric carbon and the catalytic nucleophilic oxygen of Asp204. Thus, to avoid unnecessarily long computer time we have performed one-dimensional scan along this distance.

The geometry scan was performed at DFT/B3LYP/6-31G**. The Zn^{+2} ion was represented by LACVP**, which includes the effective core potential.¹⁸⁴ During the scan, the distance between the anomeric carbon and the catalytic nucleophile is decreased from 3.91 Å to 1.41 Å by 0.2 Å. The approximate geometries of MC, TS1 and CINT were further optimized at the same level.

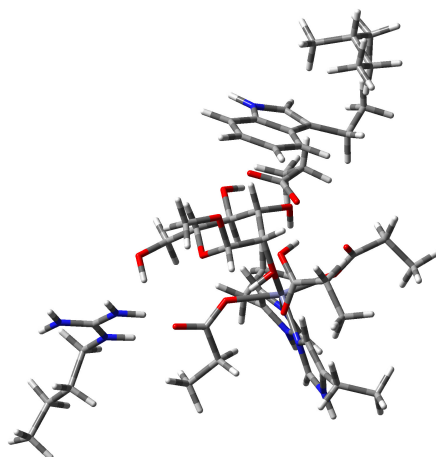


Figure 4.7. Model 3 used for the quantum mechanical study of the catalytic mechanism of GMII. The model consists of 160 atoms and the over all charge on the model is 0. The model includes the substrate, 1-methyl mannopyranoside; Zn⁺² ion; four aspartic acid residues (Asp92, Asp204, Asp341, and Asp472); Trp95; Ile96, Arg228, His90 and His471.

4.6.2 Results and Discussio

The energy profile obtained from the one-dimensional scan for Model 3 is depicted in Figure 4.8. It was possible to identify the MC, TS1 and CINT from the one-dimensional energy profile. As the geometry scan progressed, the conformation of the mannopyranosyl ring changes from ⁴C₁ to B_{2,5} at the lowest energy structure. This structure was further optimized as the Michaelis complex which resulted in slightly twisted B_{2,5} boat conformation of the mannopyranose ring in the substrate. In this conformation, the 2- and 3- hydroxyl oxygen atoms are coordinated with the Zn⁺² ion. Furthermore, interactions observed in previous models were also retained in the optimized structure of the Michaelis complex MC.

The calculated barrier for the reaction is 46.5 kcal mol⁻¹ at DFT/B3LYP/6-31G** level. In the transition state TS1, the mannopyranosyl ring adopts a conformation close to

1S_5 skew boat conformation. Interestingly, the proton abstraction observed in Model 1 and Model 2 studies was not observed in Model 3. The proton of 3-hydroxyl group forms a hydrogen bond with Asp472. Furthermore, the dihedral angle between C-5, O-5, C-1 and C-2 atoms is 2.2° , suggesting a strong double bond character in the bond between O-5 and C-1 atoms. Such an arrangement supports the maximum delocalization of the positive charge developed at the anomeric carbon during the formation of the transition state.

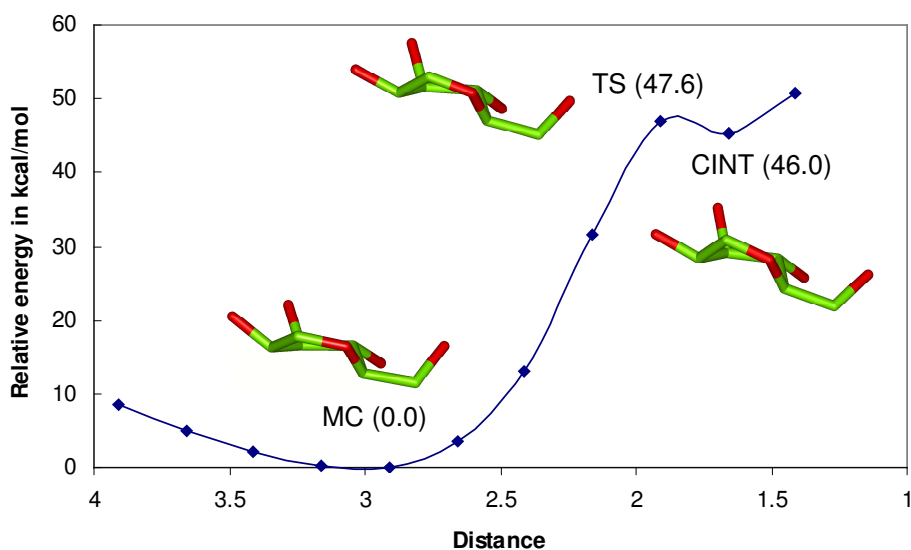


Figure 4.8. Potential energy profile obtained from the one-dimensional scan of Model 3 at DFT/B3LYP/6-31G** level (zinc is represented by LACVP** basis set) The approximate locations of the Michaelis complex, glycosyl-enzyme covalent intermediate and transition state could be identified. These approximate geometries were further optimized at same level. The geometries of the mannopyranose rings in the optimized structures have been shown.

The optimized structure of CINT displayed a skew boat conformation for the sugar ring, which lies between $B_{2,5}$ and 1S_5 conformations. X-ray structures of the wild type and a mutant dGMII in which the general acid/base catalyst has been removed, with

fluorinated sugar analogs have revealed that the glycosyl covalent intermediate adopts a 1S_5 skew boat conformation.³⁸ The optimized structure of glycosyl-enzyme covalent intermediate CINT provides an excellent opportunity to compare the bound conformation of the fluorinated sugar with that of the computed CINT conformation. Superimposition of two structures led to comparable geometrical parameters (Figure 4.9). However, the covalent bond between the catalytic nucleophile and the anomeric carbon is longer than that observed in the X-ray structure.

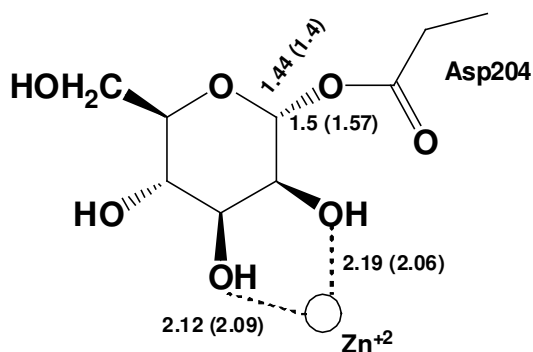


Figure 4.9. Comparison of the optimized structure of CINT with the X-ray structure of trapped covalent intermediate.

We have computed the Wiberg bond indices¹⁸⁵ for MC, TS1 and CINT (Figure 4.10), which shows the change in the bond order of O-5-C-1 bond and O-1-C-1 bond as the glycosylation progresses. An increased bond order for O-5-C-1 bond at TS1 suggests increased double bond character in this particular bond. The bond order of this bond decreases from 1.2 in TS1 to 0.99 in CINT indicating formation of an sp^3 hybridized carbon atom following formation of the glycosyl-enzyme covalent intermediate CINT. The natural population analysis (NPA) using NBO program¹⁸⁶ also suggested

delocalization of the positive charge between the endocyclic oxygen and the anomeric carbon (Figure 4.11).

While the computed energy barrier for the glycosylation step is still higher, the inclusion of two histidine residues, which coordinate with the Zn^{+2} ion, seems to prevent abstraction of the proton from 3-hydroxyl by Asp472. The higher barriers could be attributed to the lack of solvent effects, as Model 3 does not include water molecules. It is possible that water molecules present in the binding site stabilize the charge developed in the transition state, thus, reducing the activation barrier for the glycosylation step. For this reason we have investigated the catalytic mechanism of GMII using a model that included four water molecules in the binding site.

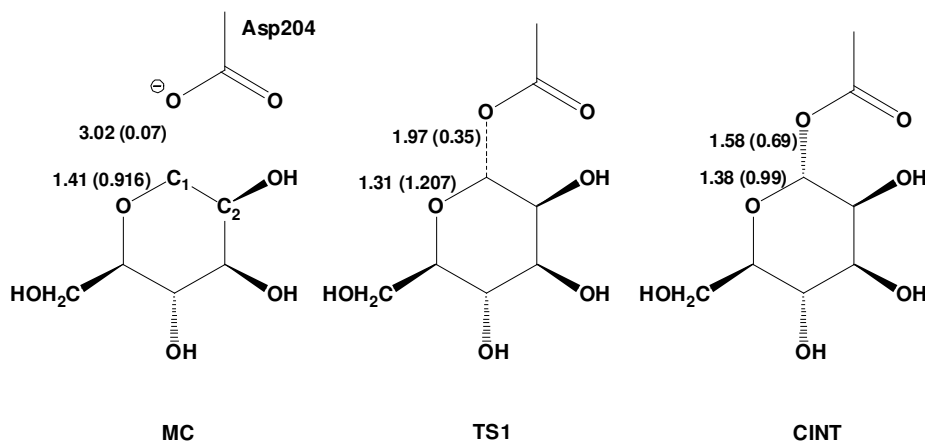


Figure 4.10. Bond order analysis for MC, TS1 and CINT obtained from QM study of Model 3. The bond distances are given for the O-5-C-1 bond and the bond between the anomeric carbon and the catalytic nucleophilic oxygen. Wiberg bond indices are given in the parenthesis. The increased sp^2 character in the O-5-C-1 bond in TS1 is clear from the reduced length of the bond and increased bond order.

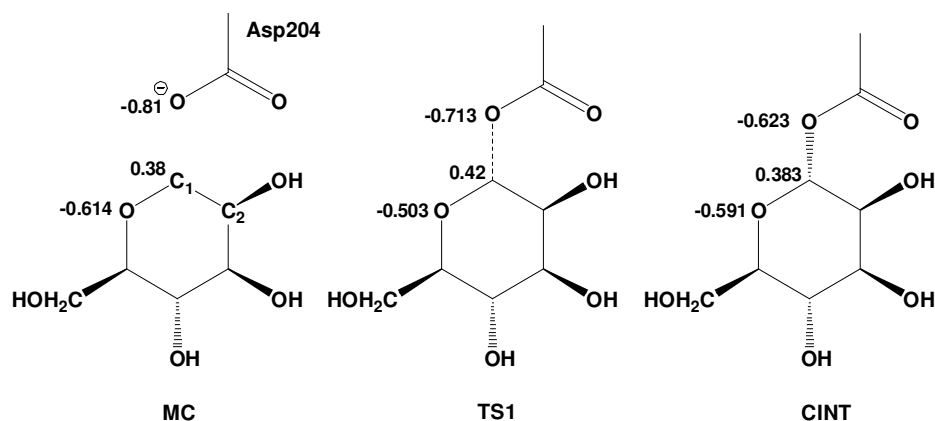


Figure 4.11. Natural population analysis for MC, TS1 and CINT obtained from QM study of Model 3. Increased charge on the ring oxygen indicates delocalization of the positive charge developed during the formation of the transition state.

4.7 Model 4

4.7.1 Description of the Model and Computational Procedure

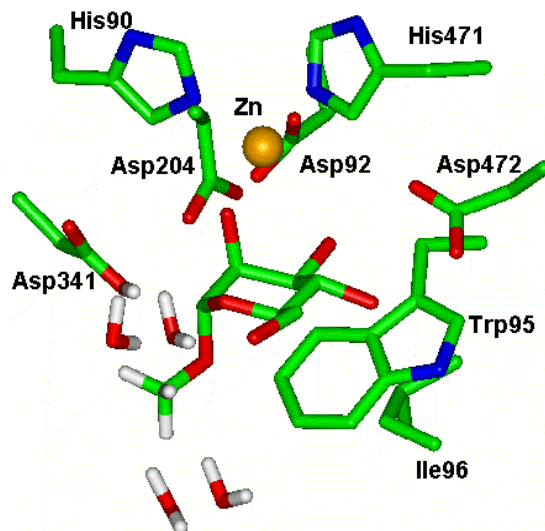


Figure 4.12. Model 4 used in the quantum mechanical (DFT/B3LYP/6-311++G**//DFT/B3LYP/6-31G**) analysis of the mechanism of hydrolysis catalyzed by GMII. Protein residues have been truncated at C α carbon, which are represented by methyl groups. The substrate is mimicked by 1-methyl mannopyranoside.

The fourth model used for investigating the catalytic mechanism of GMII consists of 150 atoms (Table 1, Figure 4.12). The overall charge on the model is -1 . This model contains four water molecules, which are conserved in the X-ray structures of swainsonine and mannostatin A complexed with dGMII. These water molecules were included to compute the effect of water on relative energies of all reactive species during the course of the hydrolysis reaction. The water molecules obtained from the X-ray structures do not contain hydrogen atoms. Hence, in the case of model 4, GWH utility in AMBER suite⁹⁷ of programs was used to add hydrogen atoms to the water molecules. This program adds hydrogen atoms depending on the electronic environment of water molecules. The computational protocol used for this model is the same as that used in the QM study of Model 3. In the case of the glycosylation step, the distance (r_1) between the anomeric carbon and the catalytic nucleophilic oxygen Asp204 OD1, which mimics the formation of a covalent bond between these two atoms, is considered as the reaction coordinate. During the scan, distance r_1 was decreased from 3.15 Å to 1.35 Å by 0.2 Å. For the deglycosylation step, the distance (r_2) between the anomeric carbon and the oxygen of the closest water molecule, which mimics the attack of water on CINT, is chosen as the reaction coordinate. All optimizations were performed at DFT/B3LYP/6-31G** level. Similar to Model 3, zinc was represented by LACVP** basis set which include effective core potential. Optimized structure of the glycosyl-enzyme covalent intermediate CINT is taken as the starting geometry for the relaxed geometry scan for the deglycosylation step.

4.7.2 Results and Discussion

The calculated energy profiles for the glycosylation and the deglycosylation steps are presented in Figure 15. For the glycosylation step, the calculated barrier is 15.8 kcal mol⁻¹ at B3LYP/6-311++G** level. The mannopyranose ring adopts an almost perfect ¹S₅ skew boat conformation at the Michaelis complex MC where atoms C-2, C-3, C-4 and O-5 are in one plane with the dihedral angle of -1.9°. In this case, the anomeric carbon is above while the C-5 atom is below the plane made by these four atoms. In the Michaelis complex MC, the mannopyranosyl ring is stacked against the Trp95 aromatic ring, a feature common in several carbohydrate-protein complexes.¹⁵⁰⁻¹⁵² The Zn⁺² ion in the active site coordinates with Nε2 nitrogen atoms of His90 and His471, and the carboxylate oxygens of Asp204 and Asp92. Furthermore, 2- and 3- hydroxyl groups coordinate with the Zn⁺² ion present in the active site, resulting in T₆ type of coordination geometry for Zn⁺² ion. Such coordination geometry has also been reported in many ligand-dGMII complexes where the ligands possessed a *cis*-diol moiety that coordinates with the zinc.^{38, 75, 80, 81} The orientation of the mannopyranosyl ring is further fixed by a strong hydrogen bond between 4-hydroxyl group and Asp472OD1 (1.8 Å between the hydroxyl hydrogen and carboxylate oxygen). In this conformation, the anomeric oxygen forms a very strong hydrogen bond (1.61 Å) with the proton from general acid Asp341, suggesting that this interaction may facilitate protonation of the leaving group and its subsequent departure.

The conformation of the transition state TS1 lies between an ideal ¹S₅ skew boat conformation and an ideal B_{2,5} boat conformation with the dihedral angle of 9.6° between atoms C-2, C-3, C-4 and O-5, suggesting a minor conformational change in the sugar ring form its conformation in the Michaelis complex. The bond between C-1 and O-1 atoms is

completely cleaved with these atoms separated by 2.38 Å. Furthermore, atoms C-5, O-5, C-1 and C-2 are co-planar with a dihedral angle of -0.5° , a condition which supports the maximum proposed sp^2 character on the anomeric carbon and the ring oxygen during the formation of the transition state. The 2- and 3-hydroxyl groups remain coordinated to Zn^{+2} ion at 2.18 Å and 2.14 Å, respectively, whereas the 4-hydroxyl group remained hydrogen bonded to carboxylate oxygen of Asp472.

The conformation of the mannopyranosyl ring further changes at the glycosyl-enzyme covalent intermediate (CINT) where it is closer to an ideal $B_{2,5}$ boat conformation. The relative energy of CINT is $4.8 \text{ kcal mol}^{-1}$ at B3LYP/6-311++G** level when compared with MC. Interestingly, the nucleophilic oxygen Asp204OD1 moves away from the Zn^{+2} ion after the formation of covalent linkage between the anomeric carbon and Asp204OD1 (Table 2). This movement is consistent with the X-ray structures of trapped covalent intermediates for dGMII and may be a result of decreased negative charge on the nucleophilic oxygen following the covalent bond formation.

For the deglycosylation step, the calculated barrier is relatively high ($30.0 \text{ kcal mol}^{-1}$) at DFT/B3LYP/6-311++G** level. The transition state TS2 conformation lies between an ideal $B_{2,5}$ boat conformation and oS_2 skew boat conformation. Interestingly, the dihedral angle between C-5, O-5, C-1, and C-2 is -24.5° as compared with -0.5° in TS1, indicating that these atoms are not co-planar as expected for an oxacarbenium ion-like transition state. Interactions made by 2-, 3- and 4-hydroxyl groups with protein residues were similar to those observed in TS1 and CINT.

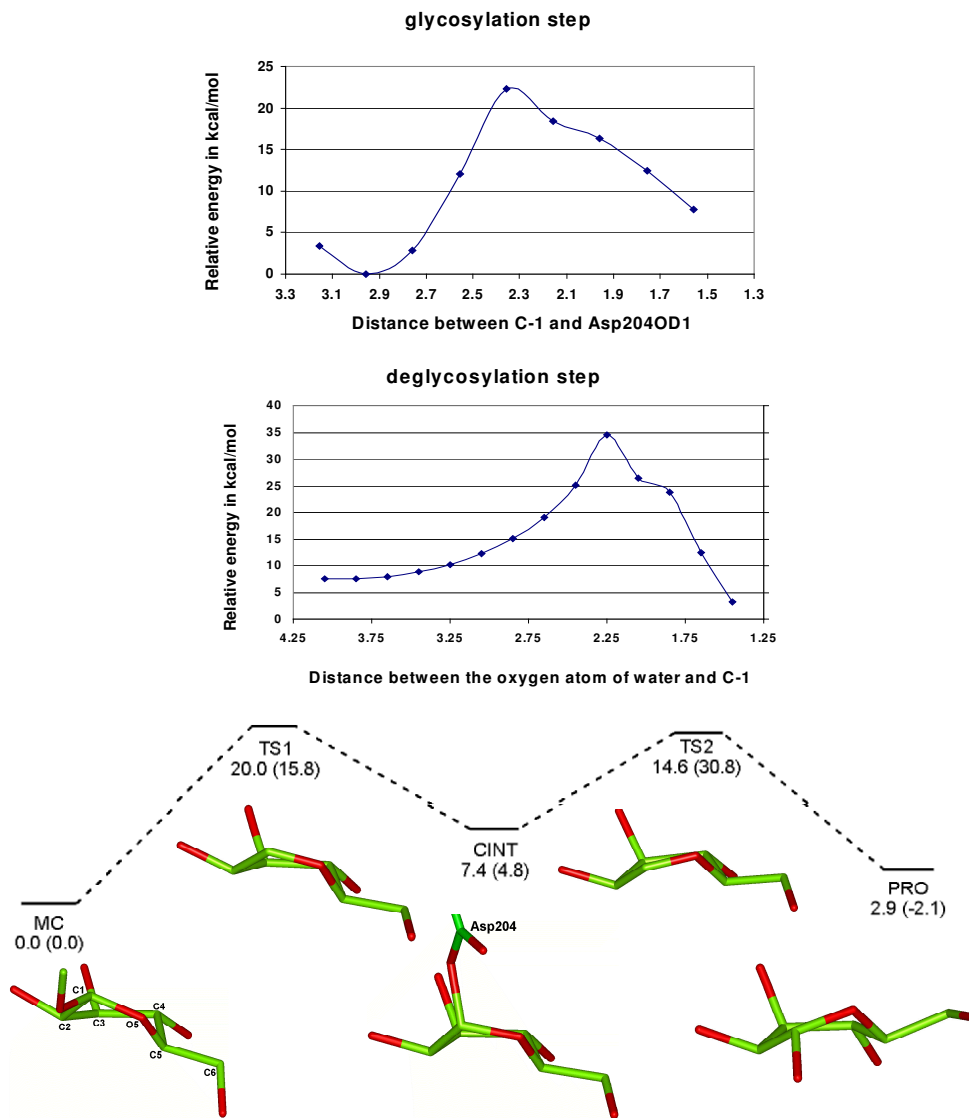


Figure 4.13. Energy profile and schematic representation of relative energies (in kcal mol⁻¹, DFT/B3LYP/6-31G** // DFT/B3LYP/6-311++G**) for the glycosylation and deglycosylation steps involved in the hydrolysis reaction catalyzed by GMII. Values in parenthesis are the single point energies at DFT/B3LYP/6-311++G**. The conformation of the mannopyranosyl ring in the Michaelis complex is ¹S₅. At the transition state the conformation lies between an ideal ¹S₅ and B_{2,5} boat conformation, with atoms C-5, O-5, C-1 and C-2 in one plane as expected for an oxacarbenium ion-like transition state. In the case of CINT the conformation was found to be slightly distorted B_{2,5} boat and was comparable to that in the trapped covalent intermediate (PDB id 1QWN). For the deglycosylation step, the transition state conformation lies between B_{2,5} and ⁰S₂ skew boat conformation while in the hydrolyzed product it was found to be very close to an ideal ⁰S₂.

The hydrolyzed product displayed a conformation very close to an ideal $^{\circ}S_2$ conformation with relative energy of $-2.1 \text{ kcal mol}^{-1}$ when compared with MC. In this structure, unlike CINT, the nucleophilic carboxylate oxygen Asp204OD1 again moves close to the Zn^{+2} ion and forms a T_6 type of geometry. Furthermore, the 4-hydroxyl group remained hydrogen bonded to carboxylate oxygen of Asp472.

Table 4.2. Computed (DFT/B3LYP/6-31G**) bond lengths for different geometries observed in the glycosylation step.

	Distances in Å					
	r_1	$r_{\text{C1-O1}}$	$r_{\text{O2-Zn}}$	$r_{\text{O3-Zn}}$	$r_{\text{204OD1-Zn}}$	C1-O5
Starting geometry	3.70	1.41	2.18	3.63	2.13	1.41
MC	3.11	1.42	2.19	2.12	2.07	1.43
TS1	2.42	2.38	2.18	2.14	2.14	1.28
CINT	1.49	3.02	2.12	2.11	2.66	1.39
TS2	2.16 ^a	3.02	2.21	2.15	2.09	1.29
PRO	1.42 ^a	3.57	2.2	2.11	2.08	1.41

^a Distance is between C-1 and the oxygen of attacking water molecule.

Analysis of important distances (Table 4.2) suggests that significant conformational changes occur during early stages of glycosylation step where the sugar donor undergoes distortion from the initial 4C_1 conformation, resulting in 1S_5 conformation in MC. It is known that glycosidases distort the substrate to yield the Michaelis complex structure. First proposed for the hen egg white lysozyme,²⁰ such substrate distortion has also been unambiguously observed in high-resolution X-ray structures of Michaelis complexes for two structurally unrelated endoglucanases (from glycosyl hydrolase families 5 and 7),^{21, 22} and hexosaminidase (family 20).²³

Furthermore, X-ray structure of Michaelis complex for Mannase 26A, which is a retaining endo- β -(1-4)-mannose, displayed 1S_5 conformation of the substrate.²⁴ During the initial optimization, similar distortion was observed in the mannopyranoside ring resulting in a $B_{2,5}$ conformation. This change in the conformation seems to be mainly controlled by the interaction between the C-3 hydroxyl oxygen and the Zn^{+2} ion. The distance between these atoms decreases from 3.63 Å in 4C_1 conformation to 2.12 Å in the MC (1S_5 conformation). Furthermore, in this conformation, C-2 hydroxyl group moves in pseudo-equatorial orientation as against axial orientation in 4C_1 conformation, thereby reducing the activation energy for the formation of the covalent glycosyl-enzyme intermediates. The distance between O-2 and Zn^{+2} ion, however, does not change (2.18 Å in 4C_1 to 2.19 Å in 1S_5 conformation) during this transformation. Thus, it appears that the coordination of C-2 and C-3 hydroxyl oxygen atoms with the Zn^{+2} ion controls the conformational itinerary in early stages of the hydrolysis reaction.

The role of Zn^{+2} ion in GMII has been recently proposed by Kuntz et al. based on the co-crystal structure of noeuromycin bound to dGMII⁸⁰ and previous crystallographic studies.^{38, 75, 80, 81} In addition to maintaining the deprotonated state of the catalytic nucleophile Asp204, it was proposed that Zn^{+2} ion drives the conformational itinerary of the substrate with the help of the interaction between C-2 and C-3 hydroxyl groups, and Zn^{+2} ion. Our calculations support this hypothesis. Furthermore, in 4C_1 conformation, O-2 is coordinated with Zn^{+2} ion resulting in T_5 geometry (square pyramidal) of zinc coordination sphere. This type of coordination geometry is one of the most common geometries observed in zinc binding proteins and was also proposed to be favorable compared to the T_6 octahedral geometry.⁷⁸ Substrate distortion driven by O-2 and O-3

interaction with Zn^{+2} ion, thus, helps achieving otherwise unfavorable T_6 coordination geometry. Moreover, natural population analysis (Table 4) reveals that the charge on zinc remains unchanged during the progress of reaction suggesting that the role of zinc is mainly structural and coordination of substrate with Zn^{+2} ion is essential for driving the conformational itinerary towards the transition state.

Table 4.3. Computed (DFT/B3LYP/6-31G**) dihedral angles for the mannopyranosyl ring along the reaction coordinate.

	Dihedral angle in °					
	C5-O5-C1-C2	O5-C1-C2-C3	C1-C2-C3-C4	C2-C3-C4-C5	C3-C4-C5-O5	C4-C5-O5-C1
Starting geometry	-59.6	55.4	-55.0	53.4	-54.5	59.3
MC	11.4	-50.8	26.5	31.2	-70.9	49.5
TS1	-0.5	-44.6	28.4	23.8	-65.1	55.5
CINT	2.5	-53.0	41.8	14.5	-63.5	57.0
TS2	-24.5	-27.1	32.5	9.5	-57.8	70.4
PRO	-38.3	-15.9	36.2	-6.4	-41.1	68.9

It is thought that the transition state structures on either side of the covalent intermediate of retaining glycosidases have significant oxacarbenium ion character.²⁵⁻²⁹ It has also been proposed that the transition state for the glycosylation step is ‘dissociative’ in nature suggesting a significant cleavage of the scissile bond.²⁹ The computed structure of the transition state is consistent with these experimental observations. In the optimized structure of TS1, atoms C-5, O-5, C-1 and C-2 are planar (dihedral angle of -0.5°) and the bond between C-1 and O-5 shortens to 1.28 Å from 1.43 Å in the Michaelis complex as a result of delocalization of the positive charge developed during the formation of the transition state. Indeed, NPA of TS1 reveals increased charge on O-5, thus indicating the delocalization of charge between C-1 and O-5. In order to get a quantitative measure of

the extent of bond-formation or bond-breaking process in the glycosylation step, we performed bond order analysis on the optimized geometries of MC, TS1 and CINT. Wiberg bond indices¹⁸⁵ have been calculated (Table 4.5) for the four bonds involved the transformation using NBO program¹⁸⁶ as implemented in Jaguar.¹¹¹ An increased bond order of C-1–O-5 bond (from 0.88 in MC to 1.38 in TS1) confirms an induced double bond (sp^2) character. In the case of CINT, the bond order for this bond decreases to 0.97 indicating the anomeric carbon becomes sp^3 hybridized, following the formation of covalent linkage between C-1 and Asp204OD1. The scissile glycosidic bond is completely cleaved in TS1 suggesting the dissociative nature of the transition state.

Table 4.4. Charge distribution along the reaction coordinate calculated using natural population analysis at DFT/B3LYP/6-31G**.

	C-1	O-5	O-1	Zn
MC	0.383	-0.634	-0.624	1.64
TS1	0.469	-0.445	-0.803	1.646
CINT	0.38	-0.591	-0.827	1.645
TS2	0.46	-0.47	-0.824	1.643
PRO	0.38	-0.61	-0.803	1.643

Table 4.5. Bond order analysis performed with NBO program using Wiberg bond indices.

Bond	MC	TS1	CINT	TS2	PRO
C1–O1	0.88	0.13	0.01	0.01	0.0
C1–O5	0.89	1.33	0.97	1.27	0.91
C1–OD1	0.01	0.13	0.77	0.07	0.0
C1–O _{Wat}	0.0	0.0	0.0	0.25	0.90

Analysis of the pseudorotational wheel for pyranose ring suggests that there are only four possible conformers that can satisfy the condition of the planarity of C-5, O-5, C-1 and C-2. They are 3H_4 , 4H_3 , ${}^{2,5}B$ and 1S_5 . Indeed, the transition states for the glycosylation steps of family-5 and 7 retaining celluloses^{21, 22}, and family-11 xylanases²³ have been proposed to adopt 4H_3 and ${}^{2,5}B$ conformations, respectively. Furthermore, $B_{2,5}$ transition state has also been suggested for β -mannase 26A.²⁴ In the case of class I α -mannosidase, the transition state is proposed to adopt 3H_4 conformation.¹⁸⁷ However, our calculations show that in the case of glycosylation step, the substrate can adopt 1S_5 skew boat conformation while still maintaining the planarity among C-5, O-5, C-1 and C-2 atoms. This conformation seems to be a result of the hydrogen bond formation between the anomeric oxygen and the proton from the general acid Asp341. This interaction also facilitates the protonation of the leaving group by general acid Asp341.

While 1S_5 skew boat conformation in MC facilitates the protonation of the leaving group by the formation of a hydrogen bond between glycosidic hydrogen and the proton from Asp341, the conformation of the mannopyranose ring in CINT seems to assist with the deglycosylation step. In this conformation the leaving group is placed anti-periplanar to the lone pair of the ring oxygen, a requirement for the departure of the leaving group according to Deslongchamp's anti-periplanar lone-pair hypothesis.⁷⁹ Furthermore, steric clashes between the *syn*-hydrogens at C-3 and C-5, and the attacking water molecule are minimal in the 1S_5 skew boat conformation. This facilitates the attack of water leading to deglycosylation of the glycosyl-enzyme covalent intermediate.

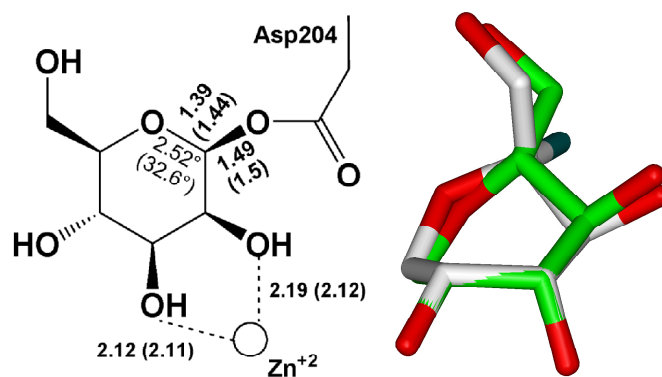


Figure 4.14. Comparison of the geometrical parameters and superimposition of glycosyl-enzyme covalent intermediate obtained from PDB 1QWN (white) and optimized structure of glycosyl covalent intermediate (green). While a good correlation can be seen in different functionalities on the sugar rings, the conformations of the ring are slightly different. The values in parenthesis are for the X-ray structure.

X-ray structures of the wild type and a mutant dGMII in which the general acid/base catalyst has been removed, with fluorinated sugar analogs have revealed that the glycosyl covalent intermediate adopts a 1S_5 skew boat conformation.³⁸ With optimized structure of glycosyl-enzyme covalent intermediate in our hand, we compared the bound conformation of the fluorinated sugar with that of the computed CINT conformation. Superimposition of two structures led to staggering similarities (Figure 4.14), with many of the geometrical parameters comparable.

The transition state for the deglycosylation was also expected to be similar to the oxacarbenium ion. Interestingly, the dihedral angle between atoms C-5, O-5, C-1, and C-2 was found to be -24.5° as compared with -0.5° in TS1, indicating the transition state for the deglycosylation step may have a reduced oxacarbenium ion character in the C-1–O-5 bond. However, the bond order analysis revealed an increased bond order of C-1–O-5 bond (from 0.97 in CINT to 1.27 in TS2) suggesting that a double bond character is induced in that bond during the formation of TS2. Furthermore, the bond length of C-1–

O-5 also reduces from 1.39 Å in CINT to 1.28 Å in TS2, which is an indicative of charge delocalization between the two atoms. This is also supported by an increased charge on the ring oxygen (from -0.59 in CINT to -0.47 in TS2, Table 4.4). This charge again decreases to -0.61 in the hydrolyzed product. The bond between C-1 and O-5 atoms also lengthens to 1.41 with decreased bond order of 0.91.

Ducros et al.²⁴ recently solved X-ray structures of Michaelis complex and glycosyl-enzyme covalent intermediate for β -mannase, a family 26 β -mannosidase, and proposed conformational itinerary for the glycosylation step as ${}^1S_5 \rightarrow B_{2,5} \rightarrow {}^0S_2$. In this case, the enzyme transforms a β -mannosyl species into an α -mannoside. Similar transformation is achieved by GMII in the deglycosylation step suggesting that the conformational changes during the deglycosylation step must be similar to those in the glycosylation step in β -mannase. Indeed, computed itinerary for the deglycosylation step is consistent with this similarity proposed by Numao et al.³⁸

In the glycosylation step, as the distance between C-1 and the nucleophilic carboxylate oxygens decreases, the mannopyranosyl ring moves closer to Asp204 (Figure 4.15). The extent of this movement is highest for O-5, which moves 1.5 Å from its position in MC. The C-5 carbon atom also moves 1.2 Å from its position in MC. In contrast, C-2 and C-3 move only 0.66 Å and 0.5 Å, respectively, from their positions in MC. This restricted motion is a result of coordination these two atoms with Zn^{+2} ion. This forces the conformation of the sugar ring towards a $B_{2,5}$ boat conformation from an ideal 1S_5 skew boat conformation in MC. In the case of deglycosylation step, however, maximum movement is seen in C-1, which moves 1.12 Å from its positioning CINT. This movement brings C-1, C-3, C-4, and C-5 atoms close to be planar (dihedral angle is

-12.9°) where the atom O-5 lies above where as C-2 lies below this plane resulting in a conformation close to an ideal 0S_2 skew boat conformation.

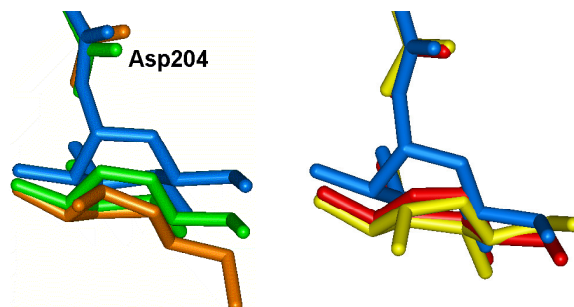


Figure 4.15. Superimposition of the active site in MC (orange), TS1 (green), CINT (blue), TS2 (red) and PRO (yellow) reveals the movement of the mannopyranosyl ring in the active site of dGMII.

Potent inhibitors of glycosidases are thought to mimic oxocarbenium ion-like transition states. For example, the inhibitory activity of the natural product swainsonine has long been attributed to its 5-membered ring resembling a flattened six-membered ring, which had been forced to attain an oxocarbenium-like structure. In fact, the crystal structure of swainsonine complexed with dGMII shows the inhibitor to be tilted in such a way as to bring the equivalent of its anomeric carbon close to the presumed catalytic nucleophile.⁷⁵ On the other hand, recently solved co-crystal structure of mannostatin A complexed with dGMII revealed that in the bound conformation mannostatin A mimics best the covalent intermediate.¹⁷⁴ Studies presented here provide an excellent opportunity to compare the bound conformations of swainsonine and mannostatin A with the transition state for the glycosylation step, TS1.

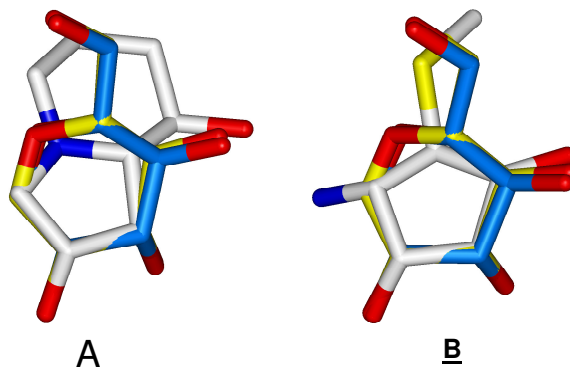


Figure 4.16. Superimposition of optimized structures of transition state (TS1, yellow) and glycosyl-enzyme covalent intermediate (CINT, blue) onto bound conformations of swainsonine (A) and mannostatin A (B). Clearly either inhibitor seems to mimic both TS1 and CINT. Interestingly, the ring nitrogen in swainsonine lies near the endocyclic oxygen of the sugar rings, whereas the amine nitrogen of mannostatin A lies near the anomeric carbon.

In the case of swainsonine, superimposition of the *cis*-diol onto 2- and 3-hydroxyl groups in TS1 resulted in extremely good overlay (Figure 4.16, RMSD = 0.06) between these hydroxyl functionalities. The 6-hydroxyl group seems to mimic 4-hydroxyl moiety in the mannopyranose ring with the hydroxyl oxygen placed at 1.5 Å from the 6-hydroxyl oxygen in swainsonine. It is believed that the ring oxygen in swainsonine mimics the positive charge developed on the ring oxygen in the actual substrate. Indeed, as can be seen in Figure 4.16, the ring nitrogen in swainsonine lies very close to the ring oxygen of the substrate (1.0 Å) suggesting that this nitrogen, in the protonated state, may mimic the positive charge on the ring oxygen developed during the formation of the transition state. In the case of mannostatin A, unlike swainsonine, the amine nitrogen lies close to the anomeric carbon (1.1 Å), thus possibly mimicking the positive charge build up on the anomeric carbon. The 3- and 4-hydroxyl groups in mannostatin display excellent overlay (RMSD = 0.07) with corresponding *cis*-diol moiety in the TS1. The 2- hydroxyl group in

mannostatin lies in the same region as that of 4-hydroxyl group in TS1 at 1.3 Å from the 4-hydroxyl oxygen of TS1.

The superimposition study performed here supports the belief that swainsonine and mannostatin are transition state mimics. It is also clear from Figure 4.16 that these inhibitors also mimic the glycosyl-enzyme covalent intermediate. This is a result of similarity between the conformations of the mannopyranose rings in TS1 and CINT. Both these conformations lie between an ideal 1S_5 skew boat conformation and $B_{2,5}$ boat conformation, suggesting that the structural differences between them are minor.

While the calculations described in this study involve a reasonably large region of the active site, it is possible that inclusion of more residues in the model may alter the results (geometries and energies) to some extent. For this reason we are currently investigating the effect of protein environments on the results reported here by using mixed quantum mechanical / molecular mechanical (QM/MM) calculations where a small portion of the active site is treated at QM level whereas, the rest of the protein is treated at MM level. Furthermore, we are also performing QM calculations on a bigger model in order to compare results from QM/MM calculations with QM calculations. All these calculations use optimized geometries of MC, TS1, CINT, TS2 and PRO as starting geometries.

4.8 Conclusions

Glycosidases are enzymes that play crucial roles in the biosynthesis of glycoproteins. Inhibitors of these enzymes have garnered much attention as lead compounds for drug discovery for diseases such as viral- and bacterial infections,

diabetes, Gauchers disease and cancer. However, efforts to design more potent and/or more selective inhibitors often are limited due to a dearth of knowledge pertaining to the catalytic mechanisms and the mechanism of inhibition by natural inhibitors of these enzymes. Computational methods are, in principle, capable of elucidating the details of an enzymatic catalytic reaction. When combined with experimental observation, such computational insights are significant in understanding the conformational changes that occur in the substrate *en route* to the transition state.

Golgi α -mannosidase II, an α -retaining mannosidase, which acts late in the *N*-glycan biosynthesis pathway, has been validated as a target for blocking tumor growth and metastasis. The enzyme catalyzes a hydrolysis reaction by a double displacement mechanism. Although general aspects of this mechanism has been accepted and refined over the years using experimental techniques, the nature of the transition state and the conformational itinerary of the mannopyranosyl ring in the glycone has been a subject of debate. Furthermore, the knowledge of the transition state structure would also facilitate the efforts of designing potent transition state analogues. In this work, a high-level quantum mechanical study of the hydrolysis reaction catalyzed by GMII has been conducted with the main focus on the conformational analysis of the substrate as the reaction progresses.

In all, four models, which differ in the size and the overall charge, have been investigated. In the first three models, which lack explicit water molecules, the reaction barriers for the glycosylation step were very high (46.5 – 61.5 kcal mol⁻¹). For this reason the deglycosylation step was not performed for these models. Although these models did not yield more realistic energy profiles, the results obtained were beneficial for the

refinement of the model. From the QM study of Model 1 – Model 3, it was concluded that all the residues that coordinate with the metal ion present in the active site must be included in the quantum mechanical calculations. Model 3, which includes complete coordination sphere for the Zn^{+2} ion, resulted in more stable complex. Unlike Model 1 and Model 2, this model did not display proton abstraction from 2-hydroxyl group by Asp472.

The best results were obtained for Model 4, where the computed activation barrier for the glycosylation step is $15.8 \text{ kcal mol}^{-1}$ at DFT/B3LYP/6-311++G** level. This model includes four water molecules in addition to all the residues in Model 3. In the optimized Michaelis complex, the mannopyranosyl ring in the substrate adopts a perfect 1S_5 skew boat conformation, where C-2, C-3, C-4 and O-5 atoms are in one plane. This conformation seems to facilitate the departure of the leaving group by forming a hydrogen bond between the anomeric oxygen and the proton from general acid catalyst Asp341.

It has been previously proposed that in the transition state the mannopyranose ring adopts one of 3H_4 , 4H_3 , $B_{2,5}$, and ${}^{2,5}B$ conformation. Our calculations suggested a slightly twisted $B_{2,5}$ conformation at the transition state that lies between $B_{2,5}$ boat conformation and 1S_5 skew boat conformation. In this conformation, the atoms C-5, O-5, C-1 and C-2 are in one plane suggesting that the transition state resembles mannopyranosyl oxacarbenium ion. Bond order analysis and natural bond order analysis revealed an increased sp^2 character was observed in the C-1–O-5 bond along with delocalization of positive charge between C-1 and O-5 atoms. At the transition state the C-

1–O-1 bond is completely cleaved, suggesting the dissociative nature of the transition state for the glycosylation step in accord with the experimental observations.

The optimized structure of CINT revealed that the sugar ring adopts a skew boat conformation that is very close to ideal 1S_5 conformation. This conformation seems to facilitate the deglycosylation step, as in this conformation the leaving group (the catalytic nucleophile) is anti-periplanar to the lone pair in the ring oxygen. Furthermore, comparison of the optimized CINT structure with the trapped covalent intermediate resulted in staggering similarities. The catalytic nucleophilic oxygen moves away from the Zn^{+2} ion. Similar movement of Asp204 was also observed in the X-ray structures of trapped covalent intermediates.

Unlike the glycosylation step, that transition state for the deglycosylation step (TS2) revealed that atoms C-5, O-5, C-1 and C-2 are not co-planar. However, increased sp^2 character was observed for the C-1–O-5 bond along with the delocalization of the charge across this bond. In this structure the conformation of the sugar ring is slightly skewed boat conformation that lies between $B_{2,5}$ and 0S_2 skew boat conformation. This conformation of the mannopyranosyl ring changes in the hydrolyzed product to a conformation very close to an ideal 0S_2 skew boat conformation.

The calculations presented here suggest that the Zn^{+2} ion in the active site is essential for substrate binding to the active site, and the coordination 2- and 3- hydroxyl group with the Zn^{+2} ion is the main driving force for the conformational changes in the substrate in the early stages of the hydrolysis reaction. Furthermore, the natural population analysis revealed that the charge on zinc remains unchanged over the course of the reaction. The role of zinc is, thus, structural and not electronic in nature.

It is thought that potent inhibitors of mannosidases mimic the transition state structure of the substrate. We have compared the bound conformation of mannostatin A and swainsonine to the mannopyranosyl ring in the optimized TS1. These superimposition studies revealed that mannostatin A and swainsonine in bound conformation mimic the transition state for the glycosylation step, which has been shown to adopt a conformation that lies between $B_{2,5}$ and 1S_5 skew boat conformation. In particular, the zinc-coordinating 3- and 4-hydroxyls of **1** display a good overlap with the corresponding *cis*-diol of the mannosyl residue. Furthermore, the amine nitrogen of mannostatin A is positioned close to the C-1 carbon of TS1, whereas in the case of swainsonine the amine nitrogen is close to the ring oxygen suggesting that it may mimic the charge build up at the ring oxygen during the formation of the transition state. Collectively these studies indicate that mannostatin A and swainsonine are transition state mimics.

4.9 Supporting information

Table S1. Optimized geometries of Michaelis complex, transition state and glycosyl-enzyme covalent intermediate for Model 2.

Michaelis complex (Model 2)				Transition state TS1 (Model 2)			
$E_{\text{absolute}} = -2867.34354482303$ hartree				$E_{\text{absolute}} = -2867.26110158471$ hartree			
Zn1	0.0578635532	0.0138279425	0.0230321071	Zn1	0.0082149349	0.0110415875	0.0130147353
C2	0.0515042443	0.0357764100	4.8540410579	C2	0.0101624129	0.0148942770	4.8440828103
H3	0.9044713233	0.0027593623	4.2083016256	H3	0.8622706602	-0.0082246727	4.1967841512
H4	0.1550299828	-0.7229469291	5.6016687275	H4	0.1270339280	-0.7448653363	5.5886847714
H5	-0.0594791675	0.9894437132	5.3259185260	H5	-0.1634825230	0.9572731698	5.3197253633
C6	-1.1703060982	-0.2304879372	3.9444866265	C6	-1.1762713906	-0.3135665265	3.8990828625
H7	-1.8980923411	-0.9077801681	4.3976220426	H7	-1.8364538951	-1.0897528255	4.2924839313
H8	-1.6847674920	0.7115157180	3.7158660941	H8	-1.7879124803	0.5820727814	3.7277469319
C9	-0.7390536709	-0.8004602287	2.6056386725	C9	-0.7074399322	-0.7517561077	2.5177190347
O10	0.1666326211	-0.1029839191	1.9755564348	O10	0.1905449600	0.0296573589	1.9545924963
O11	-1.2497481406	-1.8663089477	2.2016156946	O11	-1.1931859813	-1.7674534950	1.9962058854
C12	-6.1590717869	0.4847225607	4.2401550135	C12	-6.2177445584	0.0489657134	4.2429181649
H13	-5.7357866497	0.6598781338	5.2075844842	H13	-5.8051864462	0.2485877211	5.2102428501

H14	-6.3701562938	1.4227459648	3.7687850721	H14	-6.4921449264	0.9724376232	3.7754371988
H15	-7.0647116910	-0.0750599946	4.3436978044	H15	-7.0836299822	-0.5706139763	4.3459947935
C16	-5.1693669436	-0.3348493393	3.3831336783	C16	-5.1988164552	-0.6992483416	3.3599270329
H17	-4.8562007580	-1.2199776228	3.9529787801	H17	-4.8618674683	-1.6040698586	3.8855968841
H18	-4.2539829659	0.2497095947	3.2160739991	H18	-4.2972104748	-0.0839913520	3.2275156229
C19	-5.7309757977	-0.7899355739	2.0590364681	C19	-5.7433309344	-1.0942400871	2.0108607459
C20	-5.3798536566	-2.0008937476	1.3506880100	C20	-5.1923854610	-2.0943025827	1.1225105662
C21	-6.1706764709	-2.0469292639	0.1679443735	C21	-6.0160917432	-2.1415613981	-0.0355634644
C22	-4.4790597463	-3.0568665354	1.6104687318	C22	-4.0796558884	-2.9540128050	1.2014134559
C23	-6.6843399637	-0.1649897640	1.2875472512	C23	-6.8510448998	-0.5917496496	1.3719191228
N24	-6.9757069212	-0.9250823865	0.1670389048	N24	-7.0265747722	-1.2202453727	0.1495589164
C25	-6.0897904844	-3.1058195901	-0.7431988258	C25	-5.7521331305	-3.0086116822	-1.1027811203
C26	-4.4055815977	-4.1188012780	0.7138000468	C26	-3.8079977257	-3.8191596435	0.1460228674
C27	-5.2026411380	-4.1432664772	-0.4513963471	C27	-4.6411282701	-3.8402355610	-0.9950995563
H28	-3.8331739493	-3.0324577464	2.4839952499	H28	-3.4177339177	-2.9210167071	2.0610288634
H29	-7.2109145458	0.7677035755	1.4537744720	H29	-7.5544718060	0.1637185625	1.6942110082
H30	-6.6842868947	-3.1073296662	-1.6530746795	H30	-6.3906518362	-3.0290539770	-1.9834013764
H31	-3.7182196270	-4.9455946587	0.9069947537	H31	-2.9290586591	-4.4631587529	0.1702667949
H32	-5.1161719338	-4.9841297790	-1.1361304705	H32	-4.3962697386	-4.5203904132	-1.8074886037
C33	-8.5110614298	-2.5490541919	4.7426118150	C33	-8.3602039755	-3.1374106916	4.7378284478
H34	-9.0127345136	-2.5943731014	5.6865785848	H34	-8.8558056439	-3.2197557804	5.6824977426
H35	-7.5796307843	-2.0345826804	4.8584973891	H35	-7.4650931675	-2.5621300083	4.8540291867
H36	-9.1221336340	-2.0260876087	4.0381467566	H36	-9.0063550740	-2.6539348853	4.0364626988
C37	-8.2379298454	-3.9768232527	4.2559731076	C37	-7.9849533246	-4.5449545447	4.2604036344
H38	-7.2967524413	-4.3250420606	4.6281292682	H38	-7.0256470523	-4.8261116830	4.6428351456
C39	-9.3033156544	-4.9541516738	4.7877468842	C39	-8.9981533378	-5.5928757586	4.7531163639
H40	-9.1467701206	-5.9687404579	4.3999072200	H40	-8.7587847705	-6.5937775214	4.3718217800
H41	-9.2728603421	-5.0075077846	5.8832066751	H41	-9.0035002112	-5.6458618158	5.8495574538
H42	-10.3162164388	-4.6432897652	4.5048487256	H42	-10.0196753923	-5.3507523398	4.4337496582
C43	-8.1160967369	-4.0617662253	2.7145557627	C43	-7.7970381761	-4.6055367273	2.7201195474
H44	-7.7289836582	-5.0558116013	2.4509930449	H44	-7.3515358484	-5.5774904923	2.4650793682
H45	-7.3539888323	-3.3475486976	2.3892627797	H45	-7.0546585222	-3.8509566964	2.4305129934
C46	-9.4025885202	-3.8136600462	1.9175796198	C46	-9.0591699808	-4.4110232580	1.8693089503
H47	-9.1890189128	-3.8376467742	0.8434366552	H47	-8.8013415540	-4.4297300525	0.8039949951
H48	-10.1666423969	-4.5736047284	2.1188156128	H48	-9.7994591895	-5.2013277959	2.0434994814
H49	-9.8434871695	-2.8337345653	2.1374442105	H49	-9.5484926116	-3.4490720229	2.0663126543
C50	3.0249653416	1.7132866061	-4.1120876266	C50	2.8469914125	1.9206907923	-4.1204704807
H51	3.1392551191	0.9981735865	-4.8996310828	H51	3.0073678426	1.2177614611	-4.9109403759
H52	3.9809541854	2.1234529050	-3.8624269596	H52	3.7738612482	2.3929997392	-3.8708268641
H53	2.3740653354	2.4984533120	-4.4358522037	H53	2.1443850616	2.6617253465	-4.4401462779
C54	2.5612260910	1.0740070790	-2.8144435388	C54	2.2867801057	1.1592872818	-2.9063153713
H55	3.3110580241	0.3493867401	-2.4635414078	H55	3.0862472022	0.5841662900	-2.4169549111
H56	2.4808910334	1.8260435850	-2.0196995206	H56	1.8876147952	1.8427267581	-2.1476031119
C57	1.2491600771	0.3357141324	-2.9106421837	C57	1.2142605729	0.1413041542	-3.2886871757
O58	0.6970902547	0.0096895486	-1.8204069906	O58	0.4259895143	-0.2463708619	-2.3189351471
O59	0.7932219316	0.0472440878	-4.0455202333	O59	1.1494819119	-0.3099399469	-4.4407947540
C60	3.6967082360	2.4859406039	-10.3483765617	C60	3.4532220027	2.7598398697	-10.3548779403
H61	4.2019819899	1.5759721557	-10.0965704817	H61	4.0186682968	1.8847322396	-10.1074728640
H62	4.3783409152	3.3063983533	-10.2685420103	H62	4.0786282947	3.6237396633	-10.2730795025
H63	3.3295823285	2.4234159245	-11.3512989434	H63	3.0891081242	2.6766315441	-11.3573955267
C64	2.5558498307	2.7225908718	-9.3232385172	C64	2.2763097709	2.8387444857	-9.3549453918
H65	2.9553306778	3.3139551039	-8.4881029786	H65	2.5872949772	3.3837138304	-8.4533982701
H66	1.7666180939	3.3393987473	-9.7735449048	H66	1.4386820942	3.4062868372	-9.7823409142
C67	1.9426160029	1.4441918476	-8.7235435200	C67	1.8158062100	1.4363336886	-8.9261329772
H68	2.7357243386	0.8419891490	-8.2622674537	H68	2.6563304101	0.9231313570	-8.4412572768
H69	1.4998676009	0.8183681078	-9.5126484748	H69	1.5703950515	0.8400110378	-9.8189867823

C70	0.8924115102	1.7804164596	-7.6476586501	C70	0.6323869630	1.4536199597	-7.9424629930
H71	-0.0082325883	2.2078297547	-8.1037348139	H71	-0.3206573264	1.6273664966	-8.4571301587
H72	1.2998538166	2.5511000921	-6.9843380439	H72	0.7576580660	2.2793808203	-7.2354232244
N73	0.5035282983	0.6609521003	-6.7791287582	N73	0.5240553236	0.2444746473	-7.1202756188
H74	0.9270765057	0.5954595159	-5.8423078241	H74	0.9003043047	0.2618539658	-6.1658397861
C75	-0.6256435220	-0.0517853358	-6.8963699367	C75	-0.0511529267	-0.9043741719	-7.4743711474
N76	-1.3072536461	-0.0533827716	-8.0726567168	N76	-0.4966874134	-1.0939201819	-8.7360511419
H77	-2.1259719305	-0.6338130647	-8.1546032942	H77	-0.9488764159	-1.9598362972	-8.9896462275
H78	-0.7943114119	0.1128244359	-8.9280114714	H78	-0.1435269649	-0.5256348916	-9.4905246958
N79	-1.0806580539	-0.7254030421	-5.8491814005	N79	-0.1998712815	-1.8636308991	-6.5573247211
H80	-1.8679121445	-1.3596471217	-5.8921158275	H80	-0.6158709189	-2.7570659856	-6.7782752527
H81	-0.6423798689	-0.5725500690	-4.9234554454	H81	-0.1097899658	-1.6227827657	-5.5687140621
C82	1.5252589176	-7.0426056574	1.3724852507	C82	1.5397449806	-7.0373117327	1.3336901532
H83	2.1874919555	-6.2987212487	0.9819506643	H83	2.1947829041	-6.2862246582	0.9448103420
H84	1.7556638567	-7.9903030139	0.9326386853	H84	1.7764564668	-7.9802462573	0.8870095490
H85	1.6425682362	-7.1011518346	2.4347254410	H85	1.6593845842	-7.0987668951	2.3955075768
C86	0.0754812577	-6.6668581700	0.9888651801	C86	0.1146251836	-6.5689033345	0.9642779884
H87	-0.6371578471	-7.1447333554	1.6760148273	H87	-0.6175222036	-7.3821296548	1.0759134531
H88	-0.0928894070	-5.5855596842	1.0664903305	H88	-0.2177476618	-5.7777515942	1.6485124092
C89	-0.2864826367	-7.1970052438	-0.3974661398	C89	-0.0073482027	-6.0164145880	-0.4809582761
O90	0.0107937383	-8.3092190053	-0.7680916932	O90	0.8625369121	-6.3249850592	-1.3176797400
O91	-1.0256686024	-6.4070714394	-1.2042047119	O91	-1.0366031366	-5.2727364733	-0.6932660823
H92	-1.0877963805	-5.4802573470	-0.9135081295	H92	-1.1052030098	-4.6983200942	-2.1488778458
C93	-4.5367970128	4.9965859389	1.2891867980	C93	-4.9068589401	4.6691934939	1.3049330017
H94	-3.8236155478	5.0119159924	0.4910269145	H94	-4.1978460073	4.7349405085	0.5056221121
H95	-4.1849652050	5.6067667799	2.0947614555	H95	-4.5949955129	5.2987536601	2.1120608228
H96	-5.4737577991	5.3755702393	0.9362143691	H96	-5.8677665486	4.9858986160	0.9549784876
C97	-4.6445782610	3.5313705937	1.8064172814	C97	-4.9665731028	3.1819781660	1.7706485339
H98	-4.0970338017	3.4101455226	2.7446052167	H98	-4.4707634630	3.0472885750	2.7346327320
H99	-5.6910772232	3.2650299755	1.9956936824	H99	-6.0058530125	2.8535076189	1.8779971590
C100	-4.0903447488	2.5454961879	0.7869746974	C100	-4.2958472029	2.2796283468	0.7484718191
O101	-4.5642933110	2.5001478106	-0.3540235954	O101	-4.7190028855	2.1673173144	-0.4020064878
O102	-3.0852762908	1.8295388949	1.2220191795	O102	-3.2042172438	1.6976288708	1.2079474611
O103	-1.415898024	-3.8305230219	-2.4450376475	O103	-1.1984970662	-4.2706336617	-3.083426224
C104	-0.891806216	-4.4239241005	-3.6238024350	C104	-0.6925596670	-5.210180666	-4.0074433297
H105	-0.840951015	-5.4929014519	-3.4361164559	H105	0.0578599868	-5.8539714979	-3.5309796032
H106	0.1145237219	-4.0379028959	-3.8402767333	H106	-0.2146770540	-4.680234827	-4.8538124819
H107	-1.5403218792	-4.228956913	-4.4867207893	H107	-1.4894477194	-5.846654542	-4.4335583383
C108	-1.4138026716	-2.418748552	-2.4688705474	C108	-0.6895522683	-1.653451230	-2.7775753040
H109	-0.410007019	-2.0517788240	-2.7039880543	H109	0.1167292360	-2.3560803351	-2.9355802271
C110	-1.8271551298	-1.976269922	-1.0562981588	C110	-1.4595768084	-1.752283898	-1.4962670105
H111	-2.494703727	-2.7591494075	-0.6877219393	H111	-2.069849043	-2.6571731816	-1.5808702894
O112	-0.630919280	-2.0091285046	-0.2666356505	O112	-0.476047552	-1.9338825935	-0.4818066375
H113	-0.893799718	-2.1433254270	0.7048960916	H113	-0.877510421	-2.2131245368	0.3966780235
C114	-2.616277855	-0.6152470488	-0.9102711882	C114	-2.3942722056	-0.507515265	-1.2563490480
H115	-3.4178986579	-0.831137953	-0.1927525265	H115	-3.2629932683	-0.880101414	-0.6975637340
O116	-1.8486328307	0.4588587669	-0.4077956096	O116	-1.7668071910	0.531726830	-0.5404328181
H117	-2.5935203334	1.2212865206	0.4491002088	H117	-2.6929232625	1.1939190283	0.4642069619
C118	-3.325433900	-0.2348009214	-2.2279781923	C118	-2.8990870525	0.0536663345	-2.6043651220
H119	-2.6484627631	0.4336655323	-2.7828196517	H119	-2.2320876527	0.8955869344	-2.8537506926
O120	-4.5820741708	0.3918659579	-2.0170849399	O120	-4.2474153541	0.4792207062	-2.5551999504
H121	-4.4675641044	1.2157363025	-1.4716517807	H121	-4.3692137425	1.0903573380	-1.7862210895
C122	-3.547359297	-1.4738782538	-3.1021657604	C122	-2.7817249278	-0.968155313	-3.7342739064
H123	-4.076196637	-2.2544529234	-2.5447985682	H123	-3.3443467835	-1.880279430	-3.5118081332
C124	-4.3403338408	-1.186544900	-4.3800342781	C124	-3.2038990229	-0.412462889	-5.0975391899
H125	-4.3259601644	-2.086269626	-5.0095973979	H125	-2.9551849953	-1.142581985	-5.8772349553

H126 -3.8342457361 -0.372481427 -4.9333609971	H126 -2.6135225318 0.5022832685 -5.2967176110
O127 -5.6894679510 -0.882925369 -4.1166145266	O127 -4.588985728 -0.1860295124 -5.1607995109
H128 -5.6499431996 -0.219761675 -3.3960996089	H128 -4.8260852730 0.2690878796 -4.3264338398
O129 -2.2492503696 -1.9331982759 -3.508379529	O129 -1.366808954 -1.3498588194 -3.8686722525
H130 -7.474913507 -0.5813695026 -0.6404117239	H130 -7.7290276913 -0.978227771 -0.5308673032
Transition state TS2 (Model 2)	Covalent intermediate (Model 2)
E_{absolute} = -2867.26125014924 hartree	E_{absolute} = -2867.29332013373 hartree
Zn1 -0.0297687033 0.0002933136 0.0506679399	Zn1 -0.0000534791 -0.0008410127 -0.0024686421
C2 -0.0343311928 -0.0143523629 4.8817135897	C2 0.0027932190 0.0010553370 4.8286001410
H3 0.8189078675 -0.0041016465 4.2355738727	H3 0.8550752229 -0.0022125499 4.1811256510
H4 0.1099071097 -0.7720637075 5.6235993840	H4 0.1106498416 -0.7603527777 5.5728785389
H5 -0.2451134553 0.9187277149 5.3606695231	H5 -0.1427956772 0.9479755955 5.3046382437
C6 -1.2061912088 -0.3846972441 3.9335660908	C6 -1.1587789098 -0.3051684833 3.8617636217
H7 -1.8379742967 -1.1855913193 4.3241136556	H7 -1.5777617238 -1.3041869581 4.0216436170
H8 -1.8503952496 0.4880409647 3.7632465991	H8 -1.9982427159 0.3899998455 3.9909557103
C9 -0.7211267273 -0.8016451342 2.5509055192	C9 -0.7987655819 -0.2511027773 2.3728479501
O10 0.1509892667 0.0123364369 1.9925906913	O10 0.3226841544 0.2954461587 1.9814550492
O11 -1.1727282655 -1.8301054730 2.0237376216	O11 -1.6065227760 -0.7346608624 1.5598506941
C12 -6.2580565318 -0.2201241621 4.2715612036	C12 -6.2214721170 0.2197469117 4.2285338505
H13 -5.8548459184 -0.0083336430 5.2402387381	H13 -5.8030270059 0.4066863250 5.1958639561
H14 -6.5675414336 0.6937716714 3.8071821721	H14 -6.4684855389 1.1511220204 3.7614587387
H15 -7.0993307894 -0.8732909233 4.3710205215	H15 -7.1053060048 -0.3739639856 4.3315211295
C16 -5.2133835700 -0.9273044160 3.3839380018	C16 -5.2375656155 -0.5583954930 3.3281018372
H17 -4.8522074876 -1.8283641066 3.8998147353	H17 -4.9102967875 -1.4687057446 3.8510345534
H18 -4.3298973504 -0.2847220153 3.2624127946	H18 -4.3202431684 0.0245093063 3.1628844573
C19 -5.7414829638 -1.3199854505 2.0271387675	C19 -5.8369072017 -0.9490859275 1.9998925135
C20 -5.1642496017 -2.2951242647 1.1272735955	C20 -5.3291653088 -1.9391287625 1.0753866275
C21 -5.9816405439 -2.3428026294 -0.0355933856	C21 -6.2347795637 -2.0089707137 -0.0197526488
C22 -4.0345886324 -3.1337927194 1.1986450402	C22 -4.1972093503 -2.7732840587 1.0728388959
C23 -6.8573172485 -0.8330605233 1.3898664680	C23 -6.9900098579 -0.4638189246 1.4330956175
N24 -7.0109138364 -1.4443671849 0.1563777956	N24 -7.2414957900 -1.1010299607 0.2289725946
C25 -5.6961472520 -3.1886423189 -1.1141721712	C25 -6.0522963442 -2.8940252423 -1.0875512250
C26 -3.7433362913 -3.9800237854 0.1330888265	C26 -4.0128586378 -3.6580649876 0.0165727396
C27 -4.5707173267 -4.0011669574 -1.0123608398	C27 -4.9350795069 -3.7218056869 -1.0492525861
H28 -3.3761889513 -3.0994011660 2.0611546127	H28 -3.4562920158 -2.6969362468 1.8617492598
H29 -7.5791268537 -0.0985984616 1.7197802044	H29 -7.6780257657 0.2860646355 1.7979224285
H30 -6.3293693711 -3.2073982116 -1.9985528530	H30 -6.7557154803 -2.9326740058 -1.9160573559
H31 -2.8557823386 -4.6116953873 0.1538160761	H31 -3.1342248161 -4.2982459952 0.0022150448
H32 -4.3097633493 -4.6655603505 -1.8328365619	H32 -4.7718670020 -4.4312075740 -1.8580601784
C33 -8.2756486295 -3.4892648874 4.7512529609	C33 -8.4572556936 -2.9019915948 4.7225820614
H34 -8.7689166086 -3.5944464896 5.6948764744	H34 -8.9549245121 -2.9699975036 5.6673056968
H35 -7.4037372388 -2.8800700167 4.8709441109	H35 -7.5454852050 -2.3535116862 4.8388498596
H36 -8.9391864903 -3.0285830762 4.0507789875	H36 -9.0889225658 -2.3993208255 4.0215163929
C37 -7.8448652371 -4.8794665303 4.2699087364	C37 -8.1257584715 -4.3190825804 4.2410325490
H38 -6.8760884980 -5.1243300832 4.6534256089	H38 -7.1742707962 -4.6297734306 4.6201290022
C39 -8.8179454287 -5.9677188522 4.7555497289	C39 -9.1674456427 -5.3376479020 4.7378996987
H40 -8.5388363766 -6.9570474543 4.3711074485	H40 -8.9617212106 -6.3445135618 4.3520121755
H41 -8.8244418283 -6.0252167944 5.8517645348	H41 -9.1672350779 -5.3940437432 5.8340917569
H42 -9.8471204467 -5.7640347604 4.4339407831	H42 -10.1832899892 -5.0638262448 4.4262871605
C43 -7.6500603113 -4.9258403445 2.7298913084	C43 -7.9499810529 -4.3856597220 2.6998859414
H44 -7.1664039969 -5.8785979994 2.4718810822	H44 -7.5362308474 -5.3714862777 2.4427796831
H45 -6.9365032604 -4.1417525515 2.4460795819	H45 -7.1882329612 -3.6535277576 2.40239971095
C46 -8.9159473300 -4.7760397048 1.8757232242	C46 -9.2123222368 -4.1546394518 1.8585078661
H47 -8.6539797807 -4.7785413173 0.8112706124	H47 -8.9631772263 -4.1816069804 0.7913058317
H48 -9.6253317061 -5.5956325429 2.0430202933	H48 -9.9748982962 -4.9219422902 2.0394415064

H49	-9.4431683456	-3.8350727853	2.0763422094	H49	-9.6702377668	-3.1780997572	2.0582504336
C50	2.7380456897	2.0347399690	-4.0713876517	C50	2.8933477501	1.8255418310	-4.1357079282
H51	2.9266732944	1.3416210283	-4.8642802421	H51	3.0327124920	1.1184826086	-4.9264782007
H52	3.6455202990	2.5417634715	-3.8185984699	H52	3.8338362270	2.2701024073	-3.8860427761
H53	2.0075782183	2.7491217809	-4.3892813604	H53	2.2129384122	2.5871800878	-4.4549739756
C54	2.2038249357	1.2453102764	-2.8630009457	C54	2.2627658673	0.9783552641	-3.0176225008
H55	3.0233898311	0.6995313358	-2.3732850326	H55	3.0446038980	0.4549447195	-2.4512499367
H56	1.7756746560	1.9087543282	-2.1022239093	H56	1.6658094932	1.5654990567	-2.3150719867
C57	1.1731830156	0.1873103113	-3.2538053629	C57	1.3991405461	-0.1110379419	-3.6432076935
O58	0.4021962641	-0.2406742194	-2.2867879705	O58	0.1907689590	-0.1599666379	-3.1379209967
O59	1.1274512892	-0.2580637886	-4.4087871912	O59	1.8216487893	-0.8401214693	-4.5490822454
C60	3.3193942434	2.9207831427	-10.3016753200	C60	3.5231439506	2.6488211949	-10.3698951957
H61	3.9181138221	2.0673759261	-10.0567607707	H61	4.0624718987	1.7572581391	-10.1229279315
H62	3.9106281455	3.8080234753	-10.2156873378	H62	4.1738681952	3.4937926964	-10.2878708876
H63	2.9601109702	2.8273361299	-11.3050333012	H63	3.1565628794	2.5768238505	-11.3723814818
C64	2.1387724316	2.9527224434	-9.3037696845	C64	2.3622974378	2.7571647788	-9.3500448085
H65	2.4282602217	3.5053529354	-8.3996997458	H65	2.6928806157	3.3380637462	-8.4780729463
H66	1.2820983658	3.4915382823	-9.7307039647	H66	1.5126684249	3.3058040115	-9.7781446121
C67	1.7275802207	1.5336108845	-8.8803439000	C67	1.9183916103	1.3689112106	-8.8592257342
H68	2.5849465265	1.0483822279	-8.3961605346	H68	2.7931260443	0.8531414888	-8.4397970172
H69	1.5033939661	0.9314102791	-9.7747660877	H69	1.5692156619	0.7502223429	-9.6967359123
C70	0.5435291146	1.5079706861	-7.8977466187	C70	0.8353042982	1.4225057640	-7.7721309342
H71	-0.4142831559	1.6543114606	-8.4121925883	H71	-0.1375704133	1.6912077181	-8.1950278552
H72	0.6416293391	2.3339785624	-7.1866994970	H72	1.0749087082	2.1999151065	-7.0379822363
N73	0.4736456927	0.2922954488	-7.0814656224	N73	0.7279663861	0.1653627941	-7.0225868910
H74	0.8552570838	0.3158117929	-6.1294560352	H74	1.4268216869	-0.0045578071	-6.2990406789
C75	-0.0631702727	-0.8733542456	-7.4406584761	C75	-0.1752974324	-0.8058257568	-7.1381051170
N76	-0.5138807419	-1.0682334209	-8.6997344868	N76	-1.2534141916	-0.6708382545	-7.9419768129
H77	-0.9310634540	-1.9501261463	-8.9582876278	H77	-1.9517130526	-1.4015210137	-7.9134368405
H78	-0.1927275402	-0.4781478115	-9.4517421031	H78	-1.6147593455	0.2538530434	-8.1274029157
N79	-0.1655013224	-1.8464246137	-6.5313447191	N79	0.0314066251	-1.9792980633	-6.5080155691
H80	-0.5710704021	-2.7445764114	-6.7530542291	H80	-0.8026125827	-2.4074209797	-6.1148716198
H81	-0.0797526104	-1.6087728282	-5.5414013484	H81	0.7831113830	-1.9515153548	-5.8132334719
C82	1.7543696059	-6.9929796192	1.3468302681	C82	1.6932747495	-7.0126916527	1.3149526887
H83	2.3822783376	-6.2171684991	0.9617566221	H83	2.3308044169	-6.2465924307	0.9262601520
H84	2.0262728527	-7.9254840243	0.8982931277	H84	1.9508554492	-7.9492411344	0.8663898060
H85	1.8747571720	-7.0541408663	2.4085801203	H85	1.8145118334	-7.0718222583	2.3767209092
C86	0.3146097187	-6.5711231707	0.9762628570	C86	0.2806417211	-6.5031262043	0.8848153890
H87	-0.3881623737	-7.4119887500	1.0703016343	H87	0.0380051295	-6.8466375837	-0.1253907363
H88	-0.0502125540	-5.8035461513	1.6707003631	H88	-0.5094522840	-6.8715765698	1.5508981130
C89	0.1806469712	-6.0001312381	-0.4611206317	C89	0.2446623515	-4.9671681142	0.9157765459
O90	1.0670010447	-6.2647199222	-1.2961063642	O90	0.6392072128	-4.3084977861	1.8524206529
O91	-0.8723476104	-5.2901950002	-0.6693302535	O91	-0.2413548357	-4.4117725684	-0.2254213076
H92	-0.9818393366	-4.7379716495	-2.1385313732	H92	-0.1545628435	-4.5985603568	-2.1676147106
C93	-5.1239458599	4.4588348735	1.3530310951	C93	-4.7748407516	4.8002886514	1.2921112458
H94	-4.4169741265	4.5551692925	0.5550144569	H94	-4.0643220361	4.8453277921	0.4927023781
H95	-4.8378602339	5.0969363362	2.1629950804	H95	-4.4443423749	5.4200220885	2.0994286615
H96	-6.0959798710	4.7392853724	1.0028723777	H96	-5.7260067942	5.1454433283	0.9424469253
C97	-5.1232486744	2.9683040271	1.8114839788	C97	-4.7936604603	3.2885425945	1.7015577936
H98	-4.6229552869	2.8491242327	2.7752018165	H98	-4.2310024493	3.1329115566	2.6256285961
H99	-6.1481134023	2.5966238241	1.9165543383	H99	-5.8157991653	2.9294193996	1.8541214733
C100	-4.4152956701	2.0993485412	0.7852086867	C100	-4.1590360125	2.4477229828	0.5930446207
O101	-4.8252886956	1.9859253941	-0.3698892479	O101	-4.7689123728	2.1890066318	-0.4444424764
O102	-3.3080831748	1.5489299547	1.2466807879	O102	-2.9086833536	2.1102171331	0.8410855203
O103	-1.097742978	-4.3173170796	-3.0714741846	O103	-0.306968996	-4.6361318577	-3.1310329142
C104	-0.472500046	-5.1886754382	-3.9902297963	C104	-1.515950540	-5.3453971408	-3.3343510653

H105 0.3048960033 -5.7813419909 -3.4913907309	H105 -1.475045840 -6.3709816722 -2.9355045241
H106 -0.001130685 -4.6009893768 -4.8017230178	H106 -1.6786601108 -5.414154583 -4.4157854033
H107 -1.1943510528 -5.876560158 -4.4671961399	H107 -2.385823427 -4.8394268223 -2.8879135732
C108 -0.6520543599 -1.682693772 -2.7454432183	C108 -0.650993168 -1.3852863691 -3.2421137071
H109 0.1802295221 -2.3534222524 -2.9073179014	H109 0.014243405 -2.2148105818 -3.4770884339
C110 -1.416955674 -1.8172108416 -1.4637402118	C110 -1.2293540559 -1.508735329 -1.8368179648
H111 -1.9885884337 -2.745893856 -1.5493915621	H111 -1.8900687377 -2.389545206 -1.8486827915
O112 -0.427377042 -1.9606106658 -0.4489166101	O112 -0.1600753709 -1.713401894 -0.9573472266
H113 -0.819780359 -2.2618004925 0.4264446854	H113 -0.196425577 -3.4027828016 -0.2132006002
C114 -2.403291776 -0.6133899097 -1.2213028318	C114 -2.1646648637 -0.258821446 -1.5229768041
H115 -3.253133802 -1.0231249613 -0.6596113811	H115 -2.9211965896 -0.630344058 -0.8172220146
O116 -1.820106022 0.4534130350 -0.5075426225	O116 -1.4814879474 0.8527996291 -0.9726132741
H117 -2.7757563394 1.0717615497 0.5008496037	H117 -2.4365648215 1.5950443357 0.0754764437
C118 -2.9360864065 -0.075521679 -2.5675923349	C118 -2.9047607668 0.2011380215 -2.8042255915
H119 -2.306941255 0.7940200536 -2.8203688366	H119 -2.3403999125 1.0649970855 -3.1930697881
O120 -4.3012971833 0.2923410669 -2.5134941457	O120 -4.2634867390 0.5476076310 -2.5754233871
H121 -4.4435635206 0.9057146103 -1.7501910026	H121 -4.3434875619 1.1572930350 -1.8003222568
C122 -2.7765836899 -1.093563416 -3.6956515160	C122 -2.9299377007 -0.871921998 -3.8954676386
H123 -3.293030031 -2.0317853567 -3.4687575262	H123 -3.467121329 -1.7563985010 -3.5300797750
C124 -3.230969237 -0.5615775612 -5.0579860779	C124 -3.5986810067 -0.390054501 -5.1886765907
H125 -2.9539520799 -1.2818904608 -5.837278511	H125 -3.458374194 -1.1591373497 -5.9644565641
H126 -2.6836772141 0.3783707538 -5.2630602109	H126 -3.0670072529 0.5211185959 -5.5288213174
O127 -4.6251011399 -0.39809976 -5.1141738843	O127 -4.979696924 -0.1849147333 -5.0498830053
H128 -4.8777180781 0.0488222643 -4.2799411057	H128 -5.086881071 0.2579486712 -4.1795550264
O129 -1.3447524197 -1.405081667 -3.8351872547	O129 -1.579066035 -1.2483904594 -4.2726124943
H130 -7.723703508 -1.2181305566 -0.5186612501	H130 -7.9769621879 -0.854805318 -0.4141555180

Table S2. Optimized geometries of Michaelis complex, transition state and glycosyl-enzyme covalent intermediate for Model 3.

Michaelis complex (Model 3)			
Eabsolute = -3477.27757863120 hartrees			
Zn1	0.0059518077	-0.0045420373	0.0027571077
C2	0.0111847474	-0.0005226064	6.4443614577
H3	1.1006414128	0.0002560020	6.4329569189
H4	-0.4158167618	-0.2136587975	7.4244355120
H5	-0.3450975592	0.9752556681	6.1140739757
C6	-0.4241263087	-1.1456555268	5.5019067411
H7	-1.5087263738	-1.1877057923	5.3827867968
H8	-0.1283484899	-2.1011905642	5.9600277421
C9	0.1632911203	-1.0212630134	4.1383915781
N10	1.5235855233	-0.8732251740	3.8960609190
C11	-0.4245101351	-0.9463358657	2.9050157300
H12	-1.4728104356	-1.0219180024	2.6560396677
C13	1.7013522745	-0.7045020600	2.5610446007
H14	2.6633343700	-0.5517948173	2.0947827996
N15	0.5399838578	-0.7487981042	1.9392063186
C16	0.3177869213	4.7236668275	1.9601519125
H17	1.2586291168	4.2500761978	1.6781825778
H18	-0.0404457240	4.3692763268	2.9260006039
H19	0.3855501668	5.8106805161	1.9277714231
C20	-0.7218301460	4.2912241137	0.9006764148
H21	-0.3762621627	4.5780292740	-0.1017992036

H22	-1.6845146458	4.7810664074	1.0715229561
C23	-0.9675922383	2.7836221809	0.8573641860
O24	0.0502798651	2.0155460409	0.7984087392
O25	-2.1708390872	2.3994626233	0.8692770090
C26	-3.1788977475	6.4465099340	-3.1018897308
H27	-2.5610201130	6.2126631625	-3.9690305192
H28	-2.6994808666	7.1821662546	-2.4554337733
H29	-4.1789539980	6.7641787922	-3.3974984202
C30	-3.3027055574	5.1343417696	-2.2761315195
H31	-3.8992682800	5.3247024621	-1.3753814985
H32	-2.3051741539	4.8435977319	-1.9212399475
C33	-3.9093476133	3.9799899061	-3.0335353327
C34	-3.5316696077	3.5090963148	-4.2651013600
H35	-2.7182174846	3.8180573334	-4.9054569373
C36	-4.9876602584	3.1184544754	-2.5989697901
N37	-4.3450597679	2.4578720684	-4.6699993305
H38	-3.9700576836	1.7225588226	-5.2568490462
C39	-5.2334546539	2.1858836267	-3.6440899076
C40	-5.7337189385	3.0143594470	-1.4110979515
H41	-5.5309036431	3.6775548116	-0.5748406931
C42	-6.2366955371	1.2154243141	-3.5535096603
H43	-6.4369385796	0.5372743679	-4.3796298927
C44	-6.7110797625	2.0303021814	-1.3057568049
H45	-7.2815698272	1.9351217024	-0.3858669156
C46	-6.9705256768	1.1473376356	-2.3726470900
H47	-7.7489928228	0.3960593105	-2.2687686823
C48	-6.8929534527	7.2871486064	-3.0144600258
H49	-6.9893295413	7.3188500796	-4.1000119886
H50	-5.9471415442	6.8508512046	-2.6936765934
H51	-7.0854612426	8.2540483196	-2.5500730915
C52	-8.0590803717	6.3836808332	-2.5184547212
H53	-8.9920642287	6.9457805447	-2.6885287514
C54	-7.9426667057	6.1471853690	-1.0003185315
H55	-7.8123783140	7.1217207913	-0.5077454275
H56	-7.0242415054	5.5797976258	-0.7991071675
C57	-8.1522827446	5.0873610041	-3.3351610359
H58	-8.9979475468	4.4644681118	-3.0254131296
H59	-8.2874529715	5.3143271769	-4.3998180097
H60	-7.2446121187	4.4856408005	-3.2358163472
C61	-9.1332479178	5.4240375026	-0.3613194563
H62	-9.0224612432	5.3700095400	0.7275451569
H63	-10.0755127182	5.9453521031	-0.5718137813
H64	-9.2298280249	4.3983914315	-0.7313609038
C65	2.3867571408	-4.3585160874	-0.5260575894
H66	1.6232966953	-5.1358193588	-0.5647423043
H67	3.1143034003	-4.4877503947	0.2758274691
H68	2.8291625577	-4.1219961621	-1.4938940098
C69	1.5563805372	-3.1548175474	-0.0527408363
H70	2.1070746078	-2.2142116156	-0.1106075863
H71	1.2885250813	-3.2929952323	1.0025523558
C72	0.2434001893	-3.0337387407	-0.8130417572
O73	-0.2458745016	-1.8824422971	-0.9868215364
O74	-0.2940326360	-4.1094983262	-1.2166766686
C75	3.1094856551	-10.2310290119	-2.8857613782
H76	2.1917141675	-10.7908691004	-2.7071217635
H77	3.6509228639	-9.9712029481	-1.9763170096

H78	3.7390516877	-10.6544531689	-3.6682706997
C79	2.6577370788	-8.9051562791	-3.5959487035
H80	2.2681760894	-9.1934429452	-4.5835668645
H81	3.5490507120	-8.2957615363	-3.8000190684
C82	1.5969787977	-8.0053686508	-2.9248423724
H83	2.0108506932	-7.5164402757	-2.0333741899
H84	0.7330751303	-8.5962895472	-2.5957280142
C85	1.1263699148	-6.9408382217	-3.9389954733
H86	0.6284155541	-7.4619436929	-4.7652971895
H87	2.0127630099	-6.4374459742	-4.3576286027
N88	0.1892791362	-5.9531760657	-3.4008383095
H89	0.2969891503	-5.5996989733	-2.4458528642
C90	-0.6461357028	-5.2070120078	-4.1532147367
N91	-0.7383455075	-5.4203234749	-5.4967801037
H92	-1.3128075903	-4.7642990183	-6.0094690056
H93	0.0539812492	-5.7966359317	-5.9914879290
N94	-1.4338019820	-4.3091264564	-3.5910360830
H95	-1.9084793337	-3.6150499879	-4.1823972653
H96	-1.2706087432	-4.0936391400	-2.5834024768
C97	-4.4807708493	-0.4881041594	5.9085464467
H98	-5.0037248519	-1.2325944964	6.5095373451
H99	-4.4171765531	0.4473206300	6.4644341660
H100	-3.4764656966	-0.8619606393	5.7071721663
C101	-5.1698630785	-0.2409125582	4.5533388109
H102	-5.1546508874	0.8232480506	4.2883535766
H103	-6.2306906102	-0.5166029158	4.5607532601
C104	-4.5089345852	-0.9629897121	3.3849042167
O105	-3.5111249945	-1.6592977827	3.4752977789
O106	-5.1487814821	-0.7158524524	2.2408947356
H107	-4.6725270734	-1.1119515257	1.4681181567
C108	4.5734719845	1.6214117603	-4.4381554421
H109	5.3044530773	1.3920287258	-5.2141835309
H110	4.9493502120	2.3644397112	-3.7354495989
H111	3.6407839957	1.9988073005	-4.8581960937
C112	4.3551591248	0.3247910982	-3.6338992172
H113	5.3373268889	-0.0707844231	-3.3337038782
H114	3.8923532122	-0.4475509760	-4.2572337074
C115	3.4927726232	0.5252816525	-2.4331062778
N116	3.6022752324	1.6124853093	-1.5744226057
C117	2.4618686959	-0.2126858828	-1.9243762352
H118	2.0211360674	-1.1172565329	-2.3118172917
C119	2.6443241183	1.5050861409	-0.6205649161
H120	2.4282069890	2.2471418332	0.1329766751
N121	1.9538368209	0.3955538530	-0.7977390650
C122	1.7649226173	3.9603630163	-5.5961447851
H123	1.3919921398	3.2332069172	-6.3178483560
H124	2.6109660207	3.5405638317	-5.0515525795
H125	2.0731508887	4.8682079530	-6.1145304368
C126	0.6189233605	4.2594739315	-4.6097773657
H127	-0.1686643816	4.8150232729	-5.1371886174
H128	0.9582541698	4.8841414799	-3.7780491669
C129	-0.0284119631	2.9814814592	-4.0421398187
O130	-0.4463016072	2.1325134627	-4.8765469001
O131	-0.1015754376	2.8999308500	-2.7750006878
O132	-4.4460305179	-1.9019945224	-0.1516434078
C133	-4.7849628338	-3.2723253443	0.0556802272

H134	-5.6698730126	-3.2842774206	0.6962817485
H135	-5.0124284208	-3.7634351963	-0.8957893374
H136	-3.9676253497	-3.8109920548	0.5548512244
C137	-3.2631542310	-1.7259626350	-0.9398760143
H138	-2.4531912876	-2.3128048700	-0.5037763366
C139	-2.9295153564	-0.2191335036	-0.8617421991
H140	-3.8927605979	0.2957142443	-0.7589603840
O141	-2.1831192669	-0.0332433975	0.3324660304
H142	-2.2567985590	0.9717699633	0.6122981082
C143	-2.2094452635	0.4186651733	-2.1147192325
H144	-2.7320657731	1.3570700668	-2.3355728193
O145	-0.8555344268	0.7080900054	-1.8320341141
H146	-0.5746679467	1.6266288202	-2.2384321433
C147	-2.3110702479	-0.4904776819	-3.3419528437
H148	-1.4937547575	-1.2183072849	-3.2449192458
O149	-2.2304982249	0.1830158866	-4.5971445868
H150	-1.4915753102	0.8682480800	-4.5965273499
C151	-3.6206460100	-1.2890410079	-3.2929722348
H152	-4.4785822676	-0.6345557965	-3.0892496269
C153	-3.8967451778	-2.0357573616	-4.6039059968
H154	-4.5065826819	-1.4022254251	-5.2594494598
H155	-4.4569011050	-2.9504352286	-4.3887459717
O156	-2.6995596465	-2.4216996407	-5.3004148265
H157	-2.2272890455	-1.5698754278	-5.4233992277
O158	-3.4763644397	-2.2502385758	-2.2390747779
H159	2.2563470108	-0.8772475693	4.5892063904
H160	4.2246781546	2.3983001930	-1.6832550001
Transition state (Model 3)			
$E_{\text{absolute}} = -3477.04012756984$ hartrees			
Zn1	0.0053084763	0.0113637134	-0.0165702041
C2	0.0026237566	0.0074766186	6.3834280516
H3	1.0920919523	0.0095570803	6.3733674449
H4	-0.4261845554	-0.2056218865	7.3627211344
H5	-0.3537685749	0.9834727283	6.0539037829
C6	-0.4452535620	-1.1333739086	5.4396928976
H7	-1.5304958288	-1.1656654864	5.3131895752
H8	-0.1570377347	-2.0918660806	5.8988662882
C9	0.1430077921	-1.0209830775	4.0750973686
N10	1.5017315387	-0.8561334255	3.8295736064
C11	-0.4508300921	-0.9931023647	2.8414951813
H12	-1.5099307229	-1.1025034410	2.6224802659
C13	1.6806288278	-0.7206146270	2.4938534214
H14	2.6406667155	-0.5573549338	2.0261792805
N15	0.5180030459	-0.8056520883	1.8699243762
C16	0.3091385910	4.7375171680	1.9470373451
H17	1.2508870521	4.2653875293	1.6656439127
H18	-0.0498633295	4.3815113725	2.9120059718
H19	0.3756554583	5.8246493219	1.9160809354
C20	-0.7291111137	4.2908234322	0.8863301054
H21	-0.4070894216	4.6227661117	-0.1113201231
H22	-1.7056757994	4.7444612006	1.0803185868
C23	-0.9351424414	2.7751494875	0.7795643659
O24	0.1028400278	2.0291526081	0.7304842229
O25	-2.1260619047	2.3597749634	0.7103185248
C26	-3.1818428462	6.4859569877	-3.1101617546

H27	-2.5623617219	6.2579400727	-3.9777109743
H28	-2.7042904023	7.2183660339	-2.4586583189
H29	-4.1818227543	6.8041776934	-3.4054349834
C30	-3.3624806040	5.1778201930	-2.2920959526
H31	-3.8418584402	5.4196216351	-1.3327255377
H32	-2.3768687599	4.7633076409	-2.0353139998
C33	-4.1823813531	4.1191283243	-2.9877607790
C34	-4.4658375489	4.0315573678	-4.3282903417
H35	-4.1756769796	4.6841100852	-5.1400932629
C36	-4.8259821896	2.9755992062	-2.3730925299
N37	-5.2499826881	2.9175033253	-4.5849425529
H38	-5.5339229100	2.6101008516	-5.5012992484
C39	-5.4773521053	2.2425044469	-3.4048913591
C40	-4.9120051750	2.5024043123	-1.0481615612
H41	-4.3948324084	3.0181476412	-0.2446757552
C42	-6.1943332412	1.0665466523	-3.1468351250
H43	-6.6955441569	0.5270067214	-3.9485930397
C44	-5.6187979110	1.3315703537	-0.7857974195
H45	-5.6671690375	0.9360798954	0.2271744606
C46	-6.2501932852	0.6177864715	-1.8290793275
H47	-6.7789355910	-0.3011116640	-1.5909830856
C48	-6.8970253507	7.3216819150	-3.0235013639
H49	-6.9917782882	7.3596501936	-4.1089951154
H50	-5.9511869635	6.8846232574	-2.7038341889
H51	-7.0913934139	8.2856071896	-2.5537368998
C52	-8.0343250507	6.3989216362	-2.4990617418
H53	-8.9894037375	6.9145978465	-2.6932234169
C54	-7.9044890172	6.2198008783	-0.9729235147
H55	-7.7580204851	7.2098115164	-0.5155163312
H56	-6.9891977298	5.6471923754	-0.7610205476
C57	-8.0645119562	5.0591975697	-3.2465358390
H58	-8.9058475197	4.4319194039	-2.9301177569
H59	-8.1626533404	5.2177999617	-4.3285633099
H60	-7.1430304414	4.4927637131	-3.0745872111
C61	-9.0982445760	5.5368443255	-0.2957279386
H62	-8.9588458027	5.4900244779	0.7907937697
H63	-10.0298879586	6.0854493864	-0.4880578418
H64	-9.2365785985	4.5093868774	-0.6499197006
C65	2.3940136404	-4.3066707321	-0.6088230144
H66	1.6315343487	-5.0846299286	-0.6532477197
H67	3.1204853274	-4.4397615059	0.1934054140
H68	2.8376181975	-4.0639457074	-1.5745720077
C69	1.4708601175	-3.1215065575	-0.2122744632
H70	1.9476663147	-2.1483251778	-0.3273868674
H71	1.2058840834	-3.1970279369	0.8500434091
C72	0.1220027602	-3.1368806502	-0.9514454223
O73	-0.5113204491	-2.0067470925	-1.0169758635
O74	-0.3280896984	-4.2061425718	-1.4138364341
C75	3.1273143273	-10.1643518106	-3.0018937632
H76	2.2099356614	-10.7263128420	-2.8279577830
H77	3.6670521735	-9.9092408054	-2.0901074216
H78	3.7585776674	-10.5824257980	-3.7859109666
C79	2.7298098650	-8.8460288688	-3.7351199785
H80	2.3538723579	-9.1368961542	-4.7279035440
H81	3.6480834399	-8.2717835186	-3.9269417914
C82	1.6920882474	-7.9008564010	-3.1123309448

H83	2.0797178859	-7.4368053754	-2.1953028915
H84	0.7755053901	-8.4411647532	-2.8427397318
C85	1.3640946982	-6.8235829763	-4.1572235900
H86	0.9309346491	-7.3180651394	-5.0349473021
H87	2.3017661233	-6.3431342677	-4.4799255471
N88	0.4148700371	-5.8148803116	-3.6987895475
H89	0.3804457917	-5.5416890023	-2.7135080177
C90	-0.3328436327	-5.0618309036	-4.5178277672
N91	-0.2315456535	-5.2032540481	-5.8671619244
H92	-0.7843713679	-4.5755191131	-6.4367348768
H93	0.6350787624	-5.5234178564	-6.2715444078
N94	-1.2225923678	-4.2151505975	-4.0279599049
H95	-1.6273779439	-3.4830987272	-4.6310109648
H96	-1.2835727950	-4.1116912228	-3.0092156491
C97	-4.4873427572	-0.4987645382	5.8482465566
H98	-5.0063818510	-1.2485102686	6.4460898258
H99	-4.4277835291	0.4343430638	6.4084588668
H100	-3.4814226313	-0.8669383220	5.6444773976
C101	-5.1606192880	-0.2608719031	4.4818988668
H102	-5.1016158753	0.8043732213	4.2166109416
H103	-6.2312460370	-0.4941454049	4.5000494304
C104	-4.5277687591	-1.0166630674	3.2788277024
O105	-3.3902647493	-1.5261334846	3.4110518233
O106	-5.2520717333	-1.0024749958	2.2303801698
H107	-4.8851310437	-1.7635498368	0.9148400977
C108	4.5520186405	1.7004875061	-4.4950590180
H109	5.2814670828	1.4774105523	-5.2743607385
H110	4.9277009186	2.4408636111	-3.7894553533
H111	3.6170379969	2.0773585338	-4.9104476314
C112	4.3510530979	0.3821867685	-3.7195457965
H113	5.3410193686	-0.0105449231	-3.4397835588
H114	3.8948271625	-0.3759766835	-4.3661338541
C115	3.4979121244	0.5211864715	-2.5039339333
N116	3.6350365485	1.5380101394	-1.5679850063
C117	2.4624765136	-0.2371586713	-2.0355916122
H118	2.0128875483	-1.1064080931	-2.4901910917
C119	2.6907592116	1.3718207142	-0.6092874979
H120	2.4950168933	2.0651774831	0.1951035481
N121	1.9775354232	0.2883253226	-0.8578914900
C122	1.7140839117	4.0038724725	-5.6526969122
H123	1.3511983033	3.2726892072	-6.3754515343
H124	2.5651222273	3.5945550762	-5.1079084236
H125	2.0108383136	4.9162105712	-6.1698881709
C126	0.5550028010	4.2827813867	-4.6759755272
H127	-0.2459659706	4.8091706011	-5.2136234730
H128	0.8704191968	4.9222072257	-3.8456168344
C129	-0.0556166254	2.9898235300	-4.1085908594
O130	-0.4144499390	2.1103463269	-4.9367308739
O131	-0.1483961311	2.9201693178	-2.8395174969
O132	-4.8467490944	-2.2485728220	0.0116155024
C133	-5.7147505967	-3.3526195600	0.0986325490
H134	-5.4313561086	-4.0546007422	0.9007727044
H135	-6.7596353669	-3.0506177377	0.2798984326
H136	-5.6834963972	-3.9007972500	-0.8538277494
C137	-2.4764419584	-1.9672614988	-1.1792125671
H138	-2.5698102033	-2.6426173590	-0.3416552127

C139	-2.6358296185	-0.4845445216	-0.9787927047
H140	-3.7240094038	-0.3414668913	-0.9418457533
O141	-2.0694419001	-0.1232845857	0.2527063422
H142	-2.2437428149	0.8887758599	0.4725480373
C143	-2.0515200764	0.3421589721	-2.1796193062
H144	-2.6575405669	1.2487224096	-2.2888205804
O145	-0.7096742645	0.6753216628	-1.9084981905
H146	-0.4846285689	1.6291476842	-2.3103940369
C147	-2.1315057736	-0.4872186606	-3.4672601058
H148	-1.2079468703	-1.0866956831	-3.4947713171
O149	-2.2829009772	0.2439537671	-4.6649366284
H150	-1.5630723288	0.9559445307	-4.7132795601
C151	-3.2953152539	-1.4740111042	-3.3470356034
H152	-4.2009815007	-0.9963755494	-2.9600297071
C153	-3.6481758813	-2.1740138978	-4.6569397579
H154	-4.4357925615	-1.5887141566	-5.1446950429
H155	-4.0361473128	-3.1787648647	-4.4637529208
O156	-2.5306195486	-2.3014094352	-5.5467758180
H157	-2.2031185473	-1.3711671636	-5.6313016813
O158	-2.8848261777	-2.4631382858	-2.3263317326
H159	2.2311337377	-0.8177396706	4.5264864762
H160	4.2700107303	2.3208409972	-1.6271516739
Covalent intermediate (Model 3)			
$E_{\text{absolute}} = -3477.20503780738$ hartrees			
Zn1	-0.0266398513	-0.0045068011	0.0053509863
C2	0.0212312592	0.0203359865	6.4467324273
H3	1.1105887514	0.0207457068	6.4281155764
H4	-0.3965407250	-0.1950061606	7.4302957431
H5	-0.3305341494	0.9974652972	6.1155986863
C6	-0.4414812009	-1.1055401728	5.4885209667
H7	-1.5268637403	-1.1228897723	5.3604385865
H8	-0.1646789159	-2.0737044412	5.9324592051
C9	0.1365283941	-0.9941228126	4.1160080368
N10	1.4909134169	-0.8184215740	3.8558889971
C11	-0.4659543879	-1.0044136385	2.8845921732
H12	-1.5263745304	-1.1326680855	2.6800462692
C13	1.6604852164	-0.7156244749	2.5160796260
H14	2.6151483261	-0.5475829959	2.0398315651
N15	0.4942952058	-0.8307121381	1.9006331271
C16	0.2994841790	4.7299154920	1.9453203499
H17	1.2383052082	4.2551284198	1.6586652430
H18	-0.0524478894	4.3787612203	2.9146610714
H19	0.3673395138	5.8167980133	1.9089728037
C20	-0.7455757344	4.2649235172	0.8982359060
H21	-0.4438854836	4.6012343722	-0.1037439436
H22	-1.7280207008	4.6996701070	1.1022675523
C23	-0.9297941588	2.7451188545	0.7843823516
O24	0.1157002571	2.0085944288	0.7593375572
O25	-2.1131454033	2.3150459241	0.6792397712
C26	-3.2301343683	6.4374233256	-3.0990299128
H27	-2.6180724363	6.2005873151	-3.9694775834
H28	-2.7462461187	7.1750231632	-2.4581440450
H29	-4.2320359080	6.7544346214	-3.3890430534
C30	-3.4036658380	5.1365337035	-2.2666224423
H31	-3.8900299779	5.3846075316	-1.3130947504

H32	-2.4162440988	4.7354501599	-1.9977009250
C33	-4.2063803584	4.0556836152	-2.9488074434
C34	-4.4855274801	3.9442870266	-4.2883349961
H35	-4.2052600576	4.5912320641	-5.1075595084
C36	-4.8277411863	2.9069204440	-2.3188386210
N37	-5.2494556733	2.8129188277	-4.5307227664
H38	-5.5103024498	2.4775525348	-5.4429163617
C39	-5.4643714376	2.1491249645	-3.3413743107
C40	-4.8995652639	2.4438705540	-0.9890918197
H41	-4.3880140808	2.9747257074	-0.1926265054
C42	-6.1577416244	0.9623574207	-3.0696764179
H43	-6.6464765537	0.4031188507	-3.8647596280
C44	-5.5809416866	1.2615530273	-0.7137161676
H45	-5.6118128872	0.8713857293	0.3013446375
C46	-6.2032215316	0.5275384880	-1.7472830621
H47	-6.7188082951	-0.3959779142	-1.5002340992
C48	-6.9432977016	7.2794484281	-2.9897640407
H49	-7.0468419988	7.3076678035	-4.0747519052
H50	-5.9955061427	6.8439081582	-2.6738313810
H51	-7.1324623503	8.2479023017	-2.5272455599
C52	-8.0668842251	6.3513285665	-2.4476816942
H53	-9.0297027269	6.8555020794	-2.6298482374
C54	-7.9132452469	6.1775649506	-0.9232879198
H55	-7.7744992813	7.1698289839	-0.4702180141
H56	-6.9865721136	5.6200099899	-0.7243483542
C57	-8.0908460726	5.0090245800	-3.1909136119
H58	-8.9169136728	4.3709100638	-2.8602218939
H59	-8.2086315424	5.1628463973	-4.2705149148
H60	-7.1588641540	4.4568602206	-3.0328792353
C61	-9.0849966382	5.4765910903	-0.2278097127
H62	-8.9308390933	5.4356879546	0.8557759740
H63	-10.0279904862	6.0068579801	-0.4091493048
H64	-9.2093772383	4.4464646994	-0.5762925765
C65	2.3493184806	-4.3608671861	-0.5251587427
H66	1.5853953606	-5.1380557302	-0.5562744843
H67	3.0821243103	-4.4877367807	0.2723024940
H68	2.7853698512	-4.1276091706	-1.4966634913
C69	1.3988920526	-3.1763051286	-0.1633003577
H70	1.8465170424	-2.1951422488	-0.3144956131
H71	1.1346271778	-3.2138928211	0.9007951709
C72	0.0463008790	-3.2556364404	-0.8899573239
O73	-0.6095926385	-2.1051642411	-0.9762493548
O74	-0.4022039516	-4.3184918197	-1.3264086027
C75	3.0546996329	-10.2411936745	-2.8706106329
H76	2.1379695440	-10.8001684404	-2.6840879254
H77	3.6022244573	-9.9786003929	-1.9656165912
H78	3.6789456592	-10.6673383365	-3.6559003104
C79	2.6772489264	-8.9335709262	-3.6260442631
H80	2.2887666744	-9.2338194591	-4.6102802965
H81	3.6080384757	-8.3869995267	-3.8356547553
C82	1.6709506553	-7.9484655312	-3.0212470050
H83	2.0482201476	-7.5188963544	-2.0840524868
H84	0.7186155923	-8.4437715918	-2.7952239262
C85	1.4439624824	-6.8433364214	-4.0603516427
H86	1.0733107808	-7.3105475243	-4.9807134332
H87	2.4125400256	-6.3752621560	-4.2981722369

N88	0.4793131745	-5.8311732820	-3.6508625753
H89	0.3453623817	-5.6122613528	-2.6636624704
C90	-0.1627226026	-5.0275692712	-4.5105942322
N91	0.0861055132	-5.1158995138	-5.8428460781
H92	-0.4052901563	-4.4784089859	-6.4527638626
H93	0.9649441283	-5.4790615663	-6.1726341010
N94	-1.0761276241	-4.1745917275	-4.0887023457
H95	-1.4513110000	-3.4447591849	-4.7198091784
H96	-1.3049955016	-4.1184642622	-3.0966827338
C97	-4.4743164699	-0.4675661984	5.9422516400
H98	-4.9934956183	-1.2099500112	6.5490927193
H99	-4.4067691957	0.4696273004	6.4946832053
H100	-3.4714760957	-0.8423847315	5.7354392584
C101	-5.1429961292	-0.2548293100	4.5704015368
H102	-5.0998417001	0.8057250145	4.2874937419
H103	-6.2085915690	-0.5078883532	4.5784962143
C104	-4.4805682432	-1.0212376101	3.3901755205
O105	-3.3396388711	-1.5153046185	3.5571353912
O106	-5.1790642729	-1.0365757199	2.3260014952
H107	-4.7865078638	-1.8622247704	1.0775348674
C108	4.5607265153	1.6026027476	-4.4484828531
H109	5.2917874857	1.3689565375	-5.2231627003
H110	4.9383470973	2.3459581121	-3.7470586240
H111	3.6297968274	1.9822028077	-4.8704332869
C112	4.3570796443	0.2922919515	-3.6613880053
H113	5.3456700746	-0.0956320117	-3.3726065434
H114	3.9049017844	-0.4738091242	-4.3003204238
C115	3.4988900640	0.4419134187	-2.4513741329
N116	3.6237774831	1.4705317175	-1.5275983499
C117	2.4638199525	-0.3158030325	-1.9824181955
H118	2.0243017764	-1.1904143187	-2.4355979460
C119	2.6734310120	1.3112447474	-0.5734570521
H120	2.4650447849	2.0135175968	0.2201869431
N121	1.9670843337	0.2210968263	-0.8145887646
C122	1.7590725816	3.9513154250	-5.6034144696
H123	1.3811655158	3.2244221652	-6.3227903460
H124	2.6047608966	3.5289321777	-5.0602707203
H125	2.0697790863	4.8568906799	-6.1242846179
C126	0.6027389764	4.2345990099	-4.6250083521
H127	-0.1897418695	4.7803176071	-5.1539304384
H128	0.9232252598	4.8517506457	-3.7808726449
C129	-0.0255497103	2.9380670730	-4.0864261264
O130	-0.4030683772	2.0810314898	-4.9276868865
O131	-0.1096874198	2.8404874153	-2.8170827321
O132	-4.7183279167	-2.3963631460	0.2071950740
C133	-5.7533552771	-3.3450900121	0.2171246818
H134	-6.7511015593	-2.8866052100	0.3214162881
H135	-5.7410270948	-3.8980833317	-0.7332880762
H136	-5.6522968405	-4.0851517450	1.0297789252
C137	-2.2584767373	-2.0679723194	-1.1643928938
H138	-2.5827301937	-2.6978963966	-0.3397258702
C139	-2.5783374720	-0.5878507084	-0.9904887748
H140	-3.6717981175	-0.5477716430	-0.9747455960
O141	-2.0760839316	-0.1593600340	0.2543372118
H142	-2.2508459322	0.8612395173	0.4354792295
C143	-2.0182568541	0.2730657368	-2.1702016906

H144	-2.6523866038	1.1616998370	-2.2729770334
O145	-0.6851783565	0.6410900463	-1.8849135375
H146	-0.4560844453	1.6033321903	-2.3070729888
C147	-2.0573288176	-0.5369019204	-3.4707655333
H148	-1.1014188663	-1.0842548188	-3.5102469589
O149	-2.2435802124	0.2091322839	-4.6558687580
H150	-1.5355083227	0.9286214508	-4.7091229160
C151	-3.1524208505	-1.5971541402	-3.3464536543
H152	-4.0820079140	-1.1749102933	-2.9515887189
C153	-3.4889707863	-2.2762938570	-4.6734561505
H154	-4.3162606938	-1.7240020624	-5.1323600331
H155	-3.8176083710	-3.3064111377	-4.5053805164
O156	-2.3793795805	-2.3098321842	-5.5858921330
H157	-2.1087883396	-1.3619552099	-5.6405795937
O158	-2.6636221651	-2.5766406914	-2.3656133515
H159	2.2242470801	-0.7531267034	4.5454522220
H160	4.2563920284	2.2541237276	-1.5891635640

Table S4. Optimized geometries of Michaelis complex, transition state and glycosyl-enzyme covalent intermediate for Model 4.

Michaelis complex			
Eabsolute = -3419.84999610339 hartrees			
C1	-0.0136617122	0.0263772276	-0.0033454692
H2	-0.0125235050	0.0227314633	1.0677337105
H3	0.9988983893	0.0261400407	-0.3501462705
H4	-0.5043604874	0.9272321443	-0.3110995909
C5	-1.7013591156	-0.9660647165	6.1536711551
H6	-2.6917547740	-0.5670715974	6.2117271044
H7	-1.1006910237	-0.5412631660	6.9295846287
H8	-1.2764056563	-0.7230233743	5.2009135610
C9	-2.0296403239	-5.8873697069	10.0020610005
H10	-3.0901207061	-6.0551085610	10.2000334071
H11	-1.7261518055	-4.9329228284	10.4320598201
H12	-1.4441825125	-6.6896444679	10.4494600031
C13	0.9966510692	-8.2122340362	10.6489452512
H14	0.4641864046	-9.0475321446	11.0518016080
H15	1.5504428052	-7.7408457812	11.4349221829
H16	0.2878818523	-7.4919042196	10.2418124523
C17	-7.6871217939	-3.5790958934	-0.8818299485
H18	-8.2407048277	-4.4619565493	-0.6466216196
H19	-8.3029677839	-2.7167645236	-0.7297931287
H20	-7.3727903577	-3.6146479259	-1.9046114062
C21	-9.5343180138	-3.0399103556	6.3420834539
H22	-10.5540153811	-3.2495387930	6.6650806270
H23	-9.2334046070	-2.0553036248	6.7014527388
H24	-8.8612797368	-3.7947612036	6.7484487489
C25	2.5852073048	-3.5534830187	-0.1210956140
H26	2.1559329432	-2.6788412648	0.3213081365
H27	3.6465019163	-3.4351727837	-0.1831488062
H28	2.1825265573	-3.6884139614	-1.1029283107
C29	-7.4982127054	-5.1515975422	8.8496374832

H30	-8.0216150837	-6.0414999550	8.5730984790
H31	-7.7165390869	-4.9273431544	9.8730296015
H32	-7.8413258933	-4.3214725574	8.2330895785
Zn33	-4.2110508636	-4.0770526849	2.8671415791
C34	-0.7542662529	-1.1925669214	-0.5934344878
C35	-1.9921576339	-1.5360242666	0.1615110981
N36	-3.0269859532	-0.6511692065	0.4356787814
C37	-3.9245876134	-1.2891556278	1.2374818386
N38	-3.5241941234	-2.5176460432	1.4850767710
C39	-2.3301293528	-2.6857578630	0.8222941882
C40	-1.7160127103	-2.5012116945	6.3126165722
C41	-2.1158907715	-3.2585779759	5.0435806429
O42	-3.1460501163	-2.8715959026	4.4100318602
O43	-1.3710743172	-4.2286285995	4.7134805882
C44	-6.4601028158	-3.5446940308	0.0436029872
C45	-5.8576341142	-4.9440545164	0.2823912237
O46	-5.1808867453	-5.1210526774	1.3589751241
O47	-6.0711773306	-5.8201501959	-0.5764306202
C48	-9.4522973133	-3.0150743571	4.8055540292
C49	-8.0399683594	-2.8081589169	4.3717975550
N50	-7.2162703012	-1.8267169085	4.9141366650
C51	-5.9591136511	-2.0114935863	4.4357268378
N52	-5.9414008411	-3.0276998571	3.5989057956
C53	-7.2201037205	-3.5356951960	3.5554577686
H54	-0.9718840693	-1.0009632592	-1.6544653625
H55	-0.1244586448	-2.0859106294	-0.5705694659
H56	-3.1058779607	0.2965562969	0.1007704216
H57	-4.8331663170	-0.8345053146	1.6031233984
H58	-1.7919508232	-3.6200042448	0.8573107174
H59	-0.7276999552	-2.8653041765	6.6069543212
H60	-2.4187118427	-2.7960749842	7.1023534907
H61	-5.6665473196	-2.9140178746	-0.3774619701
H62	-6.7091795736	-3.1022821353	1.0117311877
H63	-9.8005827186	-3.9609709124	4.3791670988
H64	-10.1156046397	-2.2306666593	4.4116336013
H65	-7.4788344241	-1.1522553362	5.6157323979
H66	-5.0847267718	-1.4589861984	4.7445880115
H67	-7.4470888815	-4.4104579655	2.9659110427
C68	-1.7573122859	-5.8797649425	8.4779225628
C69	-1.9466898224	-7.2166186088	7.8041521912
C70	-3.1021368309	-7.9555369474	7.7643510968
N71	-2.9268787215	-9.1293734815	7.0498595773
C72	-1.6391908772	-9.1365413016	6.5492048194
C73	-1.0081165930	-10.0732678403	5.7246678742
C74	0.3151985002	-9.8302168167	5.3621982564
C75	0.9777550361	-8.6590725140	5.7956970625
C76	0.3390574290	-7.7216732056	6.6060970569
C77	-0.9853327719	-7.9563721738	7.0139830664
H78	-2.4102182771	-5.1426485284	7.9941373530
H79	-0.7298672494	-5.5379972426	8.3024441490
H80	-4.0813638396	-7.7319307488	8.1605631415
H81	-3.7114142114	-9.5084698096	6.5244069577
H82	-1.5446773369	-10.9377398720	5.3424356824
H83	0.8275196145	-10.5378117598	4.7132893441
H84	2.0118801292	-8.4938544990	5.4997040032
H85	0.8546290786	-6.8129006262	6.9064211161

C86	2.0029566762	-8.7353071805	9.5834108476
C87	3.4276815158	-8.8107139659	10.1598999691
C88	1.5573967392	-10.0818868605	8.9678627075
C89	1.6104082421	-11.2956809970	9.9064558778
H90	2.0300564916	-8.0173674921	8.7558946153
H91	3.4739445999	-9.4510639349	11.0492528488
H92	4.1367071192	-9.2119905202	9.4252568228
H93	3.7831992982	-7.8164744008	10.4570165848
H94	0.5384742741	-9.9668810073	8.5823304382
H95	2.1827226297	-10.2892385222	8.0906109490
H96	1.0040800862	-11.1518280943	10.8088392774
H97	1.2250225061	-12.1863111365	9.3983487093
H98	2.6327524893	-11.5217461377	10.2308942680
C99	2.2273327992	-4.7933552265	0.7061980855
C100	0.7691951419	-5.1787689714	0.5309302734
O101	0.0101858120	-4.6252086604	-0.2469148736
O102	0.4087098877	-6.2058584057	1.3028912064
H103	2.8280837424	-5.6613075229	0.4034407845
H104	2.4212858144	-4.6570454173	1.7765802992
H105	-0.5528202166	-6.4765491553	1.1385014591
C106	-5.9873103383	-5.3481261582	8.6623824995
C107	-5.6480384624	-5.8130891958	7.2390736449
O108	-6.1316769957	-6.9142792340	6.8730623606
O109	-4.9008059573	-5.0387529455	6.5576986610
H110	-5.4442883390	-4.4233971535	8.8805622211
H111	-5.6367471210	-6.1179959374	9.3627703748
O112	-5.1927342613	-8.4868649400	-0.5992232723
H113	-5.5302027056	-7.5655286861	-0.5366251542
H114	-4.9220431910	-8.7133352027	0.3014156068
O115	0.9275882715	-8.6744739125	2.5451053342
H116	0.7468182144	-8.5348669927	3.4891390499
H117	0.9636534382	-7.7939373183	2.1344125247
O118	-1.1019509344	-10.3797413798	1.5316566960
H119	-0.4754969625	-9.7421265841	1.9299071806
H120	-1.8206303400	-9.8091520789	1.2110848328
O121	1.6060325564	-11.4655335926	2.4768464484
H122	1.6802023907	-10.5012781056	2.3937533920
H123	0.7263858635	-11.6320587699	2.1085783984
O124	-1.8784358571	-7.3353536064	0.8203551100
C125	-2.1702642907	-7.2908974608	-0.5988016051
C126	-3.0204825750	-7.3363282102	1.6720359334
C127	-2.6436697331	-6.6535607124	2.9873054203
O128	-2.3878808823	-5.2886783767	2.7033031963
C129	-3.7305908955	-6.8335138877	4.1042947888
O130	-4.5737057678	-5.6989574617	4.1792177464
C131	-4.5556535474	-8.1217747514	3.8926131533
O132	-5.0654965887	-8.6511531968	5.1001653437
C133	-3.6312203903	-9.1484418526	3.2230265433
O134	-3.4065686037	-8.7019895095	1.8583202876
C135	-4.1288930498	-10.5935328402	3.1648197533
O136	-3.0773332348	-11.5435227627	3.2259326917
H137	-2.2096894962	-6.2489029217	-0.9310987452
H138	-1.3453926660	-7.8042238114	-1.1008549268
H139	-3.1185871739	-7.7963046783	-0.8095139731
H140	-3.8392104964	-6.7968885934	1.1895415898
H141	-1.7164907828	-7.1232594137	3.3446793410

H142	-1.8902556673	-4.8693736135	3.5274486024
H143	-3.1960127412	-6.9366808977	5.0569640182
H144	-4.7191083592	-5.4382320499	5.1846229718
H145	-5.3726955162	-7.8829804086	3.1926478011
H146	-5.4977835530	-7.9312146727	5.6351049351
H147	-2.6755828172	-9.1734792718	3.7626220453
H148	-4.7449465619	-10.7120918275	2.2575058842
H149	-4.7728392328	-10.7719152158	4.0303943174
H150	-2.3562237739	-11.2502918922	2.6312948604
Transition state (Model 3)			
E _{absolute} = -3419.81809396550 hartrees			
C1	0.0000000000	0.0000000000	0.0000000000
H2	0.0000000000	0.0000000000	1.0710859869
H3	1.0129296111	0.0000000000	-0.3457200542
H4	-0.4916254253	0.8991154856	-0.3113411458
C5	-1.6928754250	-0.9738480410	6.1585643246
H6	-2.6838888477	-0.5760470258	6.2142088115
H7	-1.0936291346	-0.5455670576	6.9336640290
H8	-1.2675549188	-0.7328815882	5.2054435526
C9	-2.0183759825	-5.8824833176	10.0233373224
H10	-3.0788311531	-6.0510339487	10.2207545244
H11	-1.7166807176	-4.9261540690	10.4504057544
H12	-1.4322739066	-6.6824091800	10.4740861440
C13	1.0104728023	-8.2008869941	10.6813436119
H14	0.4787478708	-9.0355551009	11.0864763566
H15	1.5627667626	-7.7260506125	11.4662981992
H16	0.3011311245	-7.4829414222	10.2710089926
C17	-7.6674810144	-3.6191649314	-0.8743904834
H18	-8.2200840743	-4.5019934261	-0.6367694040
H19	-8.2846915677	-2.7571831987	-0.7259466486
H20	-7.3520050853	-3.6577564408	-1.8967092904
C21	-9.5231724148	-3.0579882329	6.3456702867
H22	-10.5429222323	-3.2679419410	6.6682903803
H23	-9.2240177499	-2.0717448137	6.7020071795
H24	-8.8495181197	-3.8105105633	6.7553201558
C25	2.6039858388	-3.5766003605	-0.1027976154
H26	2.1730187455	-2.7010597951	0.3361691664
H27	3.6651800935	-3.4570174576	-0.1641233668
H28	2.2025438301	-3.7154343322	-1.0845934340
C29	-7.4868128088	-5.1582846124	8.8625671009
H30	-8.0086770197	-6.0498535399	8.5885000175
H31	-7.7065482510	-4.9308558490	9.8849566354
H32	-7.8304223816	-4.3307422380	8.2428320415
Zn33	-4.2439469913	-3.7761458922	2.9073781739
C34	-0.7182042977	-1.2201945210	-0.6098676516
C35	-2.0043430797	-1.5063663142	0.0785190217
N36	-3.0290372950	-0.5882388851	0.2727782025
C37	-3.9615478722	-1.1626531745	1.0790571528
N38	-3.5915326909	-2.3854471853	1.4022088401
C39	-2.3809924346	-2.6149786034	0.7834100092
C40	-1.7172472932	-2.5065869919	6.3104074568
C41	-2.1694820056	-3.2273750537	5.0415734466
O42	-3.1599326269	-2.7330991804	4.4088131668
O43	-1.5190502049	-4.2574389739	4.7071022490
C44	-6.4506554635	-3.5441932144	0.0659476316

C45	-5.7846875815	-4.9063627036	0.3363138824
O46	-5.2313252078	-5.0527267031	1.5004319022
O47	-5.8066516419	-5.7724084928	-0.5505404860
C48	-9.4837338754	-3.0282052912	4.8074908253
C49	-8.1143075289	-2.6937883309	4.3267396386
N50	-7.4124054205	-1.5672659178	4.7434465875
C51	-6.1450106568	-1.6531361504	4.2620739389
N52	-6.0093295948	-2.7479330687	3.5449608730
C53	-7.2179815003	-3.4051645462	3.5815045289
H54	-0.8629174985	-1.0463602009	-1.6871625559
H55	-0.1160357809	-2.1303712487	-0.5187359413
H56	-3.0726941932	0.3448179346	-0.1093081620
H57	-4.8734357831	-0.6740706004	1.3902370370
H58	-1.8472438433	-3.5516354477	0.8701009159
H59	-0.7263694611	-2.8907914183	6.5714708960
H60	-2.4018056563	-2.8021432393	7.1166535001
H61	-5.6773491001	-2.8906144110	-0.3576003705
H62	-6.7321393927	-3.0949477007	1.0214432177
H63	-9.7628278190	-4.0018729884	4.3912239115
H64	-10.2262726909	-2.3046481722	4.4376636518
H65	-7.7583190345	-0.8456219494	5.3584112530
H66	-5.3567625283	-0.9485160109	4.4816850866
H67	-7.3359482102	-4.3618922347	3.0962472146
C68	-1.7413249609	-5.8171782059	8.5011925438
C69	-1.9258106170	-7.0986645644	7.7283301994
C70	-3.0667014527	-7.8522759956	7.6258318795
N71	-2.8764346249	-8.9412444756	6.7865733071
C72	-1.5943254067	-8.8661467551	6.2730100798
C73	-0.9391824149	-9.7064755284	5.3687147025
C74	0.3840169056	-9.4133008379	5.0517737343
C75	1.0299822275	-8.2895211822	5.6104126149
C76	0.3689525611	-7.4453838538	6.4983810429
C77	-0.9589171038	-7.7320090454	6.8576430306
H78	-2.3865558388	-5.0467468450	8.0592883160
H79	-0.7114292925	-5.4675840932	8.3527979497
H80	-4.0416372266	-7.7001289784	8.0640785367
H81	-3.6566131924	-9.3144338314	6.2520529027
H82	-1.4416070827	-10.5622611793	4.9251997551
H83	0.9175354332	-10.0642268293	4.3650515826
H84	2.0660307140	-8.0855860313	5.3462930915
H85	0.8731638416	-6.5711272633	6.9031913892
C86	1.9964566802	-8.7216764902	9.6013475874
C87	3.3761487192	-9.0208306140	10.2124455242
C88	1.4283060799	-9.9359514024	8.8298317866
C89	1.3301736602	-11.2475345944	9.6227838669
H90	2.1385807270	-7.9258557689	8.8583240197
H91	3.3092693231	-9.7474220656	11.0326140040
H92	4.0660590778	-9.4292499712	9.4623947950
H93	3.8296782771	-8.1086992132	10.6216222293
H94	0.4366155909	-9.6711008308	8.4461345442
H95	2.0514796037	-10.1086220211	7.9426942637
H96	0.7168650136	-11.1441347704	10.5271017934
H97	0.8677562657	-12.0281996719	9.0072133460
H98	2.3153966467	-11.6166529425	9.9339304809
C99	2.2408283272	-4.8264280638	0.7120133001
C100	0.7847856595	-5.2819240590	0.4952167151

O101	-0.0115916264	-4.5392859598	-0.1068104945
O102	0.5098540191	-6.4502655859	0.9609605831
H103	2.8915130999	-5.6693027200	0.4451474597
H104	2.3916703561	-4.6687398211	1.7889879963
H105	-0.8469513464	-7.1279910216	0.6176032645
C106	-5.9757561341	-5.3627435418	8.6948385947
C107	-5.6200533427	-5.7714006576	7.2610333929
O108	-6.1162787530	-6.8479805942	6.8360867731
O109	-4.8534721125	-4.9748329806	6.6315860897
H110	-5.4284143035	-4.4515562298	8.9564711894
H111	-5.6467156384	-6.1614753392	9.3743314880
O112	-5.0825265986	-8.5131520610	-1.3904134361
H113	-5.3618510074	-7.6458515619	-1.0369372562
H114	-4.9692387710	-9.0734535519	-0.6038446921
O115	1.8164491436	-8.3023223612	2.3325599004
H116	1.4079020990	-8.1085134538	3.1922635133
H117	1.4416301136	-7.5850208183	1.7456805917
O118	-1.9177476996	-10.2003579900	1.4776226273
H119	-1.0062377147	-10.5103158180	1.6957167399
H120	-1.7825559216	-9.3505049843	0.9989524302
O121	0.7697846284	-10.7467914936	1.8657361402
H122	1.1502811116	-9.8302460158	1.9936495632
H123	1.0794616348	-11.0156449406	0.9880161646
O124	-1.6710986234	-7.6686266398	0.3505498701
C125	-1.8092573971	-7.5502744457	-1.0693691194
C126	-3.6334662831	-6.8650970997	1.4312525698
C127	-2.9879116157	-6.4215465917	2.7074969510
O128	-2.5469380375	-5.0997388202	2.5790456424
C129	-3.9500833382	-6.6262920161	3.9404761674
O130	-4.6570338797	-5.4342022661	4.1888883619
C131	-4.9288666503	-7.8051511347	3.7199255545
O132	-5.2019239006	-8.5296926222	4.9015519937
C133	-4.3497581552	-8.7533213187	2.6705301361
O134	-4.2815183723	-7.9659412238	1.4163967805
C135	-5.1487497642	-9.9986253666	2.3158376535
O136	-4.6231479235	-10.6515990453	1.1791826068
H137	-1.6611728882	-6.5074327595	-1.3759436889
H138	-1.0618107588	-8.1737096618	-1.5825223419
H139	-2.8122552438	-7.8909142104	-1.3468228702
H140	-3.6079370429	-6.3199220685	0.5045700659
H141	-2.1314259891	-7.0979528205	2.8486938930
H142	-2.0189186725	-4.8164298231	3.4423016231
H143	-3.3122964178	-6.8609570170	4.8006632111
H144	-4.7251113247	-5.2667927921	5.2223822637
H145	-5.8512643202	-7.3729737227	3.3032474044
H146	-5.5699391145	-7.8812841607	5.5692755468
H147	-3.3202763384	-9.0507568758	2.8938777741
H148	-6.1866931154	-9.7280429908	2.0874098830
H149	-5.1608179118	-10.6401641025	3.2107833096
H150	-3.6379635463	-10.6847951813	1.2657726007
Covalent intermediate (Model 3)			
$E_{\text{absolute}} = -3419.83818022281$ hartrees			
C1	0.0060422221	-0.0047110369	0.0052853278
H2	0.0064762705	-0.0058848107	1.0763705836
H3	1.0188290395	-0.0066306726	-0.3408474952

H4	-0.4836674226	0.8958583661	-0.3048706625
C5	-1.6865432541	-0.9814635716	6.1634693657
H6	-2.6766286399	-0.5814760248	6.2199534500
H7	-1.0860124206	-0.5553931477	6.9387931570
H8	-1.2614052624	-0.7397872705	5.2104468981
C9	-2.0216174988	-5.8935799284	10.0229977524
H10	-3.0823723948	-6.0599400137	10.2206626421
H11	-1.7175794698	-4.9384063250	10.4509900121
H12	-1.4371498428	-6.6953271780	10.4726314207
C13	1.0022280030	-8.2195703053	10.6772301217
H14	0.4687742855	-9.0534731603	11.0816654711
H15	1.5559162869	-7.7468488878	11.4624789087
H16	0.2943513862	-7.4995677229	10.2679711124
C17	-7.6699868687	-3.6055074285	-0.8699412095
H18	-8.2244958494	-4.4873395747	-0.6330616479
H19	-8.2851792544	-2.7422905508	-0.7203019867
H20	-7.3550136457	-3.6436943408	-1.8924302011
C21	-9.5214738902	-3.0480340243	6.3514856979
H22	-10.5415667781	-3.2560266283	6.6742914464
H23	-9.2199372218	-2.0628630782	6.7087802839
H24	-8.8493633303	-3.8025315431	6.7600366388
C25	2.6018620345	-3.5870962415	-0.1024901679
H26	2.1730611054	-2.7110615817	0.3376107190
H27	3.6633000213	-3.4698545226	-0.1641176295
H28	2.1997081200	-3.7239429123	-1.0842736498
C29	-7.4888666682	-5.1557028584	8.8652507758
H30	-8.0128640861	-6.0457844000	8.5904204122
H31	-7.7076710423	-4.9288966251	9.8879782300
H32	-7.8308482478	-4.3267042344	8.2465623693
Zn33	-4.2247574777	-3.5094145815	3.0563445600
C34	-0.7264585664	-1.2236331755	-0.5919321286
C35	-2.0329969194	-1.4687773644	0.0784237702
N36	-3.0410299199	-0.5258521399	0.2361424164
C37	-4.0047152752	-1.0624201408	1.0282653774
N38	-3.6728152448	-2.2934067269	1.3784578998
C39	-2.4516589286	-2.5605613610	0.7878233518
C40	-1.6856974325	-2.5058116625	6.3378104946
C41	-2.2159100570	-3.2100480355	5.1028959253
O42	-3.1635553255	-2.5943993708	4.4918282192
O43	-1.6984538819	-4.2989930803	4.7565404572
C44	-6.4424970362	-3.5940239116	0.0532960775
C45	-5.6585743277	-4.9015508241	-0.0059181420
O46	-5.0944777035	-5.2033991253	1.1910908993
O47	-5.5459857541	-5.5817825134	-1.0028415646
C48	-9.5329403018	-3.0336041019	4.8100596871
C49	-8.2202504619	-2.6165929030	4.2477745880
N50	-7.6921565292	-1.3393955483	4.3824777216
C51	-6.4228059047	-1.3510179100	3.8980369478
N52	-6.1184860800	-2.5533724177	3.4514965312
C53	-7.2252811617	-3.3478581895	3.6653330395
H54	-0.8537394273	-1.0716620784	-1.6738799417
H55	-0.1502097057	-2.1468828102	-0.4667208978
H56	-3.0543741187	0.4006733898	-0.1614316601
H57	-4.9102339217	-0.5456069272	1.3096404891
H58	-1.9378863682	-3.5064162418	0.8952986774
H59	-0.6804123618	-2.8864427693	6.5409845404

H60	-2.3179090429	-2.7992695972	7.1856027926
H61	-5.7418411796	-2.7989458886	-0.2246972830
H62	-6.7314507221	-3.3996567335	1.0868168360
H63	-9.7683262158	-4.0294730516	4.4218813617
H64	-10.3339405109	-2.3667344058	4.4596382015
H65	-8.1523365530	-0.5482756086	4.8067300605
H66	-5.7641818155	-0.4953688850	3.9131579712
H67	-7.1940094894	-4.4032445552	3.4439342390
C68	-1.7404418334	-5.7897668172	8.5009082113
C69	-1.9462191121	-7.0119025637	7.6393177749
C70	-3.1179994317	-7.6924975921	7.4175265778
N71	-2.9427917291	-8.6980592726	6.4808107906
C72	-1.6350730093	-8.6529379455	6.0374879244
C73	-0.9807608813	-9.4437351642	5.0887545557
C74	0.3698490358	-9.1987396698	4.8626617735
C75	1.0431343486	-8.1623844701	5.5441775755
C76	0.3835213533	-7.3651151060	6.4745564224
C77	-0.9721690870	-7.6127809668	6.7532666943
H78	-2.3591083488	-4.9762502012	8.0994644002
H79	-0.7039460118	-5.4557330827	8.3708218344
H80	-4.1011818298	-7.5413428497	7.8353253161
H81	-3.7199179917	-9.0343642859	5.9161338317
H82	-1.5057023725	-10.2160491060	4.5341916065
H83	0.9009235768	-9.8215865176	4.1496181518
H84	2.0971702693	-7.9883236923	5.3382687533
H85	0.9112837201	-6.5579874829	6.9771592755
C86	1.9753401275	-8.7415336425	9.5894794700
C87	3.3288752698	-9.1358634025	10.2041918820
C88	1.3547536787	-9.8899403484	8.7594412870
C89	1.1785286094	-11.2271363809	9.4932339233
H90	2.1668963639	-7.9219944077	8.8845356539
H91	3.2137509829	-9.8922482630	10.9900833140
H92	4.0080731730	-9.5458080962	9.4468217111
H93	3.8213999836	-8.2675229274	10.6585420549
H94	0.3843048766	-9.5563963495	8.3769536106
H95	1.9777247421	-10.0557328053	7.8716654737
H96	0.5584040830	-11.1319180528	10.3925803404
H97	0.6861844400	-11.9552510717	8.8396726519
H98	2.1379014677	-11.6598135720	9.8000901437
C99	2.1899963682	-4.8397883071	0.6886342222
C100	0.7236708151	-5.2298420480	0.3947171664
O101	-0.0617145712	-4.3526566908	-0.0132927459
O102	0.4302846840	-6.4648219287	0.5816564498
H103	2.8248314886	-5.6970183756	0.4386459759
H104	2.2958672946	-4.6900652943	1.7719404742
H105	-0.9646613132	-7.1420089943	0.1196486443
C106	-5.9910091095	-5.3787481052	8.6262283340
C107	-5.7803418445	-5.7475514451	7.1534389442
O108	-6.2208770294	-6.8589268481	6.7692575348
O109	-5.2071079836	-4.8592200330	6.4404994010
H110	-5.4124242362	-4.4819856927	8.8658321953
H111	-5.6365145177	-6.2030669909	9.2570825422
O112	-5.1659039131	-8.9285929361	-1.5399318713
H113	-5.2218345309	-8.0238348737	-1.2027892344
H114	-5.0631141364	-9.4552075986	-0.7243658474
O115	1.6871853163	-8.2605224525	2.0201439761

H116	1.3622942056	-8.0074614943	2.8956178056
H117	1.2843027556	-7.5678249596	1.4189723478
O118	-2.2569813176	-9.9330758258	1.3726421977
H119	-1.3680289330	-10.2947848662	1.5748903130
H120	-2.0811776318	-9.1352505487	0.8210289725
O121	0.4179912373	-10.6287467425	1.7613920825
H122	0.8720002367	-9.7424667126	1.8046102669
H123	0.7193678508	-11.0155537928	0.9307275262
O124	-1.7828945924	-7.6732877589	-0.1132214978
C125	-1.8398649164	-7.8913323060	-1.5147505524
C126	-4.1574016704	-6.3612064566	1.2267376908
C127	-3.3759927255	-6.2256525131	2.5300526382
O128	-2.7548320747	-4.9525142991	2.5584555029
C129	-4.2925006273	-6.4298617598	3.7624207224
O130	-4.9902725890	-5.2151658951	4.0259432943
C131	-5.2824381444	-7.6090167321	3.5497538038
O132	-5.4015690944	-8.4312357822	4.6984540593
C133	-4.7979816989	-8.4189219159	2.3459951925
O134	-4.8648636002	-7.5551984612	1.1775200187
C135	-5.5651620284	-9.6858313336	2.0008951461
O136	-4.9336782461	-10.4168916064	0.9594461605
H137	-1.7386536243	-6.9475943549	-2.0699480531
H138	-1.0458848528	-8.5742743543	-1.8605578203
H139	-2.8145187033	-8.3345232620	-1.7438823972
H140	-3.5122145461	-6.2767703471	0.3535149429
H141	-2.6044607055	-7.0012548516	2.5109960177
H142	-2.2136106111	-4.8259363566	3.4257262503
H143	-3.6525729793	-6.6694185087	4.6202114245
H144	-5.1075917520	-5.1017130114	5.0861134666
H145	-6.2571907211	-7.1680085429	3.2877249897
H146	-5.7541145588	-7.8560968523	5.4264329407
H147	-3.7595566067	-8.7316610382	2.5019746738
H148	-6.5775480661	-9.4366477640	1.6591693459
H149	-5.6530563025	-10.2809553186	2.9217106197
H150	-3.9588584313	-10.4124402298	1.1195461738
Transition state TS2 (Model 4)			
$E_{\text{absolute}} = -3419.79485197980$ hartrees			
C1	-0.0002514101	-0.0020821259	-0.0067253212
H2	0.0007162989	-0.0020755382	1.0643602286
H3	1.0123629569	-0.0043238575	-0.3533603922
H4	-0.4901687647	0.8981162487	-0.3176294811
C5	-1.6897110153	-0.9721469062	6.1533738939
H6	-2.6797917914	-0.5721553650	6.2099104698
H7	-1.0888192011	-0.5451871441	6.9279283846
H8	-1.2622516922	-0.7369675422	5.1997645587
C9	-2.0225719297	-5.8800266677	10.0184794768
H10	-3.0832183789	-6.0462309773	10.2168560711
H11	-1.7183772113	-4.9243641786	10.4452673519
H12	-1.4378329272	-6.6812436807	10.4687051157
C13	1.0017366904	-8.2051174731	10.6737679335
H14	0.4685338448	-9.0386053862	11.0793877263
H15	1.5557881454	-7.7314985471	11.4582193406
H16	0.2936136916	-7.4856078154	10.2640684939
C17	-7.6765026322	-3.6042905069	-0.8741588000
H18	-8.2308413903	-4.4858935635	-0.6360313928

H19	-8.2916714400	-2.7409452970	-0.7251643935
H20	-7.3620365679	-3.6435857123	-1.8967618953
C21	-9.5244248588	-3.0389681275	6.3475710007
H22	-10.5443445051	-3.2466646468	6.6711139586
H23	-9.2227684913	-2.0533863882	6.7036294899
H24	-8.8520662365	-3.7929756038	6.7566181753
C25	2.5957262683	-3.5844318164	-0.1118464213
H26	2.1670928296	-2.7079378274	0.3275024325
H27	3.6571264851	-3.4671958830	-0.1741318942
H28	2.1930913901	-3.7223838917	-1.0932780120
C29	-7.4904409517	-5.1437465314	8.8626440121
H30	-8.0145225855	-6.0341610808	8.5890557362
H31	-7.7087492070	-4.9158262506	9.8852298121
H32	-7.8327797270	-4.3154502151	8.2432129512
Zn33	-4.2200136469	-4.0108936070	2.8662118964
C34	-0.7215890178	-1.2307884824	-0.6002984541
C35	-1.9613818732	-1.5763645841	0.1468591214
N36	-2.9656054414	-0.6725694619	0.4697539808
C37	-3.8690562132	-1.3096361677	1.2611080234
N38	-3.5008643418	-2.5600380876	1.4537884310
C39	-2.3214314025	-2.7432982230	0.7651089183
C40	-1.7067402363	-2.5130774009	6.2995276137
C41	-2.2020435458	-3.3144705131	5.0801636990
O42	-3.1676037394	-2.8466920733	4.3964415950
O43	-1.6125578303	-4.4112201575	4.8567067651
C44	-6.4484695068	-3.5506367229	0.0565016601
C45	-5.7704393733	-4.9243815471	0.2504332778
O46	-5.1629751831	-5.1335179908	1.3702522277
O47	-5.8617126004	-5.7421227408	-0.6796171467
C48	-9.4583747658	-3.0121862156	4.8099772472
C49	-8.0618911933	-2.7616197031	4.3508306879
N50	-7.2748496119	-1.7210135310	4.8332428904
C51	-6.0180997579	-1.8733252183	4.3393430003
N52	-5.9675226572	-2.9263509380	3.5515134342
C53	-7.2231075351	-3.4902140331	3.5554013137
H54	-0.9341491530	-1.0417905743	-1.6630828138
H55	-0.0925328376	-2.1258080005	-0.5668845385
H56	-3.0142166199	0.2906654216	0.1764858575
H57	-4.7562698119	-0.8430865141	1.6621414341
H58	-1.7966802549	-3.6883524366	0.7336810685
H59	-0.7033791761	-2.8838250968	6.5293480907
H60	-2.3471057280	-2.8054976406	7.1425876297
H61	-5.6869368047	-2.8720263507	-0.3484550102
H62	-6.7203981016	-3.1456934670	1.0337344915
H63	-9.7855566105	-3.9673264085	4.3873182314
H64	-10.1505491336	-2.2478691403	4.4264863543
H65	-7.5591482518	-1.0203856096	5.5000174287
H66	-5.1690057139	-1.2627124245	4.6069361375
H67	-7.4187417195	-4.4013480701	3.0117080961
C68	-1.7439049404	-5.8364470651	8.4984104784
C69	-1.9534412868	-7.1303668713	7.7546598323
C70	-3.0844065489	-7.9053385416	7.7274030074
N71	-2.9261125214	-8.9953936103	6.8814989414
C72	-1.6787645262	-8.9004713238	6.2926832641
C73	-1.0664511035	-9.7232779445	5.3418261501
C74	0.2263220709	-9.4006411891	4.9400780997

C75	0.8901708472	-8.2742345696	5.4700921981
C76	0.2717631668	-7.4457494234	6.4015128263
C77	-1.0283516411	-7.7549335878	6.8356482267
H78	-2.3708738905	-5.0625825856	8.0378004825
H79	-0.7083342875	-5.5099005087	8.3434604900
H80	-4.0341846583	-7.7640000283	8.2208442677
H81	-3.7330374158	-9.3805250502	6.3956695858
H82	-1.5783793903	-10.5894054720	4.9308530248
H83	0.7163472287	-10.0169322800	4.1938946499
H84	1.9044703551	-8.0554172601	5.1434889585
H85	0.7836549333	-6.5643611911	6.7788060914
C86	1.9831700769	-8.7120180124	9.5839506121
C87	3.3606976637	-9.0353818782	10.1870699161
C88	1.4040256961	-9.9014730990	8.7832731084
C89	1.2865312008	-11.2274263321	9.5481506435
H90	2.1311022938	-7.8995674712	8.8603278474
H91	3.2884864476	-9.7778391273	10.9911116023
H92	4.0468364775	-9.4326281162	9.4291181406
H93	3.8214296292	-8.1369001029	10.6152589738
H94	0.4180200211	-9.6159491917	8.4018041267
H95	2.0282546454	-10.0615064880	7.8950580585
H96	0.6700001914	-11.1347376354	10.4501980655
H97	0.8186815074	-11.9899364428	8.9160375601
H98	2.2645910164	-11.6140857001	9.8572513461
C99	2.1709312194	-4.8363997966	0.6650677798
C100	0.7572996314	-5.2724329902	0.2337284869
O101	0.0233387345	-4.4626050329	-0.3645552400
O102	0.4377067260	-6.4889150317	0.4954573971
H103	2.8503338052	-5.6766743588	0.4826225049
H104	2.1744177040	-4.6774575766	1.7515730916
H105	-0.9340846201	-6.8158384162	-0.2828832846
C106	-5.9792818858	-5.3479126842	8.7227727532
C107	-5.6571227094	-5.8191628532	7.3106863122
O108	-6.1196413015	-6.9455687956	6.9854079300
O109	-4.9900237175	-5.0151982134	6.5895000467
H110	-5.4362600327	-4.4235168987	8.9403016195
H111	-5.6541346341	-6.1165265008	9.4353946536
O112	-4.9163440745	-8.2871388290	-1.3384031554
H113	-5.2466198978	-7.3978749236	-1.0911187605
H114	-5.0445584883	-8.8069958373	-0.5365835535
O115	1.6427059387	-7.9791376689	2.2431812419
H116	1.2546067000	-7.6726552047	3.0747586995
H117	1.2522454440	-7.3611071757	1.5485407024
O118	-2.3612774928	-8.9225750687	1.0994566565
H119	-1.4840260074	-9.2331187165	1.4478361386
H120	-2.1556151412	-8.4479226719	0.2417825143
O121	0.0311271232	-10.0196322740	1.7147941070
H122	0.6918678740	-9.2928234799	1.9109100527
H123	0.2766783810	-10.3481388535	0.8408875958
O124	-1.7848928887	-7.1795607883	-0.6746113900
C125	-1.8754848197	-6.9384533808	-2.0663482287
C126	-3.6673608016	-7.3052345359	1.6936062915
C127	-3.0974928343	-6.7964030839	2.9995545718
O128	-2.5860534299	-5.4989242103	2.7983078088
C129	-4.1764211149	-6.8218371660	4.1476574523
O130	-4.8395698564	-5.5811300030	4.1956931998

C131	-5.2081288647	-7.9874208927	4.0242710872
O132	-5.3781597581	-8.7180023121	5.2181474656
C133	-4.7564563241	-8.9453452821	2.9352086760
O134	-4.6448902137	-8.1427502026	1.7113122068
C135	-5.6321959246	-10.1168086799	2.5523292000
O136	-5.0055005973	-10.9106298655	1.5531391538
H137	-1.7908069601	-5.8655786427	-2.2796475703
H138	-1.0852412001	-7.4636525711	-2.6284638364
H139	-2.8505354052	-7.3096586349	-2.3898581814
H140	-3.4668871327	-6.8160857128	0.7462962685
H141	-2.2942020064	-7.4852841189	3.2903185598
H142	-2.1138664655	-5.1405508208	3.6616228674
H143	-3.6212526334	-6.9695202688	5.0806540384
H144	-4.9249364851	-5.3231818288	5.2107135382
H145	-6.1531596232	-7.5241919479	3.7042276038
H146	-5.6953671691	-8.0517377968	5.8982386734
H147	-3.7525383834	-9.3299240231	3.1513781528
H148	-6.6056934902	-9.7460337099	2.1970527394
H149	-5.8065765291	-10.7206721660	3.4505444617
H150	-4.2266209129	-10.4351421006	1.2191113025
Hydrolyzed producte PRO (Model 4)			
$E_{\text{absolute}} = -3419.84544562564$ hartrees			
C1	0.0019826568	0.0037881084	-0.0014307813
H2	0.0021713608	0.0033109788	1.0696550896
H3	1.0148513619	0.0038372192	-0.3473292359
H4	-0.4896043841	0.9030931334	-0.3122847447
C5	-1.6899082774	-0.9726276090	6.1569975669
H6	-2.6808706193	-0.5747487285	6.2129939416
H7	-1.0904809623	-0.5447540134	6.9321822866
H8	-1.2609695791	-0.7388447758	5.2037091791
C9	-2.0152367256	-5.8829501176	10.0196411297
H10	-3.0756745590	-6.0514787665	10.2171701959
H11	-1.7133670089	-4.9268424649	10.4470822845
H12	-1.4291382006	-6.6831374276	10.4699302776
C13	1.0134874674	-8.2019606048	10.6760807463
H14	0.4817473643	-9.0367539687	11.0809354048
H15	1.5659690121	-7.7275311669	11.4611493822
H16	0.3041479625	-7.4837588035	10.2661910060
C17	-7.6660270988	-3.6141928677	-0.8760844624
H18	-8.2186798163	-4.4970699381	-0.6387595319
H19	-8.2831222336	-2.7522134912	-0.7271479185
H20	-7.3507350356	-3.6523614991	-1.8984758649
C21	-9.5203889081	-3.0560416249	6.3445523022
H22	-10.5401036331	-3.2660335589	6.6672584250
H23	-9.2210693746	-2.0699880552	6.7012759363
H24	-8.8467403086	-3.8088161146	6.7537479916
C25	2.6055797227	-3.5730357428	-0.1062805638
H26	2.1747806919	-2.6976462363	0.3331522066
H27	3.6667755429	-3.4535353916	-0.1677399962
H28	2.2039504033	-3.7113907111	-1.0880673941
C29	-7.4838030085	-5.1576703016	8.8601536057
H30	-8.0058077960	-6.0490629990	8.5857811685
H31	-7.7033346591	-4.9306745963	9.8826831511
H32	-7.8274361924	-4.3298162220	8.2408480889
Zn33	-4.1470727252	-4.1729129194	2.8788661333

C34	-0.7247468395	-1.2274086116	-0.5843568856
C35	-1.9332156099	-1.5993810625	0.2005124999
N36	-2.9953964087	-0.7471337400	0.4698909327
C37	-3.8497040576	-1.3941461625	1.3109023694
N38	-3.3928189664	-2.5955605695	1.5885013993
C39	-2.2078945988	-2.7393550799	0.9059849777
C40	-1.6928931463	-2.4978327186	6.3814942816
C41	-2.1550200106	-3.3758546083	5.2110456524
O42	-3.1040283579	-2.9648714680	4.4723658495
O43	-1.5405189404	-4.4730932366	5.0859981607
C44	-6.4285532339	-3.5680297709	0.0316858087
C45	-5.7229178207	-4.9356957722	0.1737943815
O46	-4.9348320743	-5.0771315355	1.1742365982
O47	-5.9586473510	-5.8001999905	-0.6927628458
C48	-9.4197549739	-3.0406702175	4.8082356640
C49	-8.0003286434	-2.8540892617	4.3811256425
N50	-7.1586504811	-1.8959365931	4.9357943192
C51	-5.9091653736	-2.0863278758	4.4391832627
N52	-5.9107862078	-3.0809308309	3.5760578423
C53	-7.1976137285	-3.5719176882	3.5389859753
H54	-0.9715663948	-1.0370179513	-1.6390310498
H55	-0.0762813006	-2.1076969276	-0.5784097686
H56	-3.1216226962	0.1827368412	0.1018335564
H57	-4.7715170312	-0.9697989992	1.6793013924
H58	-1.6299175934	-3.6501449996	0.9479348329
H59	-0.6890684655	-2.8424022202	6.6474807642
H60	-2.3366268580	-2.7428849424	7.2374285585
H61	-5.6860469524	-2.8580441333	-0.3578026344
H62	-6.6857985886	-3.2049286684	1.0300311784
H63	-9.7763874106	-3.9845841015	4.3839054332
H64	-10.0697511648	-2.2511754740	4.4021373405
H65	-7.4004332388	-1.2444522198	5.6657063141
H66	-5.0235042270	-1.5559915100	4.7555215504
H67	-7.4468702134	-4.4316612142	2.9365326274
C68	-1.7083769115	-5.8118401360	8.5021083754
C69	-1.7848583619	-7.1066970839	7.7347269158
C70	-2.8705767912	-7.9365524584	7.6064440787
N71	-2.5840506756	-9.0119473659	6.7805175936
C72	-1.2932286342	-8.8621015425	6.3115211518
C73	-0.5491095833	-9.6688456792	5.4462054067
C74	0.7602511031	-9.2823948950	5.1672723901
C75	1.3053956296	-8.1014652218	5.7146045762
C76	0.5585960937	-7.2981179383	6.5704833492
C77	-0.7535408753	-7.6790500402	6.9005550082
H78	-2.3769573587	-5.0788101082	8.0334082301
H79	-0.6987560465	-5.4018061055	8.3780430728
H80	-3.8718678539	-7.8333679959	8.0002285464
H81	-3.3375094964	-9.4484482481	6.2487364399
H82	-0.9742183128	-10.5565592286	4.9885218305
H83	1.3708124107	-9.9049354806	4.5189292135
H84	2.3270493004	-7.8214937705	5.4668100421
H85	0.9816229378	-6.3806472348	6.9699741532
C86	2.0128463570	-8.7198852252	9.6075204038
C87	3.3918593170	-8.9925160172	10.2326139182
C88	1.4701918639	-9.9494724200	8.8442971577
C89	1.3748144923	-11.2510987045	9.6529104082

H90	2.1483294674	-7.9311641058	8.8575069334
H91	3.3299074919	-9.7118042965	11.0583327963
H92	4.0941145552	-9.3968486774	9.4931345716
H93	3.8281833303	-8.0710859742	10.6370549572
H94	0.4822116371	-9.7002832634	8.4440660214
H95	2.1068368029	-10.1252863440	7.9682291079
H96	0.7488410343	-11.1419775816	10.5465805928
H97	0.9286645658	-12.0447283014	9.0437649584
H98	2.3582195766	-11.6060323676	9.9826109953
C99	2.2040832182	-4.8542785879	0.6620476665
C100	0.9046930987	-5.4035801414	0.0807792829
O101	0.0434954299	-4.6815835528	-0.4021723995
O102	0.8268132164	-6.7300941447	0.0889066038
H103	2.9702212226	-5.6314267830	0.5845709480
H104	2.0532614153	-4.6661939637	1.7325033942
H105	-0.0194080847	-7.0600954502	-0.4271407687
C106	-5.9776141258	-5.3966549169	8.6836253653
C107	-5.7197532600	-5.9363230199	7.2741301475
O108	-5.9123666618	-7.1690170866	7.0979037111
O109	-5.3895755579	-5.0672351187	6.4093222546
H110	-5.4158386819	-4.4698323218	8.8380471907
H111	-5.6435132541	-6.1395844144	9.4168994768
O112	-5.1316889675	-8.5070479504	-0.8866987224
H113	-5.5117167729	-7.6013540597	-0.8098794724
H114	-4.5820015304	-8.5448161240	-0.0884069375
O115	1.1889697985	-8.7580999452	2.1135541086
H116	0.9874048768	-8.3476817761	2.9684909033
H117	1.0657963565	-8.0528520464	1.4507564481
O118	-2.1023630515	-8.1856908907	1.3062165384
H119	-1.8955190951	-9.0138296528	1.8023173195
H120	-1.6325986884	-8.0305072348	-0.2520892842
O121	-0.9657635622	-10.4409537937	2.2363883281
H122	-0.1185085724	-9.9393090037	2.1391332117
H123	-1.0315847572	-10.9975878354	1.4501913606
O124	-1.1598429233	-7.7620992031	-1.0834834796
C125	-2.0670138584	-6.9698800993	-1.8709273205
C126	-3.2103256153	-7.4650733881	1.8222339199
C127	-2.9106649422	-6.9015253668	3.2218012933
O128	-2.4437119623	-5.5682299471	3.0191138672
C129	-4.1050018878	-6.9343601120	4.2086047389
O130	-4.8853098399	-5.7531137840	4.0711598591
C131	-5.0302430523	-8.1829267838	4.0712628360
O132	-5.0778803754	-8.9737533976	5.2529811968
C133	-4.6823692404	-9.0793706339	2.8781843741
O134	-4.3871704584	-8.2322452830	1.7646519212
C135	-5.8808644512	-9.9322408045	2.4379049036
O136	-5.6700480536	-10.6309338574	1.2292018096
H137	-2.0759481196	-5.9292560204	-1.5287624177
H138	-1.7183523055	-6.9990488057	-2.9081594451
H139	-3.0767331994	-7.3897593247	-1.8158665628
H140	-3.3858824134	-6.6330781313	1.1430357087
H141	-2.1067315072	-7.5031893779	3.6664123159
H142	-2.0234305189	-5.1969983543	3.8908281154
H143	-3.6809482785	-6.9441639156	5.2180132718
H144	-5.1567160983	-5.4707795230	5.0348238006
H145	-6.0234269266	-7.7573262743	3.8686645616

H146	-5.4455982186	-8.3661001930	5.9462018023
H147	-3.8252329279	-9.7318509605	3.1079225814
H148	-6.7568850941	-9.2666251795	2.3692035398
H149	-6.0842884795	-10.6681547881	3.2231572384
H150	-5.6946827799	-9.9816673076	0.5013407023

CHAPTER 5
CONCLUSIONS

Glycosidases are enzymes that play crucial roles in the biosynthesis of glycoproteins. Inhibitors of these enzymes have garnered much attention as lead compounds for drug discovery for diseases such as viral and bacterial infections, diabetes, Gauchers disease, and cancer. In many cases, the mode of inhibition by these compounds is not well understood, complicating efforts to design and synthesize more potent and/or selective inhibitors. As a result, only a very small number of glycosidase inhibitors have been successfully developed as therapeutics. In the case of Golgi α -mannosidase II, which is a glycosyl hydrolase family 38 enzyme that acts late in the N-glycan biosynthesis pathway and cleaves selectively α 1,3- and α 1,6 glycosidic linkage between two mannose units, several aspects of the inhibition and the catalytic mechanism are not apparent. In this respect, potent inhibitors of GMII have potential as biochemical tools with which one can delineate further the catalytic and the inhibition mechanism, with a possibility of discovering or designing more potent and selective GMII inhibitors.

Mannostatins A and B, isolated from the soil microorganism *Streptoverticillus*, are some of the most potent inhibitors of class II α -mannosidases reported thus far, and are interesting lead compounds. Despite their structural simplicity, the mannostatins are some of the most potent inhibitors of GMII. A straightforward correlation of their structure with their inhibitory properties remains nonetheless elusive, at least using classical models. In particular it is not clear whether mannostatin A mimics the oxacarbenium ion-like transition state of the hydrolysis reaction catalyzed by GMII. In addition to this, the possible role of thiomethyl moiety in mannostatin A is intriguing, all the more so in that this feature is unique to mannostatin A. If the thiomethyl function plays a role in the binding of mannostatin A by GMII, the extent to which this structural

feature is important remains unclear. Finally, from the viewpoint of the catalytic mechanism of GMII, it is not known what conformational itinerary is followed by the substrate *en route* to the hydrolyzed product. An understanding of this itinerary would be significant in designing, synthesizing and evaluating novel inhibitors of GMII. Moreover, with the knowledge of the transition state structure it would be possible to determine to what extent the potent inhibitors of GMII mimic the transition state. In this dissertation, we have employed a computational approach in conjunction with experiments to address these unanswered questions.

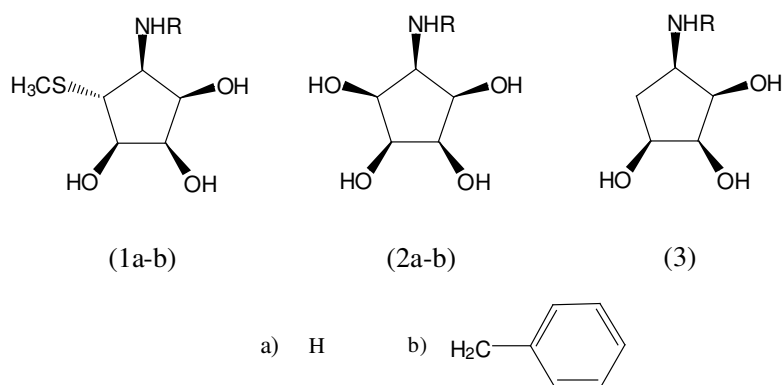


Figure 5.1. GMII inhibitors studied in this dissertation.

In order to understand the mechanism of inhibition of a protein target by a specific ligand, the knowledge of the orientation of the ligand in the binding site is essential. The first project dealt with prediction of the binding mode of mannostatin in the dGMII binding site to rationalize biological data for a set of mannostatin analogues. A range of Mannostatin analogs and structurally simpler aminocyclopentitetroles has been synthesized, which have varying benzylic moieties at their amino function. It was

observed that mannostatin A is a markedly better inhibitor than the corresponding aminocyclopentitretrol. Furthermore, the substitutions of the aminocyclopentitretrols led to significant improvements of inhibitory activity for both hGMII and hLM whereas similar substituents of Mannostatin A had only a marginal effect. Computational studies have been performed to provide a rationale for these observations.

First, the conformational properties of Mannostatin and its analogue aminocyclopentitretrol were studied by geometry optimizations of the ten possible envelope conformations, using *ab initio* molecular orbital calculations. Subsequently, the low energy conformers of each compound were docked in the binding site of dGMII and the results compared with interactions of swainsonine observed in a crystal structure with the same enzyme. It has been shown that Mannostatin and aminocyclopentitretrol could bind to GMII in a similar mode as swainsonine. Probably, the latter compounds mimic the mannosyl oxycarbenium ion, which is a putative intermediate in the hydrolysis of mannosidases. Thus, it appears that Mannostatin and aminocyclopentitretrol can inhibit GMII in a similar fashion. However, due to the flexibility of the five membered rings of **1a** and **2a**, additional low energy binding modes could be adopted. It is conceivable that the ring structure of **1a** and **2a** is flexible in the binding site of GMII allowing transitions between different binding modes. The thiomethyl moiety of Mannostatin could make favorable hydrophobic interactions with Arg228 and Tyr727. These interactions are not present in complexes with aminocyclopentitretrol (**2a**) providing a rationale for the lower inhibitory potential of this compound. It was also observed that the five membered ring of **2a** is significantly more flexible than that of **1a** allowing additional binding modes. Attachment of benzyl moieties to Mannostatin led to stacking interactions with the

aromatic moiety of Tyr269. These π - π interactions required, however, a tilting of the ring structure of **1b** resulting in a disruption of the hydrogen-bonding network observed. Due to the greater flexibility of aminocyclopentitretrol (**2a**), attachment of the benzyl moiety led to conformers that could make the stacking interactions without disrupting hydrogen bonds. This observation may provide a rationale for the improved activities of benzyl-substituted aminocyclopentitretrol.

The predicted binding modes of mannostatin A and its benzylated analogue were validated using X-ray crystallography. An excellent agreement was observed between the predictions and the bound conformations of cyclopentane rings in either inhibitor. Furthermore, from the biological data it was concluded that the thiomethyl group of mannostatin A is required for high affinity binding, as the compound which lacks this moiety was found to be 7000 times less potent than mannostatin A. Analysis of the X-ray structure of dGMII:mannostatin A complex suggested that this functionality is able to make a number of additional interactions increasing the affinity for dGMII. The thiomethyl moiety of **1a** is structurally similar to the side chain of methionine residues. Interestingly, the environment surrounding the thiomethyl group of **1a** is remarkably similar to the arrangements around methionine residues in the protein structure. Another important finding is that the methyl carbon of the thiomethyl moiety of **1a** in the complex with GMII adopts two different conformations. In both conformations, the sulfur interacts with the backbone oxygen of Arg876 through the π -orbital on the carbonyl oxygen and the antibonding σ^* orbital of the S-C bond. In cf1 conformation, the polarizable methyl group is in a hydrophilic environment interacting with three water molecules and the π -system of the Arg228 side chain. Whereas, the methyl group of the cf2 conformation is in

a hydrophobic environment where it forms C–H--- π type interactions with the phenyl rings of Phe206 and Tyr727.

The bound conformation was further compared with the proposed transition state conformers. The studies reported here indicate that Mannostatin A mimics the covalently linked mannosyl intermediate, which has been shown to adopt a 1S_5 skew boat conformation. In particular, the zinc-coordinating 3- and 4-hydroxyls of **1a** display a good overlap with the corresponding *cis*-diol of the mannosyl residue. Furthermore, the amine nitrogen of **1** is positioned close to the C-1 carbon of enzyme-linked mannosyl intermediate and therefore can interact with the carboxylic acid of the catalytic nucleophile Asp204. The thiomethyl functionality showed a good overlay with the C-6 hydroxyl of the covalently linked intermediate.

The MD simulations and NMR studies of the uncomplexed inhibitor showed that the five-membered ring could adopt two different conformational families. In the bound state, however, it is restricted to a single conformation, which is different from the conformations observed for the free ligand. This finding is surprising because it is generally believed that potent inhibitors are complexed in their ground state conformations. Probably, the flexibility of five membered rings renders the energy barrier for the conformational change relatively low.

Compound **1b** was designed in such a way that its benzyl moiety can interact with aromatic residues of the binding site of the enzyme thereby increasing its affinity. However, it was found that this compound has a slightly reduced affinity indicating that the benzyl group cannot make favorable interactions with the enzyme. The unexpected finding could be rationalized by careful examination of the crystal structure of dGMII

with **1b**. Thus, the five-membered ring of compounds **1a** and **1b** were identically positioned in the binding site of dGMII. The distance between the centroid of the aromatic ring of compound **1b** and Tyr269 was such that no edge to face binding interactions could be made. The unexpected orientation of the aromatic ring of **1b** could be rationalized by an intramolecular S---H---Ar type hydrogen bond between the thiomethyl moiety and the phenyl ring.

In addition to the mechanism of inhibition of GMII by mannostatin A, several aspects of the catalytic mechanism of the hydrolysis reaction catalyzed by GMII are not clear. In particular, it is not known which conformation is adopted by the mannopyransoyl ring at the transition state. Furthermore, the exact role of Zn⁺² ion in the catalytic mechanism is intriguing. In order to address these questions, we have studied the hydrolysis reaction catalyzed by GMII using quantum mechanical methods. We have used four models, which differ in the size and the overall charge, to investigate the mechanism. In the first three models, which lack explicit water molecules, the reaction barriers for the glycosylation step were very high (46.5 – 61.5 kcal mol⁻¹). For this reason the deglycosylation step was not performed for these models. Although these models did not result in more realistic energy profiles, the results obtained were beneficial for the refinement of the model. From the QM study of Model 1 – Model 3, it was concluded that all the residues that coordinate with the metal ion present in the active site must be included in the quantum mechanical calculations. Model 3, which includes complete coordination sphere for the Zn⁺² ion, resulted in more stable complex. Unlike Model 1 and Model 2, this model did not display proton abstraction from 2-hydroxyl group by Asp472.

The best results were obtained for Model 4, where the computed activation barrier for the glycosylation step is 15.8 kcal mol⁻¹ at DFT/B3LYP/6-311++G** level. This model includes four water molecules in addition to all the residues in Model 3. In the optimized Michaelis complex, the mannopyranosyl ring in the substrate adopts a perfect ¹S₅ skew boat conformation, where C-2, C-3, C-4 and O-5 atoms are in one plane. This conformation seems to facilitate the departure of the leaving group by forming a hydrogen bond between the anomeric oxygen and the proton from general acid catalyst Asp341.

The mannopyranosyl ring in the transition state TS1 adopts a conformation between S_{2,5} and ¹S₅. Calculation of Wiberg bond indices and natural bond order analysis supported the resemblance of the transition state with the mannopyranosyl oxacarbenium ion. An increased sp² character was observed in the C-1–O-5 bond along with delocalization of positive charge between C-1 and O-5 atoms. At the transition state the C-1–O-1 bond is completely cleaved, suggesting a dissociative nature of the transition state for the glycosylation step in accord with the experimental observations.

The optimized structure of CINT revealed that the sugar ring adopts a skew boat conformation that is very close to an ideal ¹S₅ conformation. The comparison of the optimized CINT structure with the trapped covalent intermediate resulted in staggering similarities. The catalytic nucleophilic oxygen moves away from the Zn⁺² ion. Similar movement of Asp204 was also observed in the X-ray structures of trapped covalent intermediates.

Unlike the glycosylation step, that transition state for the deglycosylation step (TS2) revealed that these atoms are not co-planar. However, increased sp² character was

observed for the C-1–O-5 bond along with the delocalization of the charge across this bond. In this structure the conformation of the sugar ring is slightly skewed boat conformation that lies between $B_{2,5}$ and 0S_2 skew boat conformation. This conformation of the mannopyranosyl ring changes in the hydrolyzed product to a conformation very close to an ideal 0S_2 skew boat conformation.

The calculation presented here suggests that the Zn^{+2} ion in the active site is essential for substrate binding to the active site and the coordination 2- and 3- hydroxyl group with the Zn^{+2} ion in the main driving force for the conformational changes in the substrate. Furthermore, the natural population analysis revealed that the charge on zinc remains unchanged over the course of the reaction. The role of zinc is, thus, structural and not electronic in nature.

Finally, we compared the bound conformation of mannostatin A and swainsonine to the mannopyranosyl ring in the optimized TS1. These superimposition studies revealed that mannostatin A and swainsonine in bound conformation mimic the transition state for the glycosylation step, which has been shown to adopt a conformation that lies between $B_{2,5}$ and 1S_5 skew boat conformation. In particular, the zinc-coordinating 3- and 4-hydroxyls of mannostatin A display a good overlap with the corresponding *cis*-diol of the mannosyl residue. Furthermore, the amine nitrogen of mannostatin A is positioned close to the C-1 carbon of TS1, whereas in the case of swainsonine the amine nitrogen is close to the ring oxygen suggesting that it may mimic the charge build up at the ring oxygen during the formation of the transition state. Collectively these studies indicate that mannostatin A and swainsonine are transition state mimics.

The studies presented in this dissertation are significant in the search of potent and /or selective inhibitors of GMII. With the knowledge of the mechanism of inhibition of GMII by mannostatin A, it is possible to design mannostatin analogues that are more potent or more selective inhibitors of GMII. Furthermore, it is also possible to design molecules, which mimic the transition state conformation. Such molecules would have higher binding affinities against GMII.

REFERENCES

- (1) Varki, A., *Glycobiology* **1993**, 3, 97-130.
- (2) Witczak, Z. J., *Curr. Med. Chem.* **1995**, 1, 392.
- (3) Sears, P.; Wong, C. H., *Proc. Natl. Acad. Sci. U. S. A.* **1996**, 93, 12086-12093.
- (4) Williams, S. J.; Davies, G. J., *Trends Biotechnol.* **2001**, 19, 356-362.
- (5) Dwek, R. A.; Butters, T. D.; Platt, F. M.; Zitzmann, N., *Nat. Rev. Drug Discov.* **2002**, 1, 65-75.
- (6) Asano, N.; Nash, R. J.; Molyneux, R. J.; Fleet, G. W. J., *Tetrahedron Asymmetry* **2000**, 11, 1645-1680.
- (7) Berecibar, A.; Grandjean, C.; Siriwardena, A., *Chem. Rev.* **1999**, 99, 779-844.
- (8) Lillelund, V. H.; Jensen, H. H.; Liang, X. F.; Bols, M., *Chem. Rev.* **2002**, 102, 515-553.
- (9) vonItzstein, M.; Thomson, R. J., *Curr. Med. Chem.* **1997**, 4, 185-210.
- (10) Yuasa, H.; Saotome, C.; Kanie, O., *Trends Glycosci. Glycotechnol.* **2002**, 14, 231-251.
- (11) Wolfenden, R.; Lu, X. D.; Young, G., *J. Am. Chem. Soc.* **1998**, 120, 6814-6815.
- (12) Zechel, D. L.; Withers, S. G., *Acc. Chem. Res.* **2000**, 33, 11-18.
- (13) Koshland, D. E., *Biol. Rev.* **1953**, 28, 416-436.
- (14) Zechel, D. L.; Withers, S. G., *Curr. Opin. Chem. Biol.* **2001**, 5, 643-649.
- (15) Sinnott, M. L., *Chem. Rev.* **1990**, 90, 1172-1202.
- (16) Rye, C. S.; Withers, S. G., *Curr. Opin. Chem. Biol.* **2000**, 4, 573-580.
- (17) Capon, B., *Chem. Rev.* **1969**, 69, 407-498.
- (18) Withers, S. G., *Carbohydrate Polymers* **2001**, 44, 325-337.
- (19) Vasella, A.; Davies, G. J.; Bohm, M., *Curr. Opin. Chem. Biol.* **2002**, 6, 619-629.

- (20) Blake, C. C. F.; Johnson, L. N.; Mair, G. A.; North, A. C. T.; Phillips, D. C.; Sarma, V. R., *Proc. Royal Soc. Lon. B* **1967**, 167, 378-&.
- (21) Davies, G. J.; Mackenzie, L.; Varrot, A.; Dauter, M.; Brzozowski, A. M.; Schulein, M.; Withers, S. G., *Biochemistry* **1998**, 37, 11707-11713.
- (22) Sulzenbacher, G.; Driguez, H.; Henrissat, B.; Schulein, M.; Davies, G. J., *Biochemistry* **1996**, 35, 15280-15287.
- (23) Tews, I.; Perrakis, A.; Oppenheim, A.; Dauter, Z.; Wilson, K. S.; Vorgias, C. E., *Nat. Struct. Biol.* **1996**, 3, 638-648.
- (24) Ducros, V. M. A.; Zechel, D. L.; Murshudov, G. N.; Gilbert, H. J.; Szabo, L.; Stoll, D.; Withers, S. G.; Davies, G. J., *Angew. Chem., Int. Ed.* **2002**, 41, 2824-2827.
- (25) Umezurike, G. M., *Biochem. J.* **1988**, 254, 73-76.
- (26) Tull, D.; Withers, S. G., *Biochemistry* **1994**, 33, 6363-6370.
- (27) Sinnott, M. L., *FEBS Lett.* **1978**, 94, 1-9.
- (28) Li, B. F. L.; Holdup, D.; Morton, C. A. J.; Sinnott, M. L., *Biochem. J.* **1989**, 260, 109-114.
- (29) Kempton, J. B.; Withers, S. G., *Biochemistry* **1992**, 31, 9961-9969.
- (30) Withers, S. G.; Rupitz, K.; Street, I. P., *J. Biol. Chem.* **1988**, 263, 7929-7932.
- (31) McCarter, J. D.; Withers, S. G., *J. Am. Chem. Soc.* **1996**, 118, 241-242.
- (32) Namchuk, M. N.; McCarter, J. D.; Becalski, A.; Andrews, T.; Withers, S. G., *J. Am. Chem. Soc.* **2000**, 122, 1270-1277.
- (33) Levvy, G. A.; Conchie, J.; Hay, A. J., *Biochem. J.* **1964**, 91, 378-384.

- (34) Levvy, G. A.; Snaith, S. M., *Advances in Enzymology and Related Areas of Molecular Biology* **1972**, 36, 151-181.
- (35) Walaszek, Z.; Horton, D.; Ekiel, I., *Carbohydr. Res.* **1982**, 106, 193-201.
- (36) Nishimura, Y.; Adachi, H.; Satoh, T.; Shitara, E.; Nakamura, H.; Kojima, F.; Takeuchi, T., *J. Org. Chem.* **2000**, 65, 4871-4882.
- (37) Strynadka, N. C. J.; James, M. N. G., *J. Mol. Biol.* **1991**, 220, 401-424.
- (38) Numao, S.; Kuntz, D. A.; Withers, S. G.; Rose, D. R., *J. Biol. Chem.* **2003**, 278, 48074-48083.
- (39) Kornfeld, R.; Kornfeld, S., *Annu. Rev. Biochem.* **1985**, 54, 631-664.
- (40) Knauer, R.; Lehle, L., *Biochim. Biophys. Acta* **1999**, 1426, 259-273.
- (41) Varki, A., *Trends Cell Biol.* **1998**, 8, 34-40.
- (42) Buckhaults, P.; Chen, L.; Fregien, N.; Pierce, M., *J. Biol. Chem.* **1997**, 272, 19575-19581.
- (43) Perng, G. S.; Shoreibah, M.; Margitich, I.; Pierce, M.; Fregien, N., *Glycobiology* **1994**, 4, 867-871.
- (44) Pierce, M.; Buckhaults, P.; Chen, L.; Fregien, N., *Glycoconjugate J.* **1997**, 14, 623-630.
- (45) Fernandes, B.; Sagman, U.; Auger, M.; Demetrio, M.; Dennis, J. W., *Cancer Res.* **1991**, 51, 718-723.
- (46) Lemaire, S.; Derappe, C.; Michalski, J. C.; Aubery, M.; Neel, D., *J. Biol. Chem.* **1994**, 269, 8069-8074.
- (47) Easton, E. W.; Blokland, I.; Geldof, A. A.; Rao, B. R.; Vandeneijnden, D. H., *FEBS Lett.* **1992**, 308, 46-49.

- (48) Do, K. Y.; Fregien, N.; Pierce, M.; Cummings, R. D., *J. Biol. Chem.* **1994**, 269, 23456-23464.
- (49) Dennis, J. W.; Kosh, K.; Bryce, D. M.; Breitman, M. L., *Oncogene* **1989**, 4, 853-860.
- (50) Dennis, J. W.; Laferte, S.; Yagel, S.; Breitman, M. L., *Cancer Cells-a Monthly Review* **1989**, 1, 87-92.
- (51) Itzkowitz, S. H.; Yuan, M.; Fukushi, Y.; Palekar, A.; Phelps, P. C.; Shamsuddin, A. M.; Trump, B. F.; Hakomori, S.; Kim, Y. S., *Cancer Res.* **1986**, 46, 2627-2632.
- (52) Kim, Y. S.; Yuan, M.; Itzkowitz, S. H.; Sun, Q.; Kaizu, T.; Palekar, A.; Trump, B. F.; Hakomori, S., *Cancer Res.* **1986**, 46, 5985-5992.
- (53) Granovsky, M.; Fata, J.; Pawling, J.; Muller, W. J.; Khokha, R.; Dennis, J. W., *Nat. Med.* **2000**, 6, 306-312.
- (54) Duronio, V.; Jacobs, S.; Romero, P. A.; Herscovics, A., *J. Biol. Chem.* **1988**, 263, 5436-5445.
- (55) Daniel, P. F.; Winchester, B.; Warren, C. D., *Glycobiology* **1994**, 4, 551-566.
- (56) Moremen, K. W.; Trimble, R. B.; Herscovics, A., *Glycobiology* **1994**, 4, 113-125.
- (57) Knight, J.; Beug, H.; Marshall, J.; Hayman, M. J., *Oncogene* **1988**, 2, 317-326.
- (58) Keegan, A. D.; Conrad, D. H., *J. Immunol.* **1987**, 139, 1199-1205.
- (59) Fischer, T.; Thoma, B.; Scheurich, P.; Pfizenmaier, K., *J. Biol. Chem.* **1990**, 265, 1710-1717.
- (60) Akiyama, S. K.; Yamada, S. S.; Yamada, K. M., *J. Biol. Chem.* **1989**, 264, 18011-18018.

- (61) Dennis, J. W.; Koch, K.; Yousefi, S.; Vanderelst, I., *Cancer Res.* **1990**, 50, 1867-1872.
- (62) Bowlin, T. L.; Sunkara, P. S., *Biochem. Biophys. Res. Commun.* **1988**, 151, 859-864.
- (63) Goss, P. E.; Baker, M. A.; Carver, J. P.; Dennis, J. W., *Clin. Cancer Res.* **1995**, 1, 935-944.
- (64) Olden, K.; Breton, P.; Grzegorzewski, K.; Yasuda, Y.; Gause, B. L.; Oredipe, O. A.; Newton, S. A.; White, S. L., *Pharm. Ther.* **1991**, 50, 285-290.
- (65) Humphries, M. J.; Olden, K., *Pharmacol. Ther.* **1989**, 44, 85-105.
- (66) Das, P. C.; Roberts, J. D.; White, S. L.; Olden, K., *Oncology Res.* **1995**, 7, 425-433.
- (67) Goss, P. E.; Reid, C. L.; Bailey, D.; Dennis, J. W., *Clin. Cancer Res.* **1997**, 3, 1077-1086.
- (68) Novikoff, P. M.; Touster, O.; Novikoff, A. B.; Tulsiani, D. P., *J. Cell Biol.* **1985**, 101, 339-349.
- (69) Tulsiani, D. R. P.; Touster, O., *Archives of Biochemistry and Biophysics* **1983**, 224, 594-600.
- (70) Berg, T.; Riise, H. M. F.; Hansen, G. N.; Malm, D.; Tranebjaerg, L.; Tollersrud, O. K.; Nilssen, O., *American Journal of Human Genetics* **1999**, 64, 77-88.
- (71) Nilssen, O.; Berg, T.; Riise, H. M. F.; Ramachandran, U.; Evjen, G.; Hansen, G. M.; Malm, D.; Tranebjaerg, L.; Tollersrud, O. K., *Human Molecular Genetics* **1997**, 6, 717-726.

- (72) Aldaher, S.; Degasperi, R.; Daniel, P.; Hirani, S.; Warren, C.; Winchester, B., *Biochem. J.* **1992**, 286, 47-53.
- (73) Liao, Y. F.; Lal, A.; Moremen, K. W., *J. Biol. Chem.* **1996**, 271, 28348-28358.
- (74) Tulsiani, D. R. P.; Hubbard, S. C.; Robbins, P. W.; Touster, O., *J. Biol. Chem.* **1982**, 257, 3660-3668.
- (75) van den Elsen, J. M. H.; Kuntz, D. A.; Rose, D. R., *EMBO J.* **2001**, 20, 3008-3017.
- (76) Howard, S.; He, S. M.; Withers, S. G., *J. Biol. Chem.* **1998**, 273, 2067-2072.
- (77) Numao, S.; He, S. M.; Evjen, G.; Howard, S.; Tollersrud, O. K.; Withers, S. G., *FEBS Lett.* **2000**, 484, 175-178.
- (78) Alberts, I. L.; Nadassy, K.; Wodak, S. J., *Protein Sci.* **1998**, 7, 1700-1716.
- (79) Deslongchamps, P., *Stereoelectronic effects in organic chemistry*. Pergamon Press: Oxford, 1983; Vol. 1.
- (80) Kuntz, D. A.; Liu, H.; Bols, M.; Rose, D. R., *Biocatalysis Biotransform.* **2006**, 24, 1-7.
- (81) Shah, N.; Kuntz, D. A.; Rose, D. R., *Biochemistry* **2003**, 42, 13812-13816.
- (82) Kuntz, D. A.; Ghavami, A.; Johnston, B. D.; Pinto, B. M.; Rose, D. R., *Tetrahedron Asymmetry* **2005**, 16, 25-32.
- (83) Boss, O.; Leroy, E.; Blaser, A.; Reymond, J. L., *Org. Lett.* **2000**, 2, 151-154.
- (84) King, S. B.; Ganem, B., *J. Am. Chem. Soc.* **1994**, 116, 562-570.
- (85) Kleban, M.; Hilgers, P.; Greul, J. N.; Kugler, R. D.; Li, J.; Picasso, S.; Vogel, P.; Jager, V., *Chembiochem* **2001**, 2, 365-368.
- (86) Ogawa, S.; Morikawa, T., *Bioorg. Med. Chem. Lett.* **1999**, 9, 1499-1504.

- (87) Ogawa, S.; Morikawa, T., *Bioorg. Med. Chem. Lett.* **2000**, 10, 1047-1050.
- (88) Popowycz, F.; Gerber-Lemaire, S.; Demange, R.; Rodriguez-Garcia, E.; Asenjo, A. T. C.; Robina, I.; Vogel, P., *Bioorg. Med. Chem. Lett.* **2001**, 11, 2489-2493.
- (89) Winkler, D. A., *J. Med. Chem.* **1996**, 39, 4332-4334.
- (90) Morris, G. M.; Goodsell, D. S.; Halliday, R. S.; Huey, R.; Hart, W. E.; Belew, R. K.; Olson, A. J., *J. Comput. Chem.* **1998**, 19, 1639-1662.
- (91) Lyne, P. D., *Drug Discov. Today* **2002**, 7, 1047-1055.
- (92) Wesson, L.; Eisenberg, D., *Protein Sci.* **1992**, 1, 227-235.
- (93) Morris, G. M.; Goodsell, D. S.; Huey, R.; Olson, A. J., *J. Comput.-Aided Mol. Design* **1996**, 10, 293-304.
- (94) Stouten, P. F. W.; Frommel, C.; Nakamura, H.; Sander, C., *Molecular Simulation* **1993**, 10, 97-&.
- (95) Mccammon, J. A.; Gelin, B. R.; Karplus, M., *Nature* **1977**, 267, 585-590.
- (96) Hansson, T.; Oostenbrink, C.; van Gunsteren, W. F., *Curr. Opin. Struct. Biol.* **2002**, 12, 190-196.
- (97) Case, D. A., et al. *Amber 7.0*, University of California: San Francisco, CA, 2002.
- (98) Verlet, L., *Physical Review* **1967**, 159, 98-103.
- (99) Jorgensen, W. L.; Chandrasekhar, J.; Madura, J. D.; Impey, R. W.; Klein, M. L., *J. Phys. Chem.* **1983**, 79, 926-935.
- (100) Friesner, R. A.; Baik, M. H.; Gherman, B. F.; Guallar, V.; Wirstam, M.; Murphy, R. B.; Lippard, S. J., *Coord. Chem. Rev.* **2003**, 238, 267-290.
- (101) Monard G., P.-R. X., Gonzalez-Lafont A. and Lluch J., *Int. J. Quantum Chem.* **2003**, 93, 229-244.

- (102) Field, M. J.; Bash, P. A.; Karplus, M., *J. Comput. Chem.* **1990**, 11, 700-733.
- (103) Antes, I.; Thiel, W., *J. Phys. Chem. A* **1999**, 103, 9290-9295.
- (104) They, V.; Rinaldi, D.; Rivail, J. L.; Maigret, B.; Ferenczy, G. G., *J. Comput. Chem.* **1994**, 15, 269-282.
- (105) Gao, J. L.; Amara, P.; Alhambra, C.; Field, M. J., *J. Phys. Chem. A* **1998**, 102, 4714-4721.
- (106) Cunningham, M. A.; Ho, L. L.; Nguyen, D. T.; Gillilan, R. E.; Bash, P. A., *Biochemistry* **1997**, 36, 4800-4816.
- (107) Mulholland, A. J.; Richards, W. G., *Proteins* **1997**, 27, 9-25.
- (108) Reuter, N.; Dejaegere, A.; Maigret, B.; Karplus, M., *J. Phys. Chem. A* **2000**, 104, 1720-1735.
- (109) Ridder, L.; Mulholland, A. J.; Rietjens, I. M. C. M.; Vervoort, J., *J. Am. Chem. Soc.* **2000**, 122, 8728-8738.
- (110) Ridder, L.; Mulholland, A. J.; Vervoort, J.; Rietjens, I. M. C. M., *J. Am. Chem. Soc.* **1998**, 120, 7641-7642.
- (111) Schrodinger, I. *Jaguar 4.2*, Portland, OR, 2001.
- (112) Frisch, M. J., et al. *Gaussian 98*, Revision A.11.3 ed; Gaussian, Inc.: Pittsburgh, PA, 2002.
- (113) Dennis, J. W.; Granovsky, M.; Warren, C. E., *Biochim. Biophys. Acta* **1999**, 1473, 21-34.
- (114) Heightman, T. D.; Vasella, A. T., *Angew. Chem., Int. Ed.* **1999**, 38, 750-770.
- (115) McCarter, J. D.; Withers, S. G., *Curr. Opin. Struct. Biol.* **1994**, 4, 885-892.

- (116) Aoyagi, T.; Yamamoto, T.; Kojiri, K.; Morishima, H.; Nagai, M.; Hamada, M.; Takeuchi, T.; Umezawa, H., *J. Antibiot.* **1989**, 42, 883-889.
- (117) Ogawa, S.; Washida, K., *Eur. J. Org. Chem.* **1998**, 1929-1934.
- (118) Ogawa, S.; Morikawa, T., *Eur. J. Org. Chem.* **2000**, 1759-1765.
- (119) Uchida, C.; Kimura, H.; Ogawa, S., *Bioorg. Med. Chem.* **1997**, 5, 921-939.
- (120) Szardenings, A. K.; Burkoth, T. S.; Look, G. C.; Campbell, D. A., *J. Org. Chem.* **1996**, 61, 6720-6722.
- (121) Schwarz, M. K.; Tumelty, D.; Gallop, M. A., *J. Org. Chem.* **1999**, 64, 2219-2231.
- (122) Salvatore, R. N.; Nagle, A. S.; Jung, K. W., *J. Org. Chem.* **2002**, 67, 674-683.
- (123) Misago, M.; Liao, Y. F.; Kudo, S.; Eto, S.; Mattei, M. G.; Moremen, K. W.; Fukuda, M. N., *Proc. Natl. Acad. Sci. USA* **1995**, 92, 11766-11770.
- (124) Lalegerie, P.; Legler, G.; Yon, J. M., *Biochimie* **1982**, 64, 977-1000.
- (125) Knapp, S.; Dhar, T. G. M., *J. Org. Chem.* **1991**, 56, 4096-4097.
- (126) Rabouille, C.; Kuntz, D. A.; Lockyer, A.; Watson, R.; Signorelli, T.; Rose, D. R.; van den Heuvel, M.; Roberts, D. B., *J. Cell Sci.* **1999**, 112, 3319-3330.
- (127) Kilpatrick, J. E.; Pitzer, K. S.; Spitzer, R., *J. Am. Chem. Soc.* **1947**, 69, 2483-2488.
- (128) Pitzer, K. S.; Donath, W. E., *J. Am. Chem. Soc.* **1959**, 81, 3213-3218.
- (129) Chung-Phillips, A.; Chen, Y. Y., *J. Phys. Chem. A* **1999**, 103, 953-964.
- (130) Cloran, F.; Carmichael, I.; Serianni, A. S., *J. Phys. Chem. A* **1999**, 103, 3783-3795.
- (131) Gordon, M. T.; Lowary, T. L.; Hadad, C. M., *J. Org. Chem.* **2000**, 65, 4954-4963.

- (132) Marten, B.; Kim, K.; Cortis, C.; Friesner, R. A.; Murphy, R. B.; Ringnalda, M. N.; Sitkoff, D.; Honig, B., *J. Phys. Chem.* **1996**, 100, 11775-11788.
- (133) Tannor, D. J.; Marten, B.; Murphy, R.; Friesner, R. A.; Sitkoff, D.; Nicholls, A.; Ringnalda, M.; Goddard, W. A.; Honig, B., *J. Am. Chem. Soc.* **1994**, 116, 11875-11882.
- (134) Boraston, A. B.; Chiu, P.; Warren, R. A. J.; Kilburn, D. G., *Biochemistry* **2000**, 39, 11129-11136.
- (135) Lemieux, R. U., *Acc. Chem. Res.* **1996**, 29, 373-380.
- (136) Lemieux, R. U.; Delbaere, L. T. J.; Beierbeck, H.; Spohr, U., *Ciba Foundation Symposia* **1991**, 158, 231-248.
- (137) McGaughey, G. B.; Gagne, M.; Rappe, A. K., *J. Biol. Chem.* **1998**, 273, 15458-15463.
- (138) Frisch, M. J. T., G. W.; Schlegel, H. B.; Gill, P. M. W.; Johnson, B. G.; Robb, M. A.; Cheeseman, J. R.; Keith, T.; Petersson, G. A.; Montgomery, J. A.; Raghavachari, K.; Al-Laham, M. A.; Zakrzewski, V. G.; Ortiz, J. V.; Foresman, J. B.; Cioslowski, J.; Stefanov, B. B.; Nanayakkara, A.; Challacombe, M.; Peng, C. Y.; Ayala, P. Y.; Chen, W.; Wong, M. W.; Andres, J. L.; Replogle, E. S.; Gomperts, R.; Martin, R. L.; Fox, D. J.; Binkley, J. S.; Defrees, D. J.; Baker, J.; Stewart, J. P.; Head-Gordon, M.; Gonzalez, C.; Pople, J. A. *Gaussian 94*, Revision E.2; Gaussian, Inc.: Pittsburgh, 1995.
- (139) Becke, A. D., *J. Chem. Phys.* **1993**, 98, 5648-5652.
- (140) Becke, A. D., *Phys. Rev. A* **1988**, 38, 3098-3100.
- (141) Lee, C. T.; Yang, W. T.; Parr, R. G., *Phys. Rev. B* **1988**, 37, 785-789.

- (142) Hariharan, P. C.; Pople, J. A., *Theor. Chim. Acta* **1973**, 28, 213-222.
- (143) Sundaralingam, M., *J. Am. Chem. Soc.* **1971**, 93, 6644-&.
- (144) Goodsell, D. S.; Morris, G. M.; Olson, A. J., *J. Mol. Recognit.* **1996**, 9, 1-5.
- (145) Chiche, L.; Gregoret, L. M.; Cohen, F. E.; Kollman, P. A., *Proc. Natl. Acad. Sci. U. S. A.* **1990**, 87, 3240-3243.
- (146) Gasteiger, J.; Marsili, M., *Tetrahedron* **1980**, 36, 3219-3228.
- (147) Mehler, E. L.; Solmajer, T., *Protein Eng.* **1991**, 4, 903-910.
- (148) Elbein, A. D., *FASEB J.* **1991**, 5, 3055-3063.
- (149) Tulsiani, D. R. P.; Harris, T. M.; Touster, O., *J. Biol. Chem.* **1982**, 257, 7936-7939.
- (150) Boraston, A. B.; Nurizzo, D.; Notenboom, V.; Ducros, V.; Rose, D. R.; Kilburn, D. G.; Davies, G. J., *J. Mol. Biol.* **2002**, 319, 1143-1156.
- (151) Chavez, M. I., et al., *Chem. Eur. J.* **2005**, 11, 7060-7074.
- (152) Fernandez, M. D.; Canada, F. J.; Jimenez-Barbero, J.; Cuevas, G., *J. Am. Chem. Soc.* **2005**, 127, 7379-7386.
- (153) Li, B.; Kawatkar, S. P.; George, S.; Strachan, H.; Woods, R. J.; Siriwardena, A.; Moremen, K. W.; Boons, G. J., *Chembiochem* **2004**, 5, 1220-1227.
- (154) Reid, K. S. C.; Lindley, P. F.; Thornton, J. M., *FEBS Lett.* **1985**, 190, 209-213.
- (155) Pal, D.; Chakrabarti, P., *J. Biomol. Struct. Dynamics* **1998**, 15, 1059-1072.
- (156) Pal, D.; Chakrabarti, P., *J. Biomol. Struct. Dynamics* **2001**, 19, 115-128.
- (157) Samanta, U.; Pal, D.; Chakrabarti, P., *Proteins* **2000**, 38, 288-300.
- (158) Iwaoka, M.; Takemoto, S.; Okada, M.; Tomoda, S., *Bull. Chem. Soc. Jpn.* **2002**, 75, 1611-1625.

- (159) Ippolito, J. A.; Alexander, R. S.; Christianson, D. W., *J. Mol. Biol.* **1990**, 215, 457-471.
- (160) Brandl, M.; Weiss, M. S.; Jabs, A.; Suhnel, J.; Hilgenfeld, R., *J. Mol. Biol.* **2001**, 307, 357-377.
- (161) Tatko, C. D.; Waters, M. L., *Protein Sci.* **2004**, 13, 2515-2522.
- (162) Alber, F.; Kuonen, O.; Scapozza, L.; Folkers, G.; Carloni, P., *Proteins* **1998**, 31, 453-459.
- (163) Pranata, J., *Bioorganic Chem.* **1997**, 25, 213-219.
- (164) Cheney, B. V.; Schulz, M. W.; Cheney, J., *Biochim. Biophys. Acta* **1989**, 996, 116-124.
- (165) Duan, G. L.; Smith, V. H.; Weaver, D. F., *Mol. Phys.* **2001**, 99, 1689-1699.
- (166) Haasnoot, C. A. G.; Deleeuw, F.; Altona, C., *Tetrahedron* **1980**, 36, 2783-2792.
- (167) Varrot, A.; Tarling, C. A.; Macdonald, J. M.; Stick, R. V.; Zechel, D. L.; Withers, S. G.; Davies, G. J., *J. Am. Chem. Soc.* **2003**, 125, 7496-7497.
- (168) Sinnokrot, M. O.; Sherrill, C. D., *J. Phys. Chem. A* **2004**, 108, 10200-10207.
- (169) Winkler, D. A.; Holan, G., *J. Med. Chem.* **1989**, 32, 2084-2089.
- (170) Morishima, H.; Kojiri, K.; Yamamoto, T.; Aoyagi, T.; Nakamura, H.; Iitaka, Y., *J. Antibiot.* **1989**, 42, 1008-1011.
- (171) Ryckaert, J. P.; Ciccotti, G.; Berendsen, H. J. C., *J. Comput. Phys.* **1977**, 23, 327-341.
- (172) Woods, R. J.; Dwek, R. A.; Edge, C. J.; Fraserreid, B., *J. Phys. Chem.* **1995**, 99, 3832-3846.
- (173) Cremer, D.; Pople, J. A., *J. Am. Chem. Soc.* **1975**, 97, 1354-1358.

- (174) Kawatkar, S. P.; Kuntz, D. A.; Woods, R. J.; Rose, D. R.; Boons, G. J., *J. Am. Chem. Soc.* **2006**.
- (175) Comba, P.; Zimmer, M., *J. Chem. Edu.* **1996**, 73, 108-110.
- (176) Cundari, T. R., *J. Chem. Soc. Dalton Transactions* **1998**, 2771-2776.
- (177) Parr, R. G.; Yang, W., *Density Functional Theory of Atoms and Molecules*.
Oxford University Press: New York, 1989.
- (178) Ziegler, T., *Chem. Rev.* **1991**, 91, 651-667.
- (179) Vacek, G.; Perry, J. K.; Langlois, J. M., *Chem. Phys. Lett.* **1999**, 310, 189-194.
- (180) Andre, I.; Tvaroska, I.; Carver, J. P., *Carbohydr. Res.* **2003**, 338, 865-877.
- (181) Tvaroska, I.; Andre, I.; Carver, J. P., *Glycobiology* **2003**, 13, 559-566.
- (182) Tvaroska, I.; Andre, I.; Carver, J. P., *J. Am. Chem. Soc.* **2000**, 122, 8762-8776.
- (183) Frisch, M. J. T., G. W.; Schlegel, H. B.; Scuseria, G. E.; Robb, M. A.;
Cheeseman, J. R.; Zakrzewski, V. G.; Montgomery, J. A.; Stratmann, Jr., R. E.;
Burant, J. C.; Dapprich, S.; Millam, J. M.; Daniels, A. D.; Kudin, K. N.; Strain,
M. C.; Farkas, O.; Tomasi, J.; Barone, V.; Cossi, M.; Cammi, R.; Mennucci, B.;
Pomelli, C.; Adamo, C.; Clifford, S.; Ochterski, J.; Petersson, G. A.; Ayala, P. Y.;
Cui, Q.; Morokuma, K.; Malick, D. K.; Rabuck, A. D.; Raghavachari, K.;
Foresman, J. B.; Cioslowski, J.; Ortiz, J. V.; Baboul, A.G.; Stefanov, B.B.; Liu,
G.; Liashenko, A.; Piskorz, P.; Komaromi, I.; Gomperts, R.; Martin, R. L.; Fox,
D. J.; Keith, T.; Al-Laham, M. A.; Peng, C. Y.; Nanayakkara, A.; Challacombe,
M.; Gill, P. M. W.; Johnson, B.; Chen, W.; Wong, M. W.; Andres, J. L.;
Gonzalez, C.; Head-Gordon, M.; Replogle, E.S. and Pople, J. A. *Gaussian 98*,
Revision A9; Gaussian, Inc.: Pittsburgh, PA, 1998.

- (184) Hay, P. J.; Wadt, W. R., *J. Chem. Phys.* **1985**, 82, 299-310.
- (185) Wiberg, K. B., *Tetrahedron* **1968**, 24, 1083-&.
- (186) Glendening, E. D.; Badenhop, J. K.; Reed, A. E.; Carpenter, J. E.; Bohmann, J. A.; Morales, C. M.; Weinhold, F. *NBO 5.0*, Theoretical Chemistry Institute, University of Wisconsin: Madison, 2001.
- (187) Karaveg, K.; Siriwardena, A.; Tempel, W.; Liu, Z. J.; Glushka, J.; Wang, B. C.; Moremen, K. W., *J. Biol. Chem.* **2005**, 280, 16197-16207.